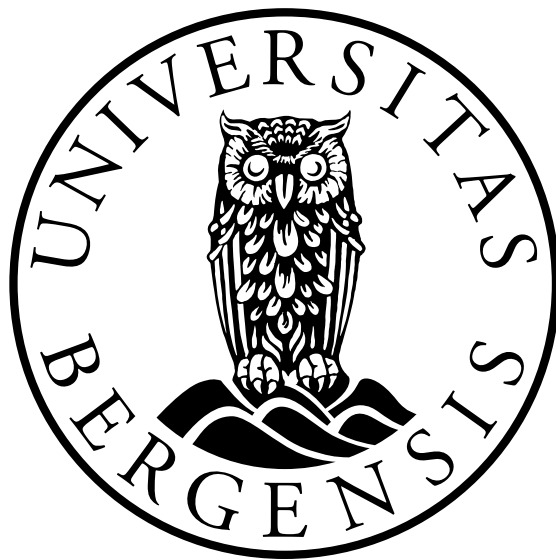


# **Multiscale analysis of selected problems in fluid dynamics**

**Sergey Alyaev**



Dissertation for the degree of Philosophiae Doctor (PhD)

Department of Mathematics  
University of Bergen

Date of defense: 03.02.2017



# **Preface**

This dissertation is submitted as a partial fulfillment of the requirements for the degree Doctor Philosophy (PhD) at the University of Bergen. The advisory committee has consisted of Jan Martin Nordbotten (University of Bergen) and Eirik Keilegavlen (University of Bergen). The work has been supported by the project of the Research Council of Norway under grant 180679: "Modelling Transport in Porous Media over Multiple Scales".



# Acknowledgements

First, I would like to thank my advisers: Jan Martin Nordbotten and Eirik Keilegavlen. Each of them played a unique role in the completion of this project. From the beginning, Jan was continuously challenging me with interesting problems and motivated with enthusiasm during our coffee-house meetings. On the other hand, Eirik has patiently discussed all difficult technical details of the research. His attention to details (hopefully) made me a better writer.

Next, I would like to thank my coauthors Boris Balakin and Sorin Pop. They further educated me as an applied mathematician and their contributions helped to diversify my work. Boris Balakin involved me in a side-project, which resulted in Paper E. With him, it was equally fun to solve problems of particle interaction and have scientific discussions in the gym. Sorin Pop taught me that one needs to be precise when doing mathematics, and we also had great time discussing life, the universe and homogenization.

I would like to acknowledge my colleagues from the department of mathematics. During my employment there, they were fulfilling the roles of both friends and family. I want to specifically thank Georgy Ivanov (my googling expert), and Trine Mykkeltvedt (my Matlab expert). We have been studying together since the start of our Master's and became closer friends over this time. Both gave me valuable feedback on my early drafts that helped to improve this thesis.

I also acknowledge my current colleagues from IRIS who treated the preparation of the thesis with a great deal of understanding. I have received a lot of empathy and helpful advice during the months of writing.

Last, but not least I would like to thank my family for being there for me, cheering and not allowing me to give up. Specifically, I would like to thank my dear wife Anna Kvashchuk who has only known me in the state of preparing the thesis. Not only did she exercise infinite patience with this hobby over the years, but she has also supported me with technical discussions, and provided some of the colorful illustrations for my thesis and for my life. I would always remember that Anna even approved integration on our sofa as quality time together. I hope I will make up for it by being an even better husband.



# Abstract

The world around us is inherently multiscale. The variety of different models depending on the reference scale is particularly diverse in problems of fluid-solid systems. For those systems, the geometry, effective parameters and even equations vary between scales. Normally, on coarser scales the fundamental laws of physics are not sufficient to provide a closed-form model. This called for experiment-based closures, which often had limited domain of applicability. An alternative approach enabled by recent developments is so-called multiscale methods. By considering the two scales simultaneously, multiscale methods do not rely on experimental closures and therefore lay a physics-based foundation for engineering problems.

In this work, we attempt to separate multiscale methods into larger classes based on a flowchart that contains questions about the structure of problems, for which they are designed. Analysis and methods, presented in the thesis, aim to fill the gaps in inter-disciplinary knowledge across several classes of multiscale methods. We conduct fit-for-purpose analysis of several selected multiscale problems in fluid dynamics: non-linear single phase flows in porous media, fractal structures formation in freezing brine, particle-particle interaction affected by capillary bridging.

The first problem is addressed by the control volume heterogeneous multiscale method (CVHMM). By coupling mass conservation with Navier-Stokes equations on the pore scale, the method captures nontrivial coarse-scale effects, which are not handled by standard single-scale models. To demonstrate the robustness of the presented methods, a multiscale convergence analysis and a derivation of a priori error estimates are developed for the method.

For the second problem, simplifications and consequent self-similar analysis identifies compact and fractal regimes of ice formation. Moreover, combining the insights obtained from numerical and analytical solutions we introduce an empirical model that can qualitatively predict properties of the formed ice.

For the third problem, we derive a new semi-analytical solution for particle interactions during viscous bridging. The solution provides basis for more efficient simulation of suspended flows of particles.



# Outline

The dissertation consists of two parts. The first part (Chapters 1 – 5) serves as an introduction to the second part (Chapter 6), which contains the publications with the main scientific results of this work.

We start by introducing the scope of the thesis and summarizing its main contributions in Chapter 1. Chapter 2 provides motivation for considering multiscale problems. It describes important concepts related to modeling and is concluded by introducing selected multiscale problems that are extensively studied in this work. Before introducing methods for multiscale problems, Chapter 3 provides basic numerical techniques that are used as solvers for each scale in relevant problems. Chapter 4 presents a classification of the multiscale methods with a brief overview of the field. It helps to position the methods developed in this thesis with respect to other developments. It pays particular attention to the methods used in the thesis. Finally, Chapter 5 summarizes the papers that constitute the main scientific contributions of the work and are attached in Chapter 6.

## List of papers

Paper A: S. ALYAEV, E. KEILEGAVLEN, AND J.M. NORDBOTTEN, **Multiscale simulation of non-Darcy flows**, *In proceedings of the XIX Computational Methods in Water Resources, CMWR* (June 17 - 21, 2012).

Paper B: S. ALYAEV, E. KEILEGAVLEN, AND J.M. NORDBOTTEN, **Analysis of control volume heterogeneous multiscale methods for single phase flow in porous media**, *Multiscale Modeling & Simulation* 12, 1 (2014), 335–363. doi: 10.1137/120885541

Paper C: S. ALYAEV, E. KEILEGAVLEN, AND J.M. NORDBOTTEN, **Multiscale simulations of non-linear flows in porous media**, Submitted to *Water Resources Research* (2016).

Paper D: S. ALYAEV, E. KEILEGAVLEN, J.M. NORDBOTTEN, AND I.S. POP, **Fractal structures in freezing brine**, Submitted to *Journal of Fluid Mechanics* (2016).

Paper E: B.V. BALAKIN, S. ALYAEV, A.C. HOFFMANN, AND P. KOSINSKI, **Micromechanics of agglomeration forced by the capillary bridge: the restitution of momentum**, *AIChe Journal* 59, 11 (2013), 4045–4057. doi: 10.1002/aic.14162



# Contents

<b>Preface</b>	<b>iii</b>
<b>Acknowledgements</b>	<b>v</b>
<b>Abstract</b>	<b>vii</b>
<b>Outline</b>	<b>ix</b>
<b>List of papers</b>	<b>ix</b>
<b>Contents</b>	<b>xi</b>
<b>1 Introduction</b>	<b>1</b>
Main contributions . . . . .	3
<b>2 Multiscale systems in fluid dynamics</b>	<b>5</b>
2.1 Eulerian and Lagrangian approaches to continuum modeling . . . . .	5
2.2 Representative elementary volume . . . . .	7
2.3 Finding similarities between scales . . . . .	9
2.3.1 Conservation laws . . . . .	10
2.3.2 Self-similarity of the solution . . . . .	10
2.4 Selected multiscale problems in fluid dynamics . . . . .	11
2.4.1 Darcy scales and permeability . . . . .	12
2.4.2 Non-linear flow in porous media . . . . .	14
2.4.3 Sea-ice and freezing brine . . . . .	16
2.4.4 Solid particle agglomerates forced by capillary bridges . . . . .	20
<b>3 Discretization strategies</b>	<b>23</b>
3.1 Control volume methods . . . . .	24
3.1.1 Two-point flux approximation . . . . .	25
3.1.2 Multi-point flux approximation . . . . .	26
3.2 Finite element methods . . . . .	28
3.2.1 Finite volume element method . . . . .	30
3.2.2 Taylor-Hood elements . . . . .	31
<b>4 Approaches to multiscale problems</b>	<b>33</b>
4.1 Relation between analytical and numerical approaches . . . . .	33
4.2 Classes of multiscale methods . . . . .	35

4.2.1	Class A: Multiresolution solvers . . . . .	36
4.2.2	Class B: Formal upscaling with closure . . . . .	36
4.2.3	Class C: Numerical upscaling using parametrization . . . . .	37
4.2.4	Class D: Fractal methods . . . . .	38
4.2.5	Class E: Hybrid method with short relaxation time . . . . .	38
4.2.6	Class F: Brief overview of space-time hybrid multiscale methods	38
4.3	Homogenization . . . . .	39
4.3.1	Homogenization for heterogeneous media . . . . .	40
4.3.2	Summary of homogenization derivation of Darcy's law . . . . .	42
4.4	Heterogenous multiscale methods . . . . .	44
4.5	Self-similarity analysis . . . . .	47
<b>5</b>	<b>Discussion of included papers</b>	<b>49</b>
5.1	Control volume HMM for non-linear flows in porous media . . . . .	49
5.1.1	Summary of Paper A . . . . .	51
5.1.2	Summary of Paper B . . . . .	51
5.1.3	Summary of Paper C . . . . .	53
5.1.4	Further directions . . . . .	54
5.2	Multiscale analysis of freezing in brine . . . . .	55
5.2.1	Summary of Paper D . . . . .	56
5.2.2	Discussion of control volume approximation of ice growth . . . . .	57
5.2.3	Further directions . . . . .	60
5.3	Semi-analytical solution for micro-mechanics of capillary bridges . . . . .	61
5.3.1	Summary of Paper E . . . . .	61
5.3.2	Paper E in the context of multiscale simulation . . . . .	62
<b>Bibliography</b>		<b>63</b>
<b>6</b>	<b>Included papers</b>	<b>71</b>
6.1	Paper A: Multiscale simulation of non-Darcy flows . . . . .	73
6.2	Paper B: Analysis of control volume heterogeneous multiscale methods for single phase flow in porous media . . . . .	83
6.3	Paper C: Multiscale simulations of non-linear flows in porous media . . . . .	115
6.4	Paper D: Fractal structures in freezing brine . . . . .	139
6.5	Paper E: Micromechanics of agglomeration forced by the capillary bridge: the restitution of momentum . . . . .	161

# Chapter 1

## Introduction

The underlying physical laws necessary for the mathematical theory of a large part of physics and the whole of chemistry are thus completely known [from quantum mechanics], and the difficulty is only that the exact application of these laws leads to equations much too complicated to be soluble.

---

Paul Dirac

The ultimate purpose of any modeling is mimicking the behavior of the modeled system, so that certain unknown characteristics of the model can be predicted based on the known parameters. These characteristics are typically specific to the macroscopic behavior and correspond to values that one can observe or measure. Historically modeling was focused on a single macroscopic scale at which the problem is formulated.

At the same time, the world around us is inherently multiscale. Depending on the size of the considered system, different behavior would be observed. Taking an extreme example: it might contain only a few elementary particles obeying the laws of quantum mechanics, a volume of gas obeying Navier-Stokes equations, or a galaxy obeying astronomical laws. The variety of different models depending on the reference size is particularly pronounced in heterogeneous continuum systems containing inclusions, e.g. suspended particle flows, flows in porous media and flows with phase transition. For those systems the geometry, effective parameters, and even equations change multiple times even when the scale is relevant for a continuum representation.

Normally, on coarser scales the fundamental laws of physics are not sufficient to describe a closed-form system. Therefore, the experiment-based (phenomenological) relations were derived to make the modeling on the system possible within that single scale. Darcy's law, Fick's law, Hooke's law and Stokes' law are just some of the well-known examples of simple constitutive relations that have been used for decades. These made it possible to find analytical and later also numerical solutions. This formed a basis for the technological advancements of the last few centuries. However, over time advancement of technology gave rise to more and more difficult problems. To cope with the new challenges the classical models were updated to include a number of corrections which were harder to estimate and justify.

An alternative to obtaining models using experiment-based closures is to consider a system on several scales simultaneously. Such kind of multiscale modeling allows to make less assumptions on the model at the scale of interest. This extends the domain of applicability of the model outside of the bounds associated with the regimes in which the constitutive relations were obtained. It was recognized by Dirac that by following the scales down to the scale of quantum-mechanical interactions the exact behavior of most systems in applied sciences can be deduced. At the same time, it is practically impossible to use them directly to study realistic problems due to resolution and complexity.

At the current stage of development, most multiscale methods are focused on two scales: the main macroscopic scale which contains the quantities of interest and a finer scale of the problem which provides an insight into the physics of the problem, which cannot be resolved on the coarsest scale. By considering the two scales simultaneously, multiscale methods lay a physical foundation for engineering problems. Moreover, for models like Darcy's law, multiscale analysis using homogenization has rigorously identified assumptions under which this phenomenological relationship accurately describes the coarse-scale behavior of the system [47]. Thus, homogenization constitutes a rigorous upscaling technique for multiscale problems. Now, we have introduced two schools of thought for multiscale problems: numerical and analytical. In this work, we emphasize the relationship between them, calling them multiscale simulation and modeling, respectively (see Section 4.1).

The advancement of theory and computational power made it possible to perform simulations that take sub-scale features into account. At the same time, many challenges should be addressed before the vision of multiscale simulation can come to everyday reality [32].

First and foremost, coupling of problems on different scales is not trivial. Since the coupling process is problem-dependent, in this work we attempt to separate multiscale methods into larger classes based on a flowchart inspired by [74], see Section 4.2. The flowchart categorizes the methods based on questions about scale dependence, scale separation in time and space, as well as the requirements on the details in solutions.

Many of studied multiscale methods assume sufficient spatial scale separation [74]. However, this assumption is not always fulfilled for multiscale systems. Paper D deals with rapid freezing in brine that results in fractal solutions. Scale similarity techniques [20] are applied to analyze the challenging fractal behavior of the problem.

When there is sufficient spatial scale separation many multiscale methods can be formulated within a unified framework of heterogeneous multiscale methods (HMM) introduced in [33], see Section 4.4. Even when utilizing this unified framework one needs to adapt the method to problem-dependent requirements. As a starting point for the multiscale methods developed in this thesis, we focus on control volume methods also called finite volume methods, see Section 3.1. Control volume methods bring the conservation laws (namely the conservation of mass and continuity of fluxes) to the discrete grid level [4, 53]. This makes them a promising choice as a coarse-scale foundation for multiscale methods for problems of fluid dynamics where those properties should be maintained on all scales.

Once the approximations on the coarse and the fine scales are defined and a methodology for coupling is established additional care should be taken to ensure that the method is consistent and convergent. In Paper B, we verify the convergence of the pre-

sented numerical multiscale method against the homogenization solution of the Stokes problem when its assumptions are valid. From there we anticipate that the consistency is maintained for regimes that cannot be easily analyzed. The self-convergence in those cases is verified numerically.

To apply multiscale methods to realistic problems it is also important to ensure that the computational cost stays within reasonable bounds. One should exploit problem-specific features to reduce excessive computational time on the fine scale. Possible but incomplete list of choices includes: auxiliary basis functions [78], dynamically constructed interpolation tables [Paper C] and semi-analytical solutions [Paper E].

## Main contributions

The present work tries to address mathematical challenges briefly discussed in the introduction by providing a problem-driven analysis of several problems in fluid dynamics. The developed analysis and methods aim to fill the gaps in inter-disciplinary knowledge. In addition to giving an insight into the problems, the analysis improves understanding in the field of multiscale modeling and simulation. This is supported by the fact that the papers included in this thesis have already inspired further work both in their respective and adjacent fields.

The specific contributions of the thesis are:

1. We present the control volume heterogeneous multiscale method (CVHMM) that takes advantage of industry-standard control volume methods to resolve the mass conservation on the coarse scale and couples it to on-demand computation of the effects arising from the fine scale. The thesis is specifically describing the coupling with Navier-Stokes equations on the pore geometry that results in non-trivial effects on the coarse scale that cannot be handled by standard single-scale models. The capabilities of the method are demonstrated on a range of relevant problems. To demonstrate the robustness of presented methods, a multiscale convergence analysis and a derivation of a priori error estimates are developed for the method.
2. A self-similar analysis of a simplified problem of rapid freezing in brine is supposed to compliment single-scale mushy-layer models for averaged dynamics of ice in brine. The analysis yields a closed form analytical self-similar solution for the continuous ice growth. The analysis is augmented by development of non-trivial control-volume method that handles moving boundaries. Using the numerical model, we demonstrate another class of self-similar solutions which are dominated by secondary nucleation resulting in fractal patterns of ice formation. Based on the coupled analysis of numerical and analytical solution we introduce an empirical model that depending on the freezing conditions can qualitatively predict properties of the formed ice.
3. An analysis of particle-particle interaction affected by formation and breakage of capillary bridge is performed. The analysis is concluded by deriving a semi-analytical solution of a problem that is experimentally validated. The newly-derived analytical model renders a computationally efficient fine-scale solver that

can be used in a Lagrangian-Eulerian multiscale coupling within computational fluid dynamics.

# Chapter 2

## Multiscale systems in fluid dynamics

Everything should be made as simple as possible, but not simpler.

---

Albert Einstein

Many of physical laws represent relations that are based on experiments. Examples include: Hooke's law of spring motion, Darcy's law for flow in porous media, Archie's law of electrical conductivity of sedimentary rocks, Avogadro's law of amount of substance of gas, Fick's laws of diffusion, Moore's law of transistor development, Stokes' law for flow of viscous fluids. The experimental setting normally imposes limits on the domain of applicability for such phenomenological laws. The scale of applicability is one of the most common limitations.

The purpose of this chapter is to identify some of the problems of fluid dynamics that span several scales thus providing an additional motivation for studying multiscale methods. However, before introducing the problems in Section 2.4, we present basic theory related to fluid dynamics and associated multiscale problems. First, in Section 2.1 we introduce the two frames of reference for continuum flow systems. Second, in Section 2.2 we give a more precise definition of what we consider a single scale of a problem and introduce a notion of REV. After that, in Section 2.3 we present some general principles used for design of multiscale methods in this thesis.

### 2.1 Eulerian and Lagrangian approaches to continuum modeling

Unlike classical mechanics, where the system normally consists of a finite number of solid objects (particles), in continuum flow systems one cannot uniquely distinguish between objects. However, it is common to introduce the notion of a fluid particle to create a setting that is analogous to classical mechanics.

One defines a fluid parcel (equivalently fluid particle, fluid element) as a very small amount of matter (of volume  $\delta V$ ) that can be tracked as it moves in the flow [21, 83]. The smallness should be understood in comparison to the domain of interest and can be formally expressed as

$$|\delta V|_* \ll |\Omega|_*, \quad (2.1)$$

where  $\delta V$  is the volume of the parcel and  $|\bullet|_*$  is a measure of characteristic size. This measure defines the scale of a physical system and is only required to be of same order

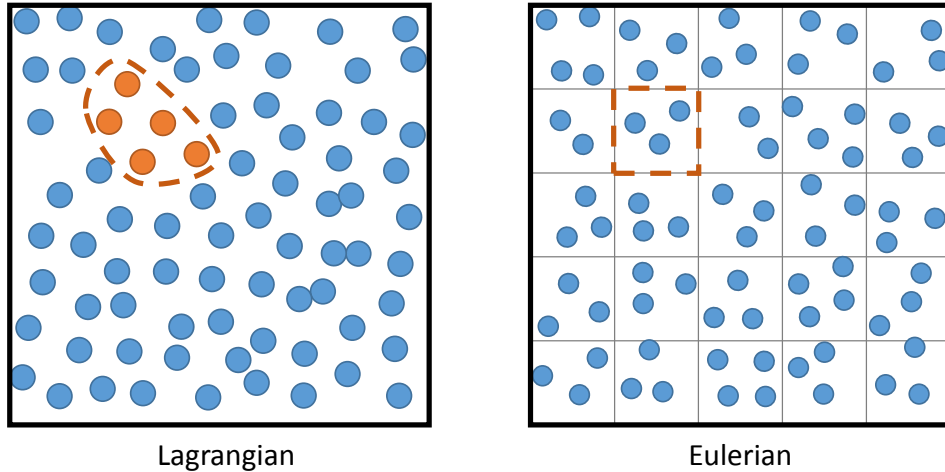


Figure 2.1: Comparison of Lagrangian and Eulerian frames of reference for a fluid with particles.

of magnitude as the actual size of measured domain. Looking at fluid flow following individual particles or fluid parcels is commonly known as the Lagrangian approach, see Figure 2.1. In computational Lagrangian-type methods, such as discrete parcel and discrete element methods, the properties of matter within one parcel are assumed to be constant [31].

On the other hand, the Eulerian approach considers fluid motion by fixing specific locations in space through which the fluid flows. In this approach one does not follow the matter itself, but tracks the exchange of substance between the neighboring locations (cells), see Figure 2.1. This leads to corresponding changes of properties associated to the cells. Examples of computational approaches in the Eulerian frame of reference, such as control volume and finite element methods, are presented in Chapter 3. For the Eulerian approach, an accurate representation of properties also requires the cells of sufficiently small size

$$|\beta|_* \ll |\Omega|_*, \quad (2.2)$$

where  $|\beta|_*$  is the typical size of a cell  $\beta$ .

The choice between the Lagrangian and Eulerian approaches is problem-specific. It is sensible to apply the approach for which the model problem is easiest to define. The problems of fluid dynamics, such as Navier-Stokes equations and flows in porous media, are better studied in Eulerian frame of reference. Therefore, we use this approach for fluid flow systems in papers A, B, C, D. At the same time, modern multiscale techniques are capable of coupling different approaches for different scales of a problem. For instance, the Lagrangian approach is used in Paper E to study the fine-scale interaction of solid particles and it is later coupled to the Eulerian description of fluid flow [18, 19]. Also, in [45] the authors use the methods from Paper B substituting the fine-scale solver with a Lagrangian solver. A further discussion highlighting the relation of the Lagrangian and Eulerian approaches to multiscale methods can be found in [32].

## 2.2 Representative elementary volume

When working with problems of fluid dynamics, it is important to keep in mind that the properties of the continuum in each point of space, are properties averaged over some reference volume. For both Lagrangian and Eulerian approaches, to resolve the dynamics of the system the averaged volume should be small compared to the domain of interest, see (2.1) and (2.2). At the same time, it should be sufficiently large so that it represents the continuum in a consistent manner, independently of its exact location.

For example, for flow of fluid with particles, the reference volume should at least contain a number of particles and some surrounding fluid to be representative, see Figure 2.1. The necessary size of such a location is called accordingly: representative elementary volume (REV). In this system one can therefore distinguish two scales of different magnitudes: the characteristic length scale of the whole domain ( $|\Omega|_*$ ) and the maximum size of features that are averaged out (**REV**):

$$\mathbf{REV} \ll |\Omega|_* . \quad (2.3)$$

If we upscale (average out) small features of sizes below **REV**, we get a single-scale problem. In definitions of (2.3) the size of a computation cell for that single-scale problem should be limited from both sides as follows

$$\mathbf{REV} \leq |\beta|_* \ll |\Omega|_* , \quad (2.4)$$

where, as earlier,  $|\beta|_*$  is the typical size of the computational parcel or cell.

More complex systems might contain more than one pair of characteristic scales **REV** and  $|\Omega|_*$ . For those systems (2.3) should be understood recursively:

$$\mathbf{REV}_{i-1} \ll |\Omega_{i-1}|_* , \quad (2.5)$$

$$\mathbf{REV}_{i-1} \ll \mathbf{REV}_i \ll |\Omega_i|_* . \quad (2.6)$$

From (2.6) we know that there exists an REV scale above  $\mathbf{REV}_{i-1}$  where the parameters can be consistently averaged out. Therefore we can limit the computational domain for the fine scale solver ( $\Omega_{i-1}$ ) to the size of  $\mathbf{REV}_i$ :

$$\mathbf{REV}_{i-1} \ll |\Omega_{i-1}|_* \sim \mathbf{REV}_i \ll |\Omega_i|_* . \quad (2.7)$$

Concept (2.7) plays a crucial role in the design of multiscale methods. For instance, it is fundamental to heterogeneous multiscale methods, which take into account several scales simultaneously (see Section 4.4). When performing a multiscale simulation, the constraint for the cell size (2.4) should be applied at every scale [8]:

$$\mathbf{REV}_i \leq |\beta_i|_* \ll |\Omega_i|_* . \quad (2.8)$$

As a more complex example, let us consider geological systems where the number of scales is particularly diverse. Figure 2.2 uses the example of permeability to show how properties of geological porous media change depending on the scale of averaging [72]. REV scale can be graphically defined as a scale at which small changes of scale or location do not change the average properties. The smallest porous-medium REV can be defined as a scale which contains a sufficient amount of pores and grains so that

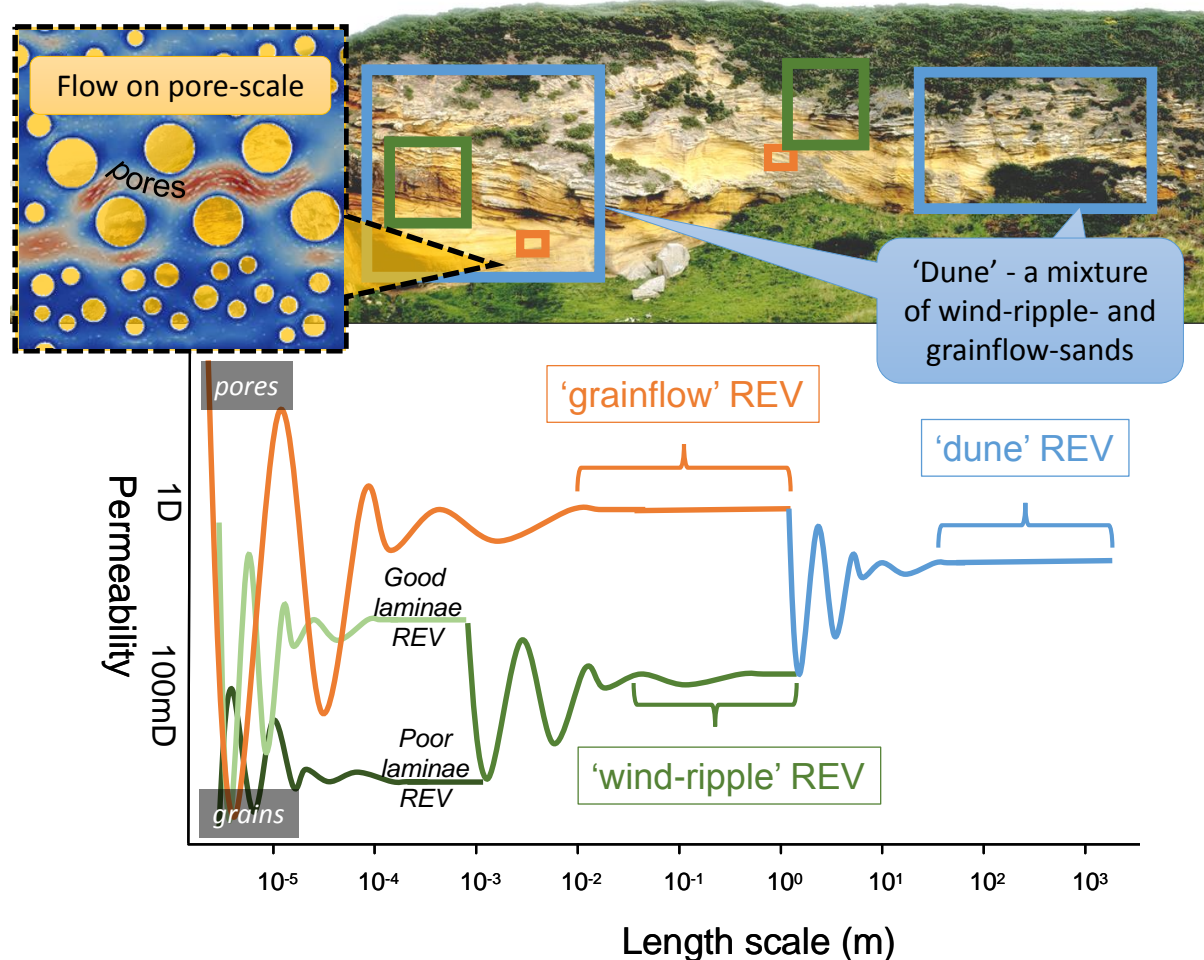


Figure 2.2: A diagram showing the influence of the scale of averaging on permeability of porous medium for a 'sand dune' reservoir. Averaging is consistent when REV is reached. Adapted from a presentation by Mark Bentley.

the properties are stable with respect to volume perturbations [22]. Similarly to [84], this can be mathematically written as:

$$\frac{1}{V_h} \int_{V_h(x_0+\delta x)} a dx \approx \frac{1}{V_h} \int_{V_h(x_0)} a dx \approx \frac{1}{V_{h+\delta}} \int_{V_{h+\delta}(x_0)} a dx, \quad (2.9)$$

where  $a$  is the property being averaged and  $V_h(x_0)$  is a volume around point  $x_0$  of size  $h$  and  $\delta$  is a small perturbation. REV is reached for the smallest  $h$  that satisfies (2.9). However, if we continue extending the averaging window, we meet heterogeneity related to deposition layering. The averaging, again, becomes inconsistent with parameters oscillating between values of good and poor lamina, see Figure 2.2. When several laminae are within the averaging volume we reach the next REV typical for a coarse deposition layer. Further, one gets the 'dune' REV which has reservoir scale.

As a result, for a geological system, one can define a tree-shaped plot of effective parameters as a function of the averaging window size and location, Figure 2.2. Such visualization of scales and REVs can facilitate decisions related to modeling of multi-scale phenomena. A particularly important consideration for problem-specific models is to ensure that available measurements are performed at an REV scale and are, therefore, consistent [72].

We have been discussing that an REV should be much smaller than the scale of the full problem domain. One can formally define the scale separation constant

$$\varepsilon = \frac{\text{REV}}{|\Omega|_*}. \quad (2.10)$$

This constant is extensively used for analysis of multiscale problems. In homogenization, the multiscale problems are studied assuming that the fine scale structure is  $\varepsilon$ -periodic, in the limit when  $\varepsilon$  goes to zero (see Section 4.3).

The same scale separation constant plays an important role in analysis of heterogeneous multiscale methods (see Section 4.4) [7, 8, Paper B]. There, the propagation of the error from the fine scale is proportional to  $\frac{|\beta_{\text{fine}}|_*}{\varepsilon}$ . This implies that in order to capture sub-scale dynamics the cell size should be small relative to the fine scale domain  $|\Omega_{\text{fine}}|_*$ , see (2.8). A discussion of the error analysis for problems specific to this work can be found in Section 5.1.2.

## 2.3 Finding similarities between scales

The definition of multiscale methods varies depending on the research community. In our work we want to explicitly differentiate multiscale methods from fine-scale methods combined with multiscale solvers, such as domain decomposition [76] or multigrid [25]. A detailed discussion of a classification is presented in Section 4.2. While multiscale solvers applied on huge grids that cover domains relevant for coarser scale do provide a detailed solution, they naturally tend to have a great computational cost. In contrast to them, multiscale methods try to utilize all available properties of the coarse system and do not solve the full fine-scale system explicitly. This results in a lower

computational cost but comes at a price of inability to reconstruct the fine-scale solution. Nevertheless, multiscale methods are desirable techniques for a vast majority of problems where only the coarse solution is required but single-scale methods (for the coarse-scale problem) fail to capture sub-scale dynamics.

This section covers some principles that can be used to extract maximum information from the coarse scale while not compromising the solution quality with specific assumptions. Such information can for example be obtained from physically sound invariants such as conservation laws and self-similarity arguments.

### 2.3.1 Conservation laws

A conservation law is a physical principle stating that a certain property of an isolated system does not change as the system evolves in time. For a continuum system for property  $\alpha$ , the conservation law in the Eulerian frame of reference can be interpreted as follows:

$$\frac{d}{dt} \int_{\beta} \alpha dx + \int_{\partial\beta} \vec{A} \cdot \vec{n} ds = \int_{\beta} \gamma dx, \quad (2.11)$$

where  $\frac{d}{dt}$  is the time derivative,  $\beta$  is a fixed volume with boundary  $\partial\beta$  with an outer normal vector  $\vec{n}$ ;  $\gamma$  is the volumetric source of  $\alpha$ ; finally,  $\vec{A}$  is the vector flux field for  $\alpha$  that may be composed of advective (due to movement of the fluid) and non-advection (specific to this property) components.

For fluid flow systems, the conservation of fluid mass is particularly important. Substituting the fluid mass (obtained as density multiplied by volumetric fraction of component  $\rho\phi$ ) for  $\alpha$  and the corresponding mass flux  $\vec{H}$  in (2.11), we get

$$\frac{d}{dt} \int_{\beta} \phi \rho dx + \int_{\partial\beta} \vec{H} \cdot \vec{n} ds = \int_{\beta} f dx. \quad (2.12)$$

Mass conservation on the coarse scale (2.12) ensures the consistency of the solution even in cases when the exact details of the flux field are hard to reproduce. In a variety of problems the conservation of mass is a required property, which is necessary for error control when coupling with a transport model [90].

In order to provide a seamless and accurate approximation of the mass conservation principle, we choose the control volume finite difference method discussed in Section 3.1. It ensures mass conservation on the coarse scale for flows in porous media considered in papers A, B, C. It is also used for numerical analysis of the salt displacement in freezing brine in Paper D, where the salt mass should be conserved.

In Paper E, which focuses on the interaction of solid particles, the conservation laws also play an important role. There, the momentum conservation equation is used to formulate the mathematical problem.

### 2.3.2 Self-similarity of the solution

There exists a class of multiscale problems that do not have scale separation (2.7). For these problems, the concept of coarse-scale REV is not defined and, consequently,

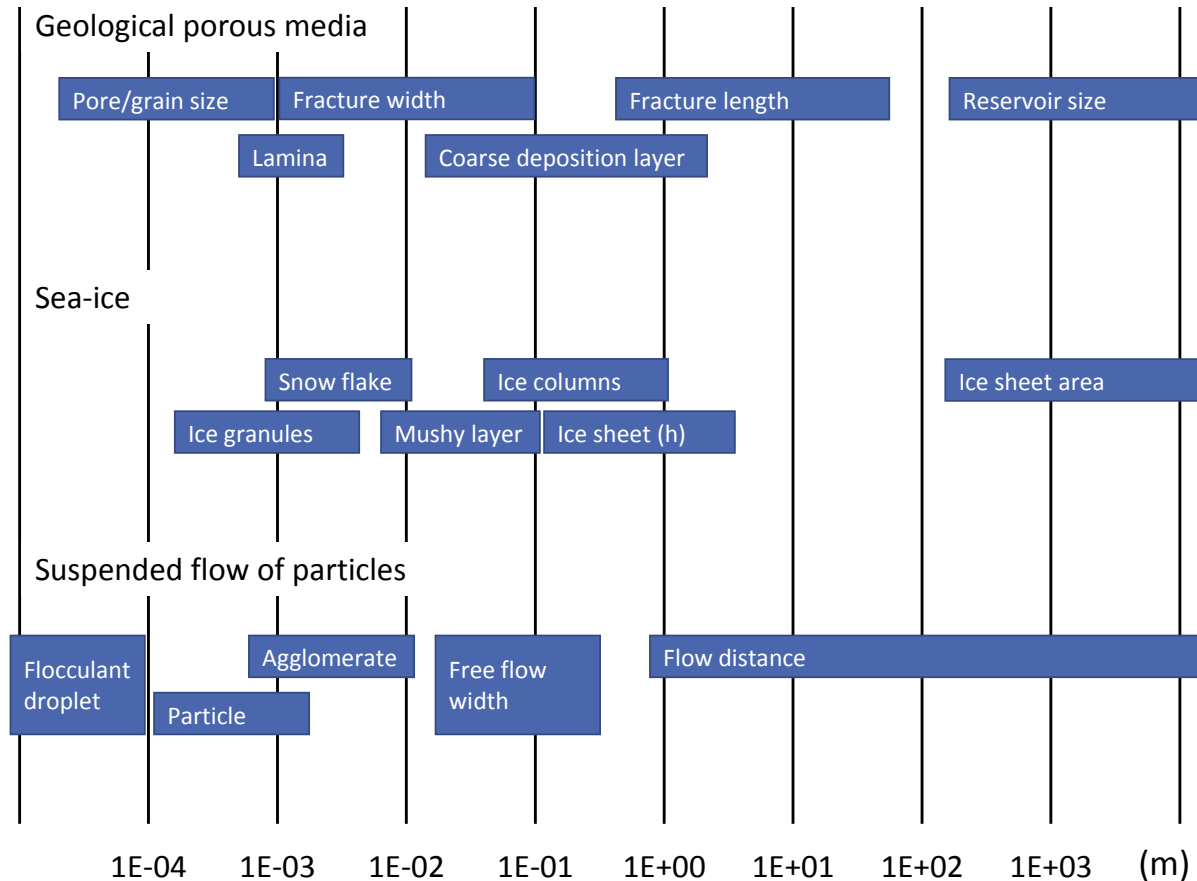


Figure 2.3: The scales of features and problems for selected physical systems.

coarse equations cannot be found. To cope with such challenges, one needs to find other characteristics that can be used to represent the coarse solution.

A possible approach is to identify solution regimes that preserve the shape-function of the solution. The problem of freezing brine considered in Paper D is an example where the approach can be applied. In the paper, we identify two regimes where the shape of the solution becomes a scale-independent invariant. Furthermore, a meaningful interpolation between the regimes leads to a reasonably accurate qualitative method for approximating coarse-scale properties of the solution.

General theory of self-similarity is beyond the scope of this thesis. For a thorough review of the theory including different problems and the corresponding methods, see [20]. Self-similar analysis is revisited in Section 4.5, where we demonstrate it on an example from Paper D.

## 2.4 Selected multiscale problems in fluid dynamics

In physical systems, where solids and fluids coexist, parameters, geometry and even equations change between the scales. In this work we consider three fluid flow systems: flow in porous media, sea-ice, and suspended flow of particles. The systems are arranged by rigidity of solid structure: consolidated for porous media; semi-consolidated for sea-ice; and free flowing for suspended particles. Figure 2.3 shows typical sizes of different features for considered systems [18, 38, 72, 73]. The variety of features and

the spatial spread over eight orders of magnitude manifest all systems as truly multiscale. Moreover, Figure 2.3 only shows the scales where continuum principles apply and omits the scales of molecular and sub-molecular interactions which were not studied in this work.

In this section we introduce specific problems spanning several scales of the systems from Figure 2.3. First, in Subsection 2.4.1 we pose the problem of multiscale permeability. This is a classical example of a well-studied multiscale problem (see Section 2.2), and it is not investigated specifically in this work. However, it also plays the role of the coarse-scale model for the problem of non-linear flow in porous medium presented in Subsection 2.4.2. Next, Subsection 2.4.3 discusses a variety of problems observed in sea-ice on different scales. It is concluded with the finest-scale continuum model of freezing brine formulated in Paper D. Finally, in Subsection 2.4.4, we touch upon the multiscale model of interactions between particles suspended in a free-flowing fluid. The model of particle-particle interaction stands out from the main theme of the thesis and is covered in less detail.

The methods presented in the rest of the thesis address particular challenges related to the problems presented here.

#### 2.4.1 Darcy scales and permeability

Section 2.2 used a geological porous medium as an example of a system with multiple REV scales. Here we focus on coarser scales where grain structure is averaged out corresponding to lamina and coarser REVs, see Figure 2.2. The classical representation of such flows is the Darcy's law. We refer to the smallest scale where the Darcy's law is valid as Darcy scale and consider it the "coarse" scale of our system.

To formulate Darcy's flow on a single (coarse) scale in a porous medium we start from the conservation of mass (2.12)

$$\frac{d}{dt} \int_{\beta} \phi \rho_c dx + \int_{\partial\beta} \rho_c \vec{u}_c \cdot \vec{n} ds = \int_{\beta} f_c dx, \quad (2.13)$$

where the subscript "*c*" emphasizes the coarse scale of the problem. This equation is normally paired with Darcy's approximation of the filtering velocity  $\vec{u}_c$  that is normally obtained from experiments

$$\vec{u}_c = -\frac{\underline{\underline{K}}_c}{\mu} \nabla p_c, \quad (2.14)$$

where  $p_c$  is the coarse-scale potential,  $\mu$  is the viscosity of the fluid and  $\underline{\underline{K}}_c$  is the permeability tensor [67]. The potential  $p_c$  in the generalized Darcy's law consists of contributions from pressure and gravity. In cases when the flow is horizontal, the gravity term is zero and the potential  $p_c$  reduces to pressure.

#### Incompressible flow and upscaling

Under the assumption of incompressibility,

$$\rho = \text{const}, \quad (2.15)$$

the first term from (2.13) disappears, resulting in a steady-state continuity equation

$$\int_{\partial\beta} \rho \vec{u}_c \cdot \vec{n} ds = \int_{\beta} f_c dx. \quad (2.16)$$

Note, that since density is constant, we replace  $\rho_c$  by  $\rho$ . For the sake of conciseness, it is convenient to write (2.16) in divergence form [67] (also dividing by density):

$$\nabla \cdot \vec{u}_c = \frac{f_c}{\rho}. \quad (2.17)$$

Substitution of (2.14) into (2.17) yields the single phase flow equation in divergence form:

$$-\nabla \cdot (\underline{\underline{A}}_c \nabla p_c) = \frac{f_c}{\rho}, \quad (2.18)$$

where

$$\underline{\underline{A}}_c = \frac{\underline{\underline{K}}_c}{\mu}. \quad (2.19)$$

We call  $\underline{\underline{A}}_c$  the Darcy coefficient. In Paper B, we use a sub-Darcy (fine) scale model to automatically obtain the Darcy coefficient  $\underline{\underline{A}}_c$ , thus substituting the experimental approximation (2.14). The fine scale model is presented in the next subsection.

In reservoir modeling applications it is common to encounter large systems with heterogeneous layering. For example in Figure 2.2, 'dune' combines 'grainflow' and 'wind-ripple' sands. In many cases, a fit-for-purpose model is not required to reproduce the solution at a very detailed resolution [72]. Therefore, upscaling techniques are frequently used. Upscaling is a reformulation of the system (2.18) on an even coarser scale. It allows us to obtain a system analogous to (2.18), which has a different effective permeability [67, 72]

$$-\nabla \cdot \left( \frac{\underline{\underline{K}}_D}{\mu} \nabla p_D \right) = \frac{f_D}{\rho}, \quad (2.20)$$

where the subscript "D" (for "Dune") emphasizes an even coarser scale than "c". Note that while the structures of the (2.18) and (2.20) are identical,  $\underline{\underline{K}}_D$  is normally different from  $\underline{\underline{K}}_c$ . Moreover,  $\underline{\underline{K}}_D$  can be a full anisotropic tensor even when the media at scale "c" are isotropic. Thus, upscaling in porous media is an interesting subject in multiscale analysis. In Section 4.3 we use this problem as an example to demonstrate a tool for mathematical upscaling: homogenization.

### Weakly compressible flow

Alongside the incompressible model, in the context of the following discussion it is important to consider weakly compressible flow on Darcy scale. Again, for convenience, we rewrite (2.13) in divergence form

$$\frac{d}{dt}(\phi \rho_c) + \nabla \cdot (\rho_c \vec{u}_c) = f_c \quad (2.21)$$

For the weakly compressible case we simplify the general continuity equation (2.21) by substituting the compressibility relation between pressure and density [22]

$$Z = \frac{1}{\rho_c} \frac{d\rho_c}{dp_c}. \quad (2.22)$$

Since the porosity  $\phi$  is constant, the equation (2.21) can be rewritten as

$$\phi Z \rho_c \frac{d}{dt} p_c + \rho_c \nabla \cdot \vec{u}_c + \nabla \rho_c \cdot \vec{u}_c = f_c. \quad (2.23)$$

The density is assumed to be slowly varying in space. As a result, its gradient is assumed small. With this in mind it is common to neglect the term  $\nabla \rho_c \cdot \vec{u}_c$  from (2.23). Dividing by the density gives

$$\phi Z \frac{d}{dt} p_c + \nabla \cdot \vec{u}_c = \tilde{f}_c, \quad (2.24)$$

where  $\tilde{f}_c$  is the volumetric source.

The closed-form equations for weakly compressible Darcy flow are not considered in this thesis. However, the weakly compressible continuity equation (2.24) is used alongside (2.16) in Paper A for the mass conservation on the coarse scale. As in Paper B, we replace Darcy's law approximation of the flux with a more general fine scale model.

## 2.4.2 Non-linear flow in porous media

Coupling equations (2.17) or (2.24) to sub-Darcy scale may result in an even more interesting multiscale problem. The equation (2.14) is a common experiment-based first-order approximation of the velocity in porous media flow. An alternative approach is to take into consideration the equations of underlying physics that govern the flow on the pore scale, see Figure 2.2. A physically sound approximation of the free flow in the pores is the Navier-Stokes equations, which consist of equations for mass and momentum conservation. For single phase flow the conservation of mass can be written similarly to (2.12):

$$\frac{d}{dt} \int_{\beta} \rho_f dx + \int_{\partial\beta} \rho_f \vec{u}_f \cdot \vec{n} ds = \int_{\beta} f_f dx, \quad (2.25)$$

which now acts on the fine (pore) scale, denoted by subscript " $f$ ". The equation is now valid only in the subdomain occupied by the fluid (i.e. pores, see Figure 2.2), and therefore the fluid fraction always equals one. It should be paired with no flow boundary condition at the interface with solid.

Instead of an empirical relation between pressures and fluxes, the Navier-Stokes system includes an equation for momentum conservation. The momentum density function is the conserved quantity that is equal to  $\rho_f \vec{u}_f$ :

$$\frac{d}{dt} \int_{\beta} \rho_f \vec{u}_f dx + \int_{\partial\beta} \underline{\underline{G}}_f \cdot \vec{n} ds = \int_{\beta} \vec{s}_f dx, \quad (2.26)$$

where tensor  $\underline{\underline{G}}_f$  is the flux of momentum density and  $\vec{s}_f$  is the body force (such as gravity) that would cause acceleration.  $\underline{\underline{G}}_f$  consists of advective and non-advection terms:

$$\underline{\underline{G}}_f = \rho_f \vec{u}_f \otimes \vec{u}_f + \underline{\underline{\sigma}}_f, \quad (2.27)$$

where  $\otimes$  denotes outer (dyadic) product and  $\underline{\underline{\sigma}}_f$  is the stress tensor, i.e. surface forces that influence momentum evolution.

Up until now we have not introduced any significant approximations to the fine-scale model. However, to close the system of equations, an approximation to the stress tensor should be introduced:

$$\underline{\underline{\sigma}}_f = -p_f \underline{\underline{I}} + \underline{\underline{\tau}}_f, \quad (2.28)$$

where  $p_f \underline{\underline{I}}$  is a fine-scale pressure multiplied by the identity matrix, and  $\underline{\underline{\tau}}_f$  is the deviatoric component of the stress tensor. For Newtonian fluids, a common approximation to the latter can be written for each component  $(ij)$  of tensor  $\underline{\underline{\tau}}_f$  as follows [21]:

$$\underline{\underline{\tau}}_{f,ij} = \mu \left( \frac{\partial \vec{u}_f{}_i}{\partial x_j} + \frac{\partial \vec{u}_f{}_j}{\partial x_i} - \frac{2}{3} \delta_{ij} \frac{\partial \vec{u}_f{}_k}{\partial x_k} \right), \quad (2.29)$$

where  $\delta_{ij}$  is Kronecker's delta and  $\mu$  is the linear viscosity of the fluid.

Additionally to stress approximation, it is common to assume that compressibility effects are not pronounced locally on the fine scale. Therefore, one can use this approximation for practical multiscale methods with scale separation, defined by (2.7). These assumptions lead to divergence-free flow that simplifies the equations to a large extent. The system is commonly written in divergence form as follows:

$$\begin{aligned} \nabla \cdot \vec{u}_f &= 0, \\ \rho_f \left( \frac{\partial \vec{u}_f}{\partial t} + \vec{u}_f \cdot \nabla \vec{u}_f \right) &= -\nabla p_f + \mu \Delta \vec{u}_f + \vec{s}_f. \end{aligned} \quad (2.30)$$

For flows in porous media these equations are equipped with no flow boundary conditions on the contact with the solid part of the domain, i.e. grains in Figure 2.2. The flow over a domain covering only a few pore sizes would stabilize quickly compared to changes in the coarse scale conditions. Therefore the steady state equations would give a reasonable approximation for local fine-scale domains:

$$\begin{aligned} \nabla \cdot \vec{u}_f &= 0, \\ \rho_f \vec{u}_f \cdot \nabla \vec{u}_f + \nabla p_f - \mu \Delta \vec{u}_f &= \vec{s}_f. \end{aligned} \quad (2.31)$$

Equations (2.31) form a non-linear system that represents local flows on the pore scale. When the flow speed is sufficiently low, the non-linear term  $\rho_f \vec{u}_f \cdot \nabla \vec{u}_f$  goes to zero. In this regime it is possible to show that the coarse-scale fluxes indeed respect Darcy's law (2.14). A sketch of the derivation is presented in Section 4.3.2.

In faster flow regimes or in highly permeable porous media the non-linearity gives a non-negligible contribution, which propagates to the coarser scales. It is challenging to adjust single-scale models to consistently handle this non-linearity. In papers A, B, C we resolve the non-linear flows on Darcy scale by directly coupling mass conservation (2.13) with local numerical solutions to Navier-Stokes equations (2.31). We emphasize that coupling of distinct equations on the two scales is non-trivial. It is furthermore complicated due to different numerical methods required for each of them. We use control volume methods (see Section 3.1) and the Taylor-Hood finite element method (see Section 3.2.2) for the coarse and the fine scales, respectively. A complete version of the multiscale method is presented in Section 4.4 and the papers are summarized in Section 5.1.

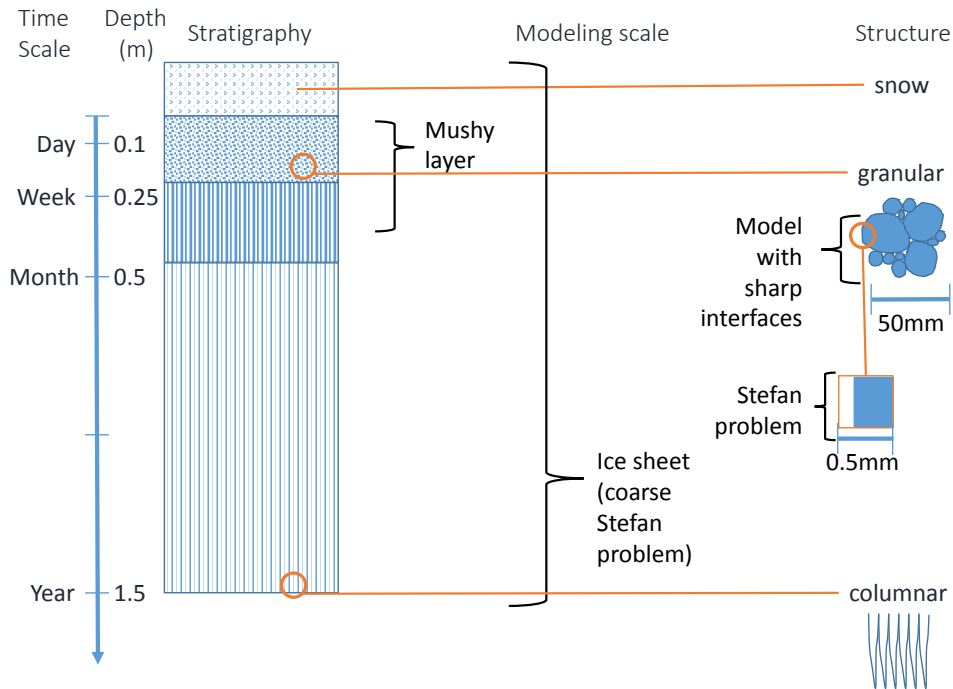


Figure 2.4: Illustration of structure, scales, and applicable models in sea-ice.

### 2.4.3 Sea-ice and freezing brine

When both the fluid and the solid are composed of the same material, it gives rise to an interesting multiscale system – ice formation in brine. Figure 2.4 presents the diversity of structures observed in sea-ice [38, 50]. Different structures give rise to a number of mathematical problems for different scales. In this section we present three important models, each having a different scale of validity: a Stefan problem, a mushy layer model and a simplified continuum model derived in Paper D (see Figure 2.4). The first two models are not studied in this work directly. However, the model in Paper D aims to provide a mathematical justification for mushy layer theory and shares a lot of similarities with the Stefan problem.

#### Stefan problem

In fresh water the ice formation and melting is usually described by a Stefan problem [82]. A Stefan problem [38, 82] is derived from conservation of energy and consists of a heat equation paired with the Stefan condition on the interface. The conservation of energy condition on the interface balances heat consumed by freezing with conductive heat flux to the interface:

$$\frac{d}{dt} \int_{\text{area}} \rho L h ds = \int_{\text{area}} \Phi ds, \quad (2.32)$$

where  $\rho$  is density,  $L$  is latent heat of freezing,  $h$  is the ice thickness, and  $\Phi$  is the conductive heat flux perpendicular to the interface. Since properties of ice are constant and assuming homogeneous ice formation across the whole area, the equation can be simplified to a 1D differential equation [59]

$$\rho L \frac{dh}{dt} = \Phi. \quad (2.33)$$

Due to presence of salt, the homogeneous freezing is rarely observed at small scales [38]. As a result, the Stefan problem (2.32) fails to resolve the complex freezing of brine for this regime. At the same time, the model gives a good rough approximation of sea-ice dynamics on the ice-sheet scale, see Figure 2.4. For this case the conductive heat flux should be in balance with the energy absorption by the ice. The latter is proportional to the coarse-scale temperature gradient in ice in the vertical direction  $\frac{\partial T_c}{\partial z}$ , with proportionality coefficient  $\kappa$  called the thermal conductivity of ice [38, 59]:

$$\Phi_c = -\kappa \frac{\partial T_c}{\partial z} \approx -\kappa \frac{T_{\text{freez}} - T_0}{h_c}. \quad (2.34)$$

Here, as before, subscript "*c*" emphasizes the coarse scale. In (2.34), the gradient is approximated as the temperature difference between the freezing temperature of ice at the water contact  $T_{\text{freez}}$  and surface temperature  $T_0$  divided by the thickness of the ice sheet  $h_c$ .

### Mushy layer model

Simulating a more complex behavior observed at a meso-scale of ice-brine systems requires a larger system of equations. A common approximation for this case is given by a so-called mushy layer model [50, 87]. The main assumption of the model is that ice and brine phases are mixed into an indistinguishable mush where the solid phase is immobile, see Figure 2.4. The system of equations operates with mean properties weighted to represent the mixture proportions:

$$\bar{X} = (1 - \phi)X_i + \phi X_b \quad (2.35)$$

where  $\bar{X}$  is an average property computed from ice ( $X_i$ ) and brine ( $X_b$ ) quantities which are weighted with the brine proportion  $\phi$ . Brine proportion  $\phi$  is analogous to porosity in the terminology of porous media. Substituting average quantities obtained from (2.35) for mass of water, salinity of water, momentum and energy, one formulates conservation equations for those quantities. These conservation equations together with a choice of constitutive relations give a closed system of mushy layer equations. A detailed description of such a system is presented in [50].

### Fine-scale model with sharp interfaces

In this thesis we consider a model on the continuum scale that is finer than the scale of the mushy layer model. That model uses the sharp approximation of interfaces like the Stefan problem rather than the averaging from (2.35), see Figure 2.4. Unlike the classical Stefan problem, the model focuses on domains with complex configurations of ice inclusions rather than a uniform ice-liquid interface. Our fine-scale model does not include all complex effects from modern mushy layer models, which allows a thorough mathematical study of early ice formation.

The conditions for phase transition can be obtained from an equilibrium phase diagram [86] that represents the state of a brine-ice system as a function of the concentration of salt and the temperature of the medium, see Figure 2.5. Under moderately high

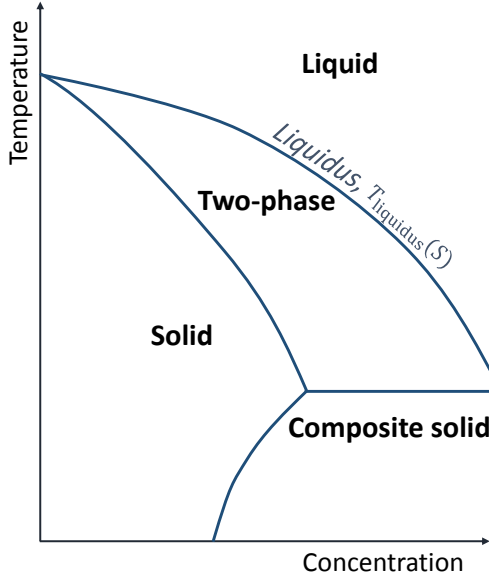


Figure 2.5: An equilibrium phase diagram for freezing brine.

temperatures that are characteristic to early ice formation, all salt remains in the liquid phase. For these conditions one can derive a monotone function that relates temperature to the critical freezing concentration of the mixture called the liquidus [86]:

$$T = T_{\text{liquidus}}(S_{\text{freez}}), \quad (2.36)$$

where  $S_{\text{freez}}$  is the critical freezing concentration (equivalently freezing salinity). The liquidus becomes the boundary condition for temperature on the fluid-liquid interface.

In our simplified model, we assume that thermal effects propagate instantaneously and that temperature is an external control to the system. The monotonicity of (2.36) allows to eliminate the temperature from the system of equations and consider the time-dependent critical concentration  $S_{\text{freez}}$  as the control mechanism for the ice-brine system. The salinity on the boundary is balanced by melting of fresh ice [50] resulting in the boundary condition

$$S_f(t, x) = S_{\text{freez}}(t), \text{ for } x \in \partial\Omega_f(t), \quad (2.37)$$

where  $\partial\Omega_f(t)$  is the moving boundary of the ice-brine domain evolving in time and  $S_f$  is the fine-scale salt concentration that becomes the primary variable in the system. As before, we emphasize the fine scale of the problem by the subscript "f". The primary equation of the system is the conservation equation for the salinity  $S_f$  which in divergence form reads

$$\frac{\partial S_f(t, x)}{\partial t} = -\nabla \cdot (S_f \vec{u}_f + \vec{q}_{fna}), \text{ for } t \geq 0, x \in \Omega_f(t), \quad (2.38)$$

where  $S_f \vec{u}_f$  and  $\vec{q}_{fna}$  are advective (due to fluid flow) and non-advective fluxes respectively. In our model we assume that the fluid is stationary and the diffusion is Fickian [60, 77], yielding

$$\vec{u}_f(t, x) = 0, \quad \text{for } t \geq 0, x \in \Omega_f(t), \quad (2.39)$$

$$\vec{q}_{fna}(t, x) = -D \nabla S_f(t, x), \quad \text{for } t \geq 0, x \in \Omega_f(t). \quad (2.40)$$

Here,  $D$  is the diffusion coefficient. With this in mind, the equation (2.38) becomes

$$\frac{\partial S_f(t, x)}{\partial t} = D \Delta S_f(t, x), \text{ for } t \geq 0, x \in \Omega_f(t), \quad (2.41)$$

which closely resembles the heat equation, but from the physical point of view is distinctly different.

For conserving the salt mass at the ice-brine boundary the normal component of the salt flux from the boundary ( $\vec{q}_{f\text{expul}} \cdot \vec{n}$ ) should be equal to the normal component of the diffusive flux  $\vec{q}_{f\text{na}}$  to ensure that the salt is expelled from the ice domain

$$-\vec{q}_{f\text{expul}} \cdot \vec{n} + \vec{q}_{f\text{na}} \cdot \vec{n} = 0, \text{ for } t \geq 0 \text{ and } x \in \partial\Omega_f(t), \quad (2.42)$$

where  $\vec{n}$  is the normal vector at the boundary  $\partial\Omega_f$  pointing inside the fluid. Note that the equation (2.42) assumes no expansion of the medium due to freezing. Since all the salt should be expelled from the ice and the concentration on the boundary is  $S_{\text{freez}}$  from (2.37), the expulsion flux becomes

$$\vec{q}_{f\text{expul}} = S_{\text{freez}} \frac{d\vec{s}_f}{dt}, \quad (2.43)$$

where the position of the ice boundary is denoted by  $\vec{s}_f$ . Substituting (2.40) and (2.43) into (2.42) results in the following equation for boundary evolution

$$-S_{\text{freez}}(t, x) \frac{d\vec{s}_f(t)}{dt} \cdot \vec{n} - D \nabla S_f(t, x) = 0, \text{ for } t \geq 0 \text{ and } x \in \partial\Omega_f(t), \quad (2.44)$$

which is a particular form of the Rankine-Hugoniot condition, see e.g. [26, 79].

The system of equations (2.37), (2.41), (2.44) from the mathematical point of view closely resembles the Stefan problem, which, as discussed earlier, cannot capture non-trivial sub-scale dynamics. One of the possible mechanisms for formation of non-trivial structures in freezing brine is the secondary nucleation [16, 69]. It is the process of formation of ice (solid) crystals within the volume of liquid that is disconnected from the boundaries formed by initial nucleation. Secondary nucleation is observed in experiments during rapid freezing of brines [69]. Mathematically speaking, secondary nucleation creates a new internal boundary within the fluid domain. It is natural to assume that it happens when the fluid is supercooled, i.e. the temperature of the fluid is much lower than the freezing temperature for the current salinity. The nucleation can be expressed in terms of freezing concentration

$$S_{\text{nucl}}(t) = v(S_{\text{freez}}, \dots) S_{\text{freez}}(t) < S_{\text{freez}}(t), \quad (2.45)$$

where nucleation salinity  $S_{\text{nucl}}(t)$  at which the fluid spontaneously turns into ice is related to the freezing salinity  $S_{\text{freez}}$  via some nucleation multiplier  $v$ . Generally speaking the nucleation multiplier is a function that might be dependent on several parameters.

The problems with moving boundaries are difficult from the mathematical perspective. Moreover, dynamically created internal boundaries result in fractal structures, which cannot be easily parametrized or upscaled. Paper D presents an attempt to handle the problem using self-similarity analysis (see Section 4.5). For analysis purposes, the nucleation multiplier  $v$  is assumed to be constant. The fine-scale continuum model with secondary nucleation captures non-trivial dynamics of ice formation in brines (observed in [69]) and opens up a new perspective on modeling on at the scale that is below the scale of mushy layers. The results of the analysis are summarized in Section 5.2.

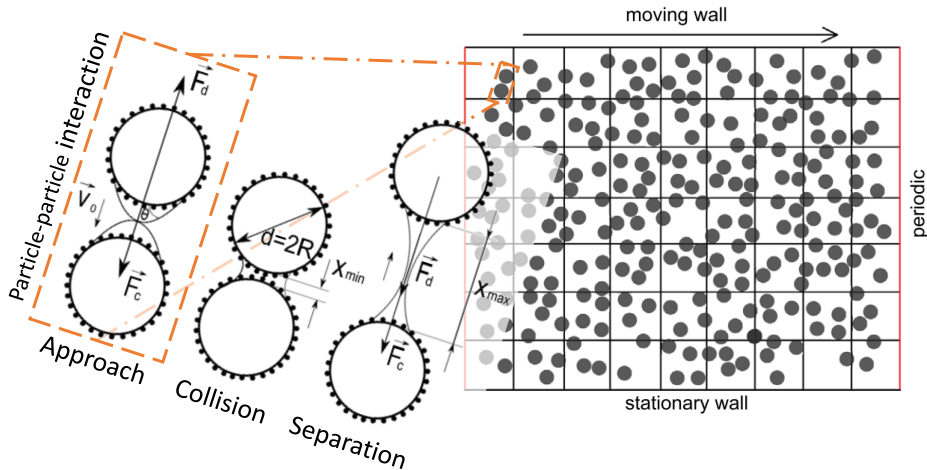


Figure 2.6: Schematics of flow of particles covered with liquid flocculant in a fluid stream; typical for e.g. rheometers or shear cells. The figure presents the free flow on the coarse scale governed by Navier-Stokes equations and a zoomed view of particle-particle interactions on the fine scale. Adapted from Boris Balakin [18].

#### 2.4.4 Solid particle agglomerates forced by capillary bridges

When the concentration of particles in the fluid is low and they are mobile, another multiscale problem arises: suspended flow of particles, see Figure 2.3. The overall flow on the coarse scale in this case is described by Navier-Stokes equations (presented in section 2.4.2). Additionally, the flow is influenced by the interaction of particles happening on a finer scale [18, 19], see Figure 2.6.

An interesting example is flow of particles covered with liquid flocculant in a fluid stream. The liquid flocculant covering particles does not change the properties of the carrier phase flow explicitly. At the same time it alters interactions between the particles on the micro-scale causing formation of viscous bridges between pairs of particles. That can ultimately lead to formation of large agglomerates of solids.

The interaction of solid particles differs drastically from the micro-scale models discussed up till now. Since they are solid and discrete, their respective masses do not change and there is no need for a mass conservation equation. The interaction of particles is governed by a classical equation for momentum conservation:

$$\frac{d}{dt}(m_p \vec{u}_p) = \vec{F}_p, \quad (2.46)$$

where  $m_p$  and  $\vec{u}_p$  are the mass and the velocity of particles respectively, and  $\vec{F}_p$  is the force that acts on a particle. Since the particles are discrete, the equations do not require integration over volume. They are therefore formulated in Lagrangian coordinates. Following [66], the force influencing liquid bridging of particles in viscous flow is composed of

- the capillary force due to liquid flocculant covering the particles;
- the dissipative viscous force from the carrier phase fluid;
- possible additional external forces that influence the dynamics of inter-particle interactions.

For the particular form of the forces we refer the reader to Paper E.

Solving the equation (2.46) numerically is relatively easy. However in the multiscale context, the system is tightly coupled with Navier-Stokes equations. A fluid dynamics simulation of the coupled system requires resolving a number of particle-particle interactions for every coarse cell at every simulation step [18]. To reduce the computational effort, it is therefore desirable to use a closed-form analytical expression to resolve the interactions. The original equation for momentum of this system does not have an analytical solution [89]. Paper E suggests a number of simplifications and approximations which allow to obtain an analytical expression for particle interactions during viscous bridging. The results of the paper are summarized in Section 5.3.



# Chapter 3

## Discretization strategies

The purpose of computing is insight, not numbers.

---

Richard Hamming

In this chapter we will present an overview of basic spatial discretization methods that were used in the dissertation for solving the problems presented in Section 2.4 on different scales. The multiscale methods that are presented in the next chapter utilize these numerical discretization strategies as building blocks.

We start by Section 3.1, which presents a numerical strategy called control volume methods. This discretization is used in the attached papers and is a standard mass conservative approximation utilized in the industry for modeling fluid flows. The second part of the chapter (Section 3.2) describes finite element methods that were traditionally preferred for numerical analysis. We focus on two finite element discretizations that possess the mass conservation property.

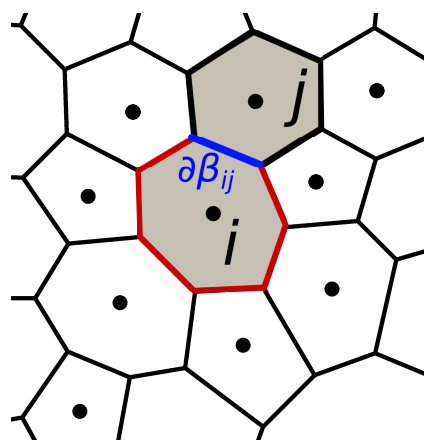


Figure 3.1: An example of a polygonal control volume discretization (adapted from Robert Klöfkorn [55]).

### 3.1 Control volume methods

Control volume methods (also called finite volume methods; CV for short) [41, 53] constitute a class of finite difference methods for flow problems that ensure mass conservation at the level of computational grid. The grid can be some polygonal (2D) or polyhedral (3D) discretization of the computational domain. Figure 3.1 presents an example of a polygonal control volume grid. We denote the computational cell number  $i$ , also called control volume  $i$ , by  $\beta_i$  and the boundary between volumes  $i$  and  $j$  as  $\partial\beta_{ij}$ .

The foundation of this method is the integral formulation of mass conservation (2.12) that is enforced for each computational volume in the grid. To derive the method we first replace an arbitrary volume in the mass conservation equation with a discrete cell  $\beta_i$  to obtain

$$\frac{d}{dt} \int_{\beta_i} \phi \rho dx + \sum_j \int_{\partial\beta_{ij}} \vec{H} \cdot \vec{n} ds = \int_{\beta_i} f dx. \quad (3.1)$$

Further, we replace primary variables such as mass fraction  $\phi$  and density  $\rho$  and source density  $f$  by their discrete approximations:

$$\frac{d}{dt} \phi_i \rho_i \int_{\beta_i} dx + \sum_j \int_{\partial\beta_{ij}} \vec{H} \cdot \vec{n} ds = f_i \int_{\beta_i} dx. \quad (3.2)$$

Finally, the mass flux  $\int_{\partial\beta_{ij}} \vec{H} \cdot \vec{n} ds$  is replaced by a finite difference approximation computed based on the values in the neighboring cells:

$$\frac{d}{dt} \phi_i \rho_i \int_{\beta_i} dx + \sum_j \vec{H}_{ij} = f_i \int_{\beta_i} dx. \quad (3.3)$$

Since the control volume method treats fluxes between any cells  $i$  and  $j$  explicitly, local mass conservation is ensured by construction:

$$\vec{H}_{ij} = -\vec{H}_{ji}. \quad (3.4)$$

The flux between the cells  $\vec{H}_{ij}$  is a function of unknown variables from cells  $i$ ,  $j$  and possibly their neighbors. Depending on which cells are considered, different control volume methods are formed. In the following subsections we will mention some of the possible methods to obtain a flux approximation. To simplify the presentation we will assume that the flux is given by Darcy's law, similar to (2.14):

$$\vec{H} = -\underline{\underline{A}}(x) \nabla p, \quad (3.5)$$

where  $\underline{\underline{A}}(x)$  is a space-dependent Darcy's tensor coefficient.

Before considering particular control volume methods, let us introduce some general conventions that each of the methods will follow:

- The primary variables, such as density and pressure, as well as parameters, such as fluid fraction or permeability, are defined for each cell as constants.

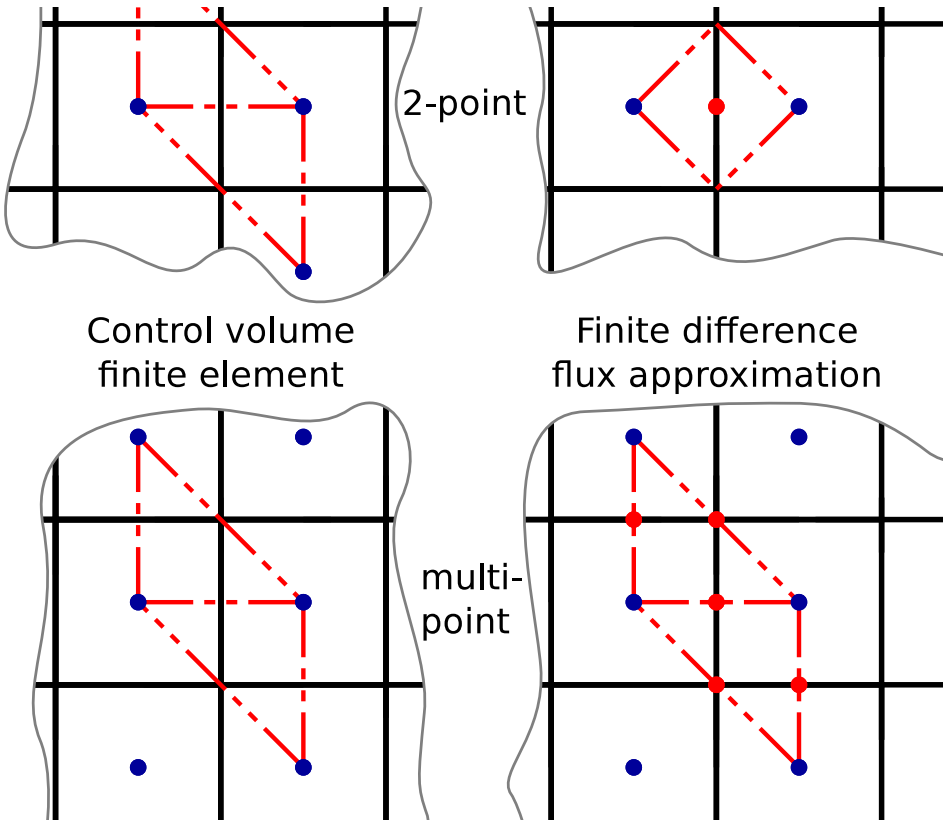


Figure 3.2: Two-point and multi point (L-method) flux approximation with highlighted interaction regions and auxiliary variable locations.

- One needs to choose a point within the volume that represents the reference location of the primary variable, which we refer to as cell center. The standard approximation for a cell center is the center of mass for the cell volume. While other choices are also possible, this choice does not influence the method description but might affect accuracy of the method.
- There exists a dual grid (specific for a given method, see Figure 3.2) that defines so-called interaction regions. The flux for the edges inside an interaction regions can be only influenced by the cells that are part of that region. Therefore the computation of fluxes can be performed locally within the region.

We emphasize that the conventions above represent our choices and are not necessary for derivations of CV methods. Discussion of CV methods that do not follow the conventions above is beyond the scope of this thesis.

The rest of the section is devoted to specific choices of defining local flux approximations that result in different CV methods.

### 3.1.1 Two-point flux approximation

The simplest control volume method approximates fluxes using two points. In this method the flux over each edge is defined only by the neighboring cells with interaction regions spanning the cell centers and the ends of the edge, see Figure 3.2. The naive

approach is to approximate the flux by the following difference approximation:

$$\vec{H}_{ij} = -\vec{e}_{i,j} \cdot \underline{\underline{A}} \vec{e}_{i,j} \frac{p_j - p_i}{\text{dist}(i, j)} \int_{\partial\beta_{ij}} ds, \quad (3.6)$$

where  $\text{dist}(i, j)$  is the distance between the cell centers and  $\vec{e}_{i,j}$  is the unit vector pointing from the center of cell  $i$  to the center of cell  $j$ .

This approach works perfectly when the edges are perpendicular to the lines connecting neighboring cell centers and the tensor coefficient does not change within the interaction region. In a more general case, when the coefficient  $\underline{\underline{A}}$  is piecewise constant within each cell but  $\underline{\underline{A}}_i \neq \underline{\underline{A}}_j$ , a more general method is required: the two-point flux approximation (TPFA). In 1D there is an analytical expression of flux for a domain with discontinuity [2]. It is desirable to preserve this invariant in the numerical scheme on the grid level for each interaction region. Similarly to the analytical approach, an auxiliary point (denoted by subscript  $ij$ ) is introduced in the middle of the edge  $\partial\beta_{ij}$  yielding a homogeneous medium in each of the cells in the interaction region. This allows to recover the exact flux expressions on each side. As required by mass conservation, the fluxes projected in the direction normal to the edge are forced to be equal on both sides of edge  $\partial\beta_{ij}$ . This can be summarized in a system of equations:

$$\vec{H}_{ij}^i = -\vec{n}_{ij} \cdot \underline{\underline{A}} \vec{e}_{i,ij} \frac{p_{ij} - p_i}{\text{dist}(i, ij)} \int_{\partial\beta_{ij}} ds, \quad (3.7)$$

$$\vec{H}_{ij}^j = -\vec{n}_{ij} \cdot \underline{\underline{A}} \vec{e}_{ij,j} \frac{p_j - p_{ij}}{\text{dist}(ij, j)} \int_{\partial\beta_{ij}} ds, \quad (3.8)$$

$$\vec{H}_{ij} = \vec{H}_{ij}^i = \vec{H}_{ij}^j, \quad (3.9)$$

where  $\vec{H}_{ij}^k$  are fluxes over edge from  $i$  to  $j$  on the side of cell  $k$ ,  $\vec{n}_{ij}$  is the unit normal to the edge and the rest of notation is naturally extended from (3.6). Equations (3.7)-(3.9) can be solved locally to eliminate the auxiliary pressure  $p_{ij}$  and to find the flux. The closed form solution for the system (3.7)-(3.9) with linear fluxes can be found in e.g. [2].

The local consistency with the analytical solution for the TPFA makes it a popular technique in reservoir simulation [62]. For this reason, we also prefer this method as a coarse-scale solver in papers A, B. However, for many problems, e.g. with anisotropic permeability tensor, TPFA fails to approximate contribution to the flux induced by the flow perpendicular to the line connecting the cells. As a result, the method gives systematic errors [3]. This further extends to multiscale methods based on TPFA principles as shown in Paper B. To achieve consistency for such general cases, multi-point flux approximation methods can be used.

### 3.1.2 Multi-point flux approximation

To approximate gradient accurately in multiple dimensions more than two points are required; the minimum number of points in 2D is three and in 3D is four. Consequently, at least the same number of control volumes is required in each interaction region to

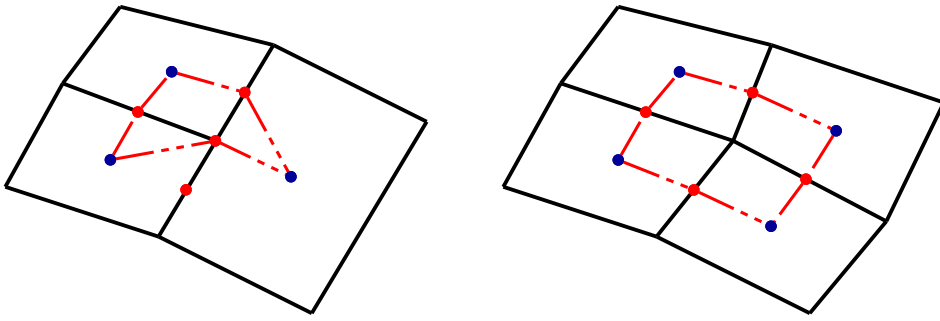


Figure 3.3: Interaction region for MPFA L-method with hanging node (left) and MPFA O-method (right).

fully define gradients and therefore provide consistent approximation of local fluxes. Multi-point flux approximation (MPFA) methods are control volume methods that use enough points to achieve this consistency.

Since for the MPFA the interaction regions involve additional nodes, it is common to subdivide the edge into two halves. This minimizes the area of influence to each half-edge and therefore improves the finite difference approximation of the gradients, see Figure 3.2 (bottom-right). Defining the shape of interaction regions and the placement of auxiliary points leads to different multi-point flux approximations. Below we present two of them. First, we present the O-method, the most common and basic MPFA. Then, we explain modifications needed to construct the L-method. The latter has a few desirable qualities which are also discussed. These qualities make an L-method-based coarse-scale solver a desirable component for the multiscale method with improved robustness, which is introduced in Paper C.

### O-method

Choosing an interaction region that goes through all cells surrounding a corner of a grid gives the O-method [4]. The method owes its name to resemblance between the shape of the region and the letter O. For the O-method, the auxiliary variables are placed in the middles of the edges. The three points per sub-cell ( $k$ ) of the interaction region allow to derive equation of the plane and therefore to define the gradient as its slope  $(\nabla p)_k$ . Substituting those approximate gradients into the expression for flux: e.g. (3.5) gives

$$\vec{H}^k = -A_{\underline{k}}(\nabla p)_k, \quad (3.10)$$

where  $\vec{H}^k$  is the flux vector in the sub-cell  $k$ . As for the case of TPFA, we want to solve the system of fluxes locally. Similarly to (3.9), we require that the fluxes normal to half edges are the same from both sides:

$$\vec{H}_{kl}^{k'} = -\vec{n}_{kl} \cdot \vec{H}^k \frac{1}{2} \int_{\partial \beta_{ij}} ds, \quad (3.11)$$

$$\vec{H}'_{kl} = \vec{H}_{kl}^{k'} = \vec{H}_{kl}^{l'}, \quad (3.12)$$

where  $\vec{H}_{kl}^{k'}$  is the flux across the half-edge between sub-cells  $k$  and  $l$ , viewed from the side of sub-cell  $k$  which should be the same as the flux across the half-edge,  $\vec{H}_{kl}'$ . Solving the system of equations (3.12) for all half-edges  $kl$  allows to eliminate the flux locally. The closed form solution for the Darcy case can be found in [5].

### L-method

The construction of the O-method does not require an auxiliary point on the intersection of half edges. As a result, the reconstructed linear solution for the pressure is guaranteed to be continuous only in the midpoints of the edges. An alternative flux approximation, the L-method, has this property [5]. It is achieved by adding a continuity points in the corners of control volumes, see Figure 3.2 (bottom-right). The interaction region for the method spans exactly three cell centers in 2D forming an L-shape and gives the method its name.

L-method is asymmetric, having two interaction regions with two auxiliary points and triangular shape, and one with three points and quadrilateral shape, see Figure 3.2 (bottom-right). Moreover, the triangular interaction regions can be rotated 90 degrees to produce another valid decomposition into interaction regions. This means that the L-method is not uniquely defined. In [5] the authors suggest a strategy of choosing the configuration of the interaction regions based on the structure of the problem, i.e. form of anisotropy of Darcy's coefficient. Following that strategy results in a method with superior monotonicity properties compared to O-methods.

Analogously to the O-method, we want to approximate the gradients in each of the sub-cells. The gradient is first approximated linearly for the quadrilateral sub-cell using the central point and the auxiliary points in the middle of the edges. This gradient is used to compute the value of the auxiliary variable on the intersection of half-edges resulting in the primary variable continuity condition. This allows us to approximate the gradients in the triangular sub-cells. This modified procedure still results in three linear functions (one for each sub-cell) defining the three gradient slopes  $(\nabla p)_k$ .

The primary variable continuity condition in the quadrilateral cell together with the two conditions of flux continuity (3.12) allows to eliminate the auxiliary variables locally and gives the fluxes across half-edges as well as piecewise linear pressure reconstruction in the interaction region. The closed form representation of the fluxes for the Darcy-type flow can be found in [4].

The L-method can be naturally extended to grids with hanging nodes by treating the hanging node as a corner of a polygon with angle of 180 degrees, as shown in Figure 3.3 (left). This allows to apply the method for a variety of challenging geometries arising on the boundaries of sub-domains.

## 3.2 Finite element methods

A generic partial differential equation (PDE) in divergence (strong) form can be written as

$$\mathcal{L}u(x) = f(x), \quad \forall x \in \Omega \quad (3.13)$$

where  $\mathcal{L}$  is some differential operator,  $u$  is an unknown function defined in  $\Omega$ . The variational (weak) formulation for equation (3.13) reads: find  $u$ , such that

$$\int_{\Omega} [\mathcal{L}u(x)]\varphi(x)dx = \int_{\Omega} f(x)\varphi(x)dx \quad (3.14)$$

for all infinitely differentiable test functions in the domain  $\Omega$ . For brevity we omit the discussion of boundary conditions and Sobolev spaces required for full understanding of finite element theory and refer to [23] and [12], respectively.

For many practical applications it is possible to formulate a variational problem that admits a larger set of solutions than the problem in the divergence form. When a function  $u$  has insufficient continuity for the differential operator  $\mathcal{L}u$  to be well defined, that function can still be a weak solution to a slightly modified variational formulation. Integrating the right-hand side of (3.14) by parts allows moving the derivative to the smooth test function and therefore weakens the continuity required of the solution. For instance, for Darcy's flow (2.20) the weak form would look like

$$\int_{\Omega} (\underline{\underline{A}}_D \nabla p_D) \cdot \nabla \varphi dx - \int_{\partial\Omega} (\underline{\underline{A}}_D \nabla p_D) \varphi \cdot \vec{n} ds = \int_{\Omega} \frac{f_D}{\rho} \varphi dx \quad (3.15)$$

where is the boundary term that would normally vanish or contribute to the right hand side, depending on boundary conditions. Therefore it is common to study a simpler equation

$$\int_{\Omega} (\underline{\underline{A}}_D \nabla p_D) \cdot \nabla \varphi dx = \int_{\Omega} \frac{f_D}{\rho} \varphi dx \quad (3.16)$$

The finite element method is a discrete representation of the weak formulation of the equations being solved. The method can be obtained from (3.14) by replacing the original functional spaces where the solution  $u$  and the test functions  $\varphi$  are defined by the corresponding discrete analogues. For a given triangulation over the domain one defines a finite set of basis functions which honor two rules:

- The basis functions have local support and are normally infinitely smooth within each triangle (element).
- They satisfy the properties of the original solution space (e.g. continuity).

The basis functions for the solution space ( $\psi_i$ ) and the test function space ( $\varphi_j$ ) do not necessarily coincide. Since the solution and the test function spaces are finite, it is possible to reformulate the PDE (3.14) as a system of algebraic equations using the fact that any test function in the new discrete space can be represented in terms of the basis:

$$\int_{\Omega} [\mathcal{L} \sum \psi_i u_i] \varphi_j dx = \int_{\Omega} f \varphi_j dx, \quad \forall j, \quad (3.17)$$

where  $\sum \psi_i u_i$  is a decomposition of solution into basis functions. Note that due to local support of  $\psi_i$  and  $\varphi_j$ , the integrals in (3.17) are non-zero only over few elements and the integration can be restricted to those elements.

More details on the finite element theory can be found in [23, 63]. In the rest of the section we discuss the finite element methods that were used in this work.

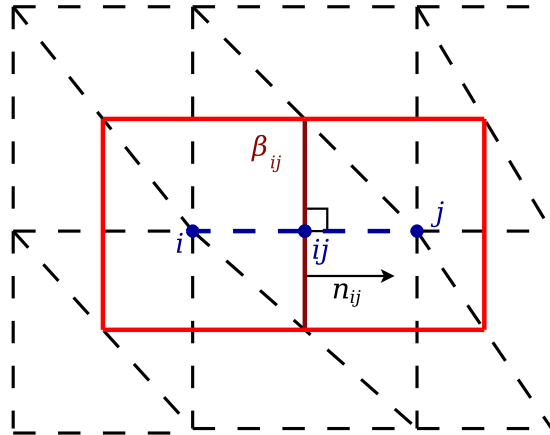


Figure 3.4: The structure of finite element grid (dashed lines) and the finite volume grid dual to it obtained as its Voronoi diagram (solid lines). Adapted from Paper B.

### 3.2.1 Finite volume element method

Finite volume element method (FVEM) [28], (also called control volume finite element method [Paper B]) is a non-standard variation of a finite element method for equations of form (3.16). It can be formally obtained by choosing the test function to be an indicator step function on each element of the finite volume grid, defined as:

$$\varphi_j(x) = \begin{cases} 1, & x \in \beta_j \\ 0, & x \notin \beta_j \end{cases}, \quad (3.18)$$

where  $\beta_j$  is the  $j$ -th element in the discretization. The function given by (3.18) is not differentiable on the boundary of triangles. Nevertheless, one can formally replace the integral over the element with the integral over the boundary of each element yielding the equation

$$\int_{\partial\beta_j} (\underline{\underline{A}}_D \nabla p_D) \cdot \vec{n} ds = \int_{\beta_j} 1 \frac{f_D}{\rho} dx. \quad (3.19)$$

The function space for the pressure  $p_D$  is chosen to be continuous functions that are piecewise linear on each triangle. The basis functions  $\psi_j$  are chosen so that for each vertex in the grid  $x_i$  the basis function is defined:

$$\psi_j(x_i) = \delta_{ij}, \quad (3.20)$$

where  $\delta_{ij}$  is the Kronecker delta. The basis functions are linearly extended to the interior of triangles. This type of element space is called Lagrange elements of order one [23].

We immediately see that the formulation (3.19) relates closely to the control volume formulation introduced in Section 3.1, hence the name of the method. The advantage of finite element formulation for a control volume method is the ability to utilize the mathematical toolkit available for finite element methods for analysis purposes, see e.g. [28, 51, 88].

To highlight the differences between FVEM and CV methods we recall the definition of the Darcy's flux introduced in (3.5) to rewrite the finite volume element method

in the form:

$$\sum_{\partial\beta_{jk}} \int \vec{H} \cdot \vec{n} ds = \int_{\beta_j} \frac{f_D}{\rho} dx. \quad (3.21)$$

While formulation (3.21) looks very similar to the control volume formulation (3.1) (omitting the time dependent term), the difference is how the flux approximation is performed.

- In control volume methods the fluxes are approximated through the computations on the dual grid composed of interaction regions.
- In FVEM the fluxes are approximated on the elements themselves and the continuity of fluxes is ensured over boundaries of the elements.

For the regular triangulation of a rectangular domain one can define interaction regions of the CV method to coincide with the triangulation of FVEM. This happens when the control volume grid is constructed as Voronoi diagram (see e.g. [2]) of a set of points where the primary variables are defined, see Figure 3.4. Following this duality, Figure 3.2 provides comparison of treating fluxes in FVEM and CV methods. Paper B uses this duality to extend the proofs for convergence properties of FVEM to a larger class of control volume methods.

### 3.2.2 Taylor-Hood elements

For discretization of the free flow considered on the pore-scale of a porous medium (see section 2.4.2) in papers A, B, C we used a finite element method. Multiplication of equations (2.31) by test functions and subsequent integration by parts results in the weak form of the steady Navier-Stokes equations

$$\int_{\Omega} (\nabla \cdot \vec{u}_f \varphi_p) dx = 0, \quad (3.22)$$

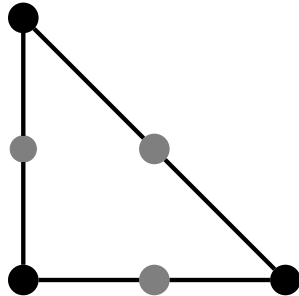
$$\int_{\Omega} (\rho (\vec{u}_f \cdot \nabla \vec{u}_f) \cdot \varphi_{\vec{u}} - p_f \nabla \cdot \varphi_{\vec{u}} + \mu \nabla \vec{u}_f : \nabla \varphi_{\vec{u}}) dx = \int_{\Omega} (\vec{s}_f \cdot \varphi_{\vec{u}}) dx, \quad (3.23)$$

where  $\varphi_p$  and  $\varphi_{\vec{u}}$  are test functions associated to pressure and velocity respectively and ":" represents Frobenius inner product of second order tensors. Since in (3.22) and (3.23) the test functions for velocity and pressure are independent of each other they can be summed up without loss of generality to form the single equation:

$$\int_{\Omega} (\nabla \cdot \vec{u}_f \varphi_p + \rho (\vec{u}_f \cdot \nabla \vec{u}_f) \cdot \varphi_{\vec{u}} - p_f \nabla \cdot \varphi_{\vec{u}} + \mu \nabla \vec{u}_f : \nabla \varphi_{\vec{u}}) dx = \int_{\Omega} (\vec{s}_f \cdot \varphi_{\vec{u}}) dx, \quad (3.24)$$

which is one of the standard weak formulations of the steady-state Navier-Stokes equations.

To complete the formulation of the finite element method for equation (3.24) we need to choose finite element spaces for the solution and the test function for both pressure and temperature component. For the problem to be solvable, compatible finite



- Node for elements of order 1 and 2
- Node for elements of order 2

Figure 3.5: Position of the nodes for Lagrange finite elements.

element spaces are required. The Taylor-Hood elements is a standard, stable functional space pair for the Stokes equations [39, 63]. The space is composed of Lagrange elements: second-order piecewise polynomials for each dimension of velocity and first-order polynomials for pressure. The same type of functions is used for both the solution and the test-function spaces. Lagrange elements of the first order were already defined in (3.20). Lagrange finite elements of second order use additional node values in the midpoints of the sides of triangles in the grid, see Figure 3.5. The basis functions are than defined similarly for all the nodes:

$$\psi_j(x_i) = \delta_{ij}. \quad (3.25)$$

Additional degrees of freedom per triangle define the unique second order polynomial within each triangle of the grid resulting in a piecewise quadratic finite element space.

# Chapter 4

## Approaches to multiscale problems

Every kind of science, if it has only reached a certain degree of maturity, automatically becomes a part of mathematics.

---

David Hilbert (translated [40])

There is a great variety of different multiscale systems in nature, and Section 2.4 just demonstrates a few examples. It is not possible to construct a single multiscale method that solves all of them. At the same time a classification of multiscale problems by their typical characteristics enables reusing approaches that have been developed for similar problems.

In this chapter we present two ways to classify the multiscale methods. First, in Section 4.1 we distinguish two fundamentally different approaches to multiscale systems that are focused on analytical (continuous) and numerical (discrete) formulations respectively. After that, Section 4.2 presents a flowchart which classifies multiscale problems based on the requirements on the solution and degree of scale separation. We argue that all the methods that cope with problems in any particular class would share very similar structure despite having different naming conventions of their components. Therefore, we extend the classification of problems to the corresponding methods. Section 4.2 also serves to position the developments of this work in the field of multiscale methods.

The rest of the chapter is devoted to a detailed description of specific multiscale techniques. We focus on those used in the attached papers: homogenization, heterogeneous multiscale methods and self-similarity analysis.

### 4.1 Relation between analytical and numerical approaches

Since there are many examples of multiscale problems in nature, scientists were confronted with solving them even before computational techniques and resources were available. One can distinguish between two approaches to multiscale systems: semi-analytical and numerical. We will refer to those approaches as multiscale modeling and

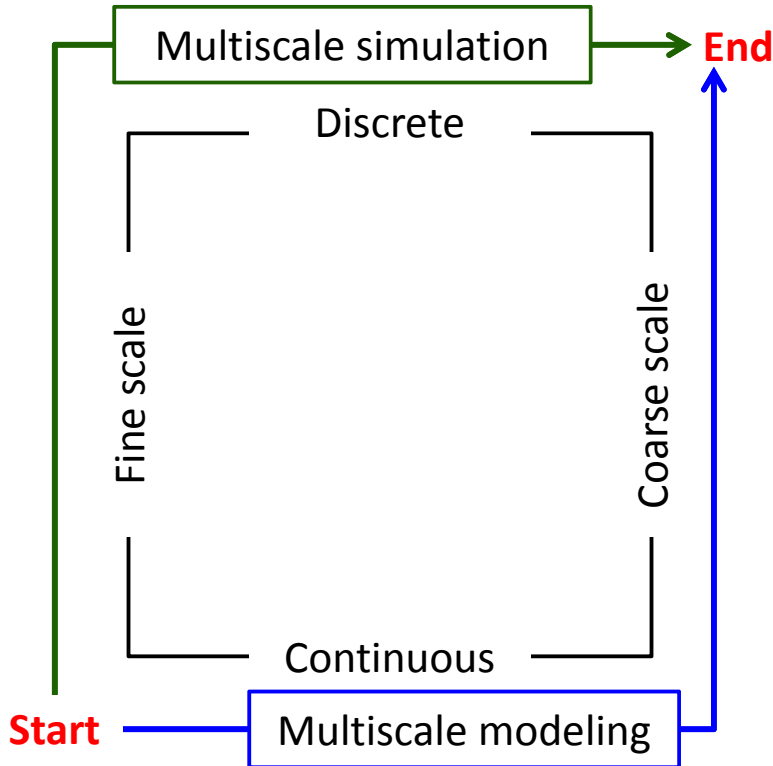


Figure 4.1: Two conceptual approaches to multiscale problems.

multiscale simulation, respectively<sup>1</sup>.

The approaches can be pictured as paths along the square, see Figure 4.1. Horizontal axis along the square is the scale: fine or coarse. The vertical axis is the type of the problem formulation: continuous or discrete. The purpose of any model is to provide relevant predictions. For multiscale methods these are values associated with coarse-scale of the problem that honor the behavior of the fine scale. Therefore, all multiscale approaches start with an original (continuous) fine-scale problem and aim at giving a solution (discrete set of values) on the coarse scale, see Figure 4.1.

A more classical approach, multiscale modeling, is to perform upscaling from the fine to the coarse scale in a continuous setting, i.e., analytically. Ultimately, the closed coarse-scale problem would be treated by either analytical or numerical techniques to give the desired answer. An example of such an approach is homogenization presented in Section 4.3.

In contrast to that, in multiscale simulation one introduces a discrete representation of both fine and coarse scales and constructs an algorithm that solves this combined system. Heterogeneous multiscale methods, presented in Section 4.4, form a framework that tries to generalize multiscale simulation approaches.

In many problems the closed form representation on a single scale cannot be found (bottom-right corner of Figure 4.1) and therefore the multiscale modeling techniques are not applicable. The need to address those problems motivates development of multiscale simulation techniques, also called multiscale methods. At the same time, mul-

<sup>1</sup>Distinguishing multiscale modeling and multiscale simulation in this way is not conventional naming. Even though in this thesis we find it convenient to introduce this separation, in other sources (e.g. [32]) both are referred to as multiscale modeling.

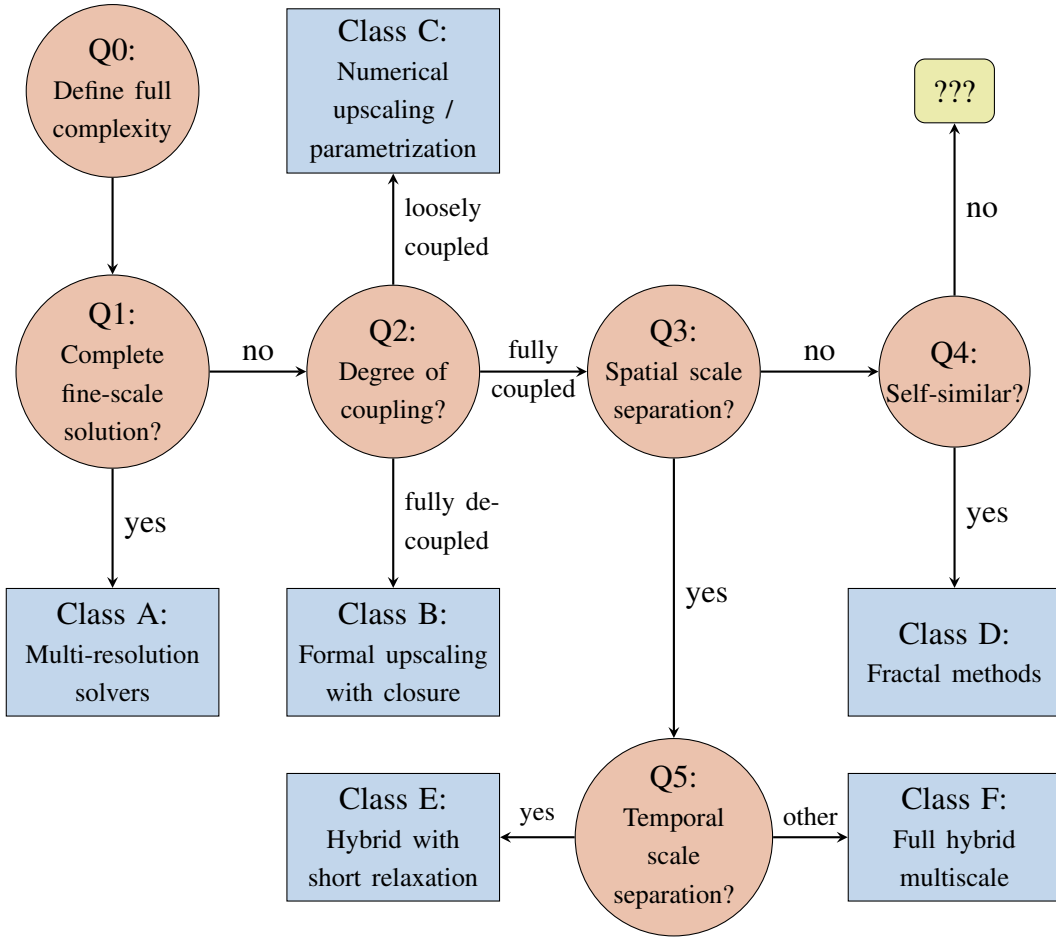


Figure 4.2: Flowchart for determining the class of a multiscale method.

tiscale modeling remains a reliable benchmark for the multiscale simulations where closed-form representation exists on the coarse scale.

## 4.2 Classes of multiscale methods

The aim of this section is to introduce a classification of the multiscale methods depending on their applicability to multiscale problems with different characteristics. The classification follows a flowchart inspired by [74]. Figure 4.2 presents the flowchart for the multiscale problem classification that is central to this section. Answers to the questions Q0-Q5 create a path along the flowchart. The terminal nodes in Figure 4.2 (denoted Class A - Class F) are classes of problems and corresponding methods. Each of them would be discussed in a separate subsection below.

Figure 4.2 and consequently this section are structured to relate the developments of this work to the field of multiscale methods. To maintain the focus it condenses all spatio-temporal multiscale methods (which are outside our scope) into meta-Class F. We refer to [24, 32, 34, 43, 54, 74] for a further review of multiscale methods.

First, one needs to decide about the hypothetically best possible fine-scale solution of the considered problem Q0. For example, we consider the problem of non-linear flow in porous media (see Section 2.4.2). It takes into account pore scale effects based on the Navier-Stokes equations on pore geometry. Therefore, the best possible solution

is resolving all the porous structures of the pore-scale with a Navier-Stokes solver.

#### 4.2.1 Class A: Multiresolution solvers

Having chosen the best possible solution we advance along the flowchart to the first classifying question. Q1 reads: is the complete fine-scale solution desirable? When that is the case, a method uses the coarse scale to help solve the full fine-scale problem. Among examples from Section 2.4, such method would be applicable to reservoir-scale flows in porous media discussed in Section 2.4.1.

This type of methods provides an efficient way to solve a fine-scale problem using the multiscale structure of the problem and are therefore classified as multiresolution solvers: Class A. Multi-level domain decomposition: linear [76] and non-linear [27, 75], and multigrid [25] are examples of methods in this class that are older than the term "multiscale methods". Both of these methods were developed as solvers to large single-scale problems but, later, became a basis for newer multiscale techniques.

Additionally to classical solvers, Class A contains methods that use decomposition of finite element spaces into coarse and fine. This idea was implemented in variational multiscale methods [13, 49, 57] and multiscale finite element methods [36, 37, 48]. The groups of methods are very similar apart from different naming. The decomposition allows for a rough accelerated solution of the coarse-scale problem fulfilling the purpose of a multiscale method. At the same time, the methods provide a possibility to reconstruct the full fine scale and therefore belong to the class of multiresolution solvers. Following the finite-element-based techniques, multiscale extensions to other classes of numerical methods were created that served the same purpose. They include multiscale mixed finite-element method [52], multiscale finite volume method [64], numerical sub-grid upscaling method [14], and more (see [15, 54] for a review and comparison). Currently, the state-of-the-art methods from this category make their way to the industrial applications in e.g. reservoir simulation [61].

#### 4.2.2 Class B: Formal upscaling with closure

In many cases when we are confronted with a multiscale problem it is not viable to obtain full fine-scale solutions. In these situations, in addition to answering Q0, one should explicitly formulate some sort of a coarse-scale problem, which would be incomplete without the fine scale information. At this point, the methods should be further classified depending on the degree of coupling between the fine and the coarse scales (Q2).

In the simplest case, the fine and the coarse scales are essentially decoupled. This leads to Class B: formal upscaling with closure. This is, arguably, the only class that can be fully solved by both multiscale modeling and multiscale simulation.

A well-known example of such upscaling is Darcy's law that was initially obtained from experiments [22]. Later, Tartar rigorously derived the law by homogenization of Stokes equations on the pore scale [47]. The homogenization is therefore a multiscale modeling paradigm that allows to decouple the fine and the coarse scale. Using it, one can compute the data (such as Darcy's permeability) needed for closure of the coarse scale problem as an offline step of the main multiscale method. Further discussion of homogenization techniques is presented in Section 4.3 (see also [47, 68] for a review).

Note that the homogenization is not the only way to perform upscaling for multiscale problems of Class B. For other methods related to flows in porous media, see [67, 74] and references therein.

Multiscale simulation where both scales are considered simultaneously is also applicable to Class B, but is not required. In Paper B we emphasize that Class B problems, where multiscale modeling is available, are essential for analysis and verification of multiscale simulation techniques.

### 4.2.3 Class C: Numerical upscaling using parametrization

For more challenging problems it is not possible to find a closed-form upscaling to the coarse scale. Let us look back to the example of flow in porous media on the Darcy scale (Section 2.4.2). When the flow on the pore scale exhibits non-linear behavior, the concept of permeability fails. The relationship between the pressure drop and the flux becomes dependent on the flow rate and direction and therefore truly multiscale numerical methods should be developed to address the problem. At the same time, for this and many other problems, the coupling (Q2) is weak and it is possible to parametrize the effect of the fine-scale model on the coarse scale by a function of few coarse scale variables. This gives rise to numerical upscaling, Class C.

E and Engquist [33] proposed a unified multiscale simulation framework for handling multiscale problems that cannot be solved by upscaling: heterogeneous multiscale methods (HMM). This class of methods loosely follows homogenization principles and uses interpolation between solutions on local fine-scale patches distributed throughout the coarse domain to find the full coarse-scale solution. It can supplement the multiscale modeling for Class C, but can be also used to handle more complex problems from classes E and F. However, for HMM methods of classes B and C, Abdulle has developed an analysis framework [8] allowing to study convergence of the coarse-scale solution. The framework was used in Paper B for proving convergence of the method. Further discussion of the HMM can be found in Section 4.4 and in [7, 32].

Papers A, B, C consider a Class C problem of non-linear steady-state flow in porous media (Section 2.4.2). The method follows the HMM principles. While the problem does not allow for closed form upscaling of permeability, the on-demand computation allows to construct an interpolation table for local pressure-dependent flow rate. This interpolation table can be later reused as a source of offline information for parametrization of the fine scale responses. The detailed discussion of the method can be found in Section 4.4 and Section 5.1. Other noteworthy developments considering sub-Darcy-scale of Class C are [9, 10, 29].

Paper E also presents a semi-analytical solver for the problem of particle interaction under the influence of capillary bridging (see Section 2.4.4). The semi-analytical solutions derived in the paper can be used to simulate an upscaled response of the small fine-scale particles on the coarse-scale flow [18, 19]. The approach therefore represents another example of Class C.

The examples above only cover a few particular examples of Class C methods. It is impossible to cover the full diversity of problems and corresponding methods in this subsection. Some examples of methods can be found in [7, 74].

#### 4.2.4 Class D: Fractal methods

In the case when the degree of coupling between scales is sufficient, we need to move along the flowchart to question Q3: the presence of spatial scale separation. Note that all methods considered up to this point assume spatial scale separation, since it is a necessary condition to decouple a multiscale system.

When scale separation is insufficient, obtaining the solution becomes tricky. In the absence of scale separation one may look for self-similarity of the solution to a problem (Q4).

When self-similarities exist we end up with fractal-type methods (Class D). This class of problems has been recognized in the multiscale modeling community quite recently [74]. More classical studies of power-law-type self-similar solutions can be found in [20, 65]. Inspired by the self-similarity analysis, in Paper D we develop methods that predict early ice formation in brine. The paper shows that ice can be formed both as a continuous front and a fractal structure. The methodology and results are summarized in Section 5.2.

The fractal methods require formulating and solving eigenvalue problems analytically and are therefore not applicable to arbitrary models. Therefore, there is an empty node in Figure 4.2 when the answer to Q4 is "no".

#### 4.2.5 Class E: Hybrid method with short relaxation time on the fine scale

Following somewhat non-standard Class D we return to problems with spatial scale separation, where the answer to Q3 is "yes" (see Figure 4.2). The sufficient degree of coupling that is carried over from the answer to Q2 means that the considered problems have some dynamics in time that cannot be upscaled. Impossibility to perform upscaling means that hierarchical hybrid methods need to be applied to problems below. Hybrid refers to necessary algorithmic coupling of fine and coarse scales and continuous interaction between the two [74]. We also describe the class of such methods as true multiscale simulation (see Section 4.1). This leads us to asking the question about temporal scale separation (Q5).

Short relaxation time on the fine scale implies temporal scale separation. Problems with this property constitute Class E. In Paper A we considered a sub-class of these methods: temporal multiscale with full decoupling in terms of time. There, the model problem is compressible non-linear single phase flow, see Section 2.4.2. However, we assume that relaxation time on the fine scale locally is sufficiently small. This allows us to solve local Navier-Stokes problems independent of time with a given density. However, since density is dynamic on the coarse scale, parametrization of the fine scale cannot be easily obtained, and the problem belongs to Class E.

#### 4.2.6 Class F: Brief overview of space-time hybrid multiscale methods

Methods that include non-trivial time-dependent effects and require continuous interaction between the fine and the coarse scales were not the focus of this work. Therefore we summarize all the problems and corresponding methods where temporal multiscale treatment is required in meta-Class F. This meta-class is further subdivided and discussed in [74].

Even though there exists a lot of variations of multiscale methods that are dependent upon availability of information about the coarse-scale solution, the general approach is similar to HMM [32]. To solve such systems, the algorithm would go back and forth between the scales compressing the information from the coarse to the fine scale, solving locally, and then reconstructing and extrapolating fine-scale data. Depending on the particular implementation of compression and reconstruction, one can end up with different multiscale methods [74]: hierarchical hybrid with time bursts, time-parallel hierarchical hybrid, hierarchical hybrid (gap tooth), concurrent hybrid.

### 4.3 Homogenization

Homogenization is a multiscale modeling technique (see Figure 4.1) that constitutes a large topic in the analysis of multiscale systems. While homogenization is not a method for multiscale simulation it is extensively used for design of many multiscale methods presented in Figure 4.2. These methods are central to this thesis. The goal of this section is to demonstrate how to use the mathematical abstraction of homogenization to formally derive physical properties of multiscale systems, such as permeability. We give a brief overview of techniques used for homogenization and references to more rigorous proofs.

Homogenization addresses two-scale problems: the class of differential equations where the scale separation is introduced explicitly by assuming that the spatial coordinate has a fast varying component

$$y = \frac{x}{\varepsilon}, \quad (4.1)$$

that also acts in space but is independent of  $x$ . While the framework is applicable to a large range of problems where  $\varepsilon$  is small, the mathematical analysis is conducted for the limiting case  $\varepsilon \rightarrow 0$ .

A function  $u^\varepsilon$  that depends on a single spatial variable is replaced by a so-called multiscale expansion of functions  $u_i$ , which are dependent on both the coarse variable  $x$  and the fine variable  $y$ :

$$u^\varepsilon(x^\varepsilon) = u(x, y) = \sum_{i=0}^{\infty} \varepsilon^i u_i(x, y), \quad (4.2)$$

where  $u_i$  are one-periodic with respect to  $y$ . The periodicity requirement on the fine-scale variable means that the coarse-scale effects can be efficiently averaged by integrating the function over the period of  $y$  that forms a unit torus  $Y$  at each point of the coarse domain when  $\varepsilon \rightarrow 0$ . To distinguish the original variable from the newly introduced coarse variable we use the superscript notation  $x^\varepsilon$ . Substituting (4.1) one can formally use the chain rule for multiple variables for a spatial derivative

$$\frac{du^\varepsilon(x^\varepsilon)}{dx^\varepsilon} = \frac{du\left(x^\varepsilon, \frac{x^\varepsilon}{\varepsilon}\right)}{dx^\varepsilon} = \frac{\partial}{\partial x} u(x, y) + \frac{1}{\varepsilon} \frac{\partial}{\partial y} u(x, y), \quad (4.3)$$

where  $d/dx^\varepsilon$  is a multiscale derivative that for the case of one variable operates similarly to full derivative. For a multivariate case to distinguish between full, multiscale

and partial derivatives we introduce indexes to the nabla operator as follows:

$$\nabla = \nabla_x + \frac{1}{\varepsilon} \nabla_y. \quad (4.4)$$

In the rest of the section we demonstrate homogenization techniques on two examples that address flows in porous media on different scales.

### 4.3.1 Homogenization for heterogeneous media

The first example of a multiscale problem is an elliptic equation with a multiscale parameter that arises from Darcy's law with heterogeneous permeability (see Section 2.4.1):

$$\nabla \cdot (a^\varepsilon \nabla u^\varepsilon) = f, \quad (4.5)$$

where  $a^\varepsilon(x^\varepsilon) = a(y) = a\left(\frac{x^\varepsilon}{\varepsilon}\right)$ . To solve the multiscale problem (4.5) we rewrite the equation using the multiscale expansion for the solution (4.2) and the two-scale representation of the derivative (4.4). Grouping the terms with associated powers of epsilon gives:

$$0 = \varepsilon^{-2} [\nabla_y \cdot (a \nabla_y u_0)] \quad (4.6)$$

$$+ \varepsilon^{-1} [\nabla_y \cdot (a \nabla_y u_1) + \nabla_y \cdot (a \nabla_x u_0) + \nabla_x \cdot (a \nabla_y u_0)] \quad (4.7)$$

$$+ \varepsilon^0 [\nabla_y \cdot (a \nabla_y u_2 + a \nabla_x u_1) + \nabla_x \cdot (a \nabla_y u_1) + \nabla_x \cdot (a \nabla_x u_0) + f] \quad (4.8)$$

+ ...

The powers of  $\varepsilon$  are independent functions. Therefore, for the equation (4.6) to hold as  $\varepsilon \rightarrow 0$ , all lines (4.6)-(4.8) that are significant (have non-positive power of  $\varepsilon$ ) should be equal to zero. This means that the corresponding brackets should be exactly zero.

It is of interest to consider the pattern of equations arising when solving equations one after another going from lower powers of  $\varepsilon$ :

$\varepsilon^{-2}$ : Equality of the  $y$ -derivative of  $u_0$  to zero implies that it is independent of the fine variable  $y$ :

$$u_0(x, y) = u_0(x). \quad (4.9)$$

$\varepsilon^{-1}$ : Equation (4.9) implies that  $\nabla_x \cdot (a(y) \nabla_y u_0(x)) = 0$  and (4.7) can be rewritten:

$$\nabla_y \cdot (a(y) \nabla_y u_1(x, y)) = -\nabla_y \cdot (a(y) \nabla_x u_0(x)). \quad (4.10)$$

It is convenient to rewrite this equation in the weak form

$$\int_Y (a(y) [\nabla_y u_1(x, y) + \nabla_x u_0(x)]) \cdot \nabla \varphi dy = 0, \quad (4.11)$$

which should hold for any test function  $\varphi$  that is one-periodic with respect to  $y$ . The equation (4.11) defines a so-called cell problem - a problem that is solved locally on the periodic cell. The equation can be solved with respect to  $u_1$  up to a constant  $C(x)$  by separation of variables:

$$u_1(x, y) = \vec{\chi}(y) \cdot \nabla_x u_0(x). \quad (4.12)$$

For the considered case substitution of (4.12) into (4.11) results in a system of two cell problems that are decoupled from the rest of the system

$$\int_Y (a(y)[\nabla_y \vec{\chi}_i(y) + \vec{e}_i]) \cdot \nabla \varphi dy = 0, \quad (4.13)$$

where  $\vec{e}_i$  is a unit vector.

$\varepsilon^0$ : Instead of solving the equation (4.8), we integrate it over the fine-scale unit torus  $\int_Y dy$ . The  $y$ -divergence term vanishes due to periodicity while the other two given (4.11) and (4.12) become:

$$\nabla_x \cdot \left[ \int_Y a(y) (\nabla_y \otimes \vec{\chi} + \underline{\underline{I}}) dy \right] \nabla_x u_0(x) + f(x) \int_Y dy = 0, \quad (4.14)$$

where  $\underline{\underline{I}}$  is the unit matrix and  $\otimes$  denotes outer product. Equation (4.14) is essentially a closure of the upscaling procedure and

$$\underline{\underline{A}} = \int_Y a(y) (\nabla_y \otimes \vec{\chi} + \underline{\underline{I}}) dy \quad (4.15)$$

is the up-scaled coefficient. It is interesting to observe that the last equation means that even scalar  $a$  can result in a tensorial coefficient when up-scaled, sometimes causing additional challenges for coarse-scale solvers.

The steps above can be summarized into a closed form upscaling (Class B) of the multiscale problem [47, 68]:

**Proposition 1** *The two-scale problem (4.5) is equivalent to the following elliptic equation*

$$-\nabla \cdot (\underline{\underline{A}} \nabla u) = f, \quad (4.16)$$

where the matrix  $\underline{\underline{A}}$  relates to the multiscale problem:

$$\underline{\underline{A}}_{ij} = \int_Y a(y) (\delta_{ij} + \frac{\partial}{\partial y_i} \vec{\chi}(y)) dy, \quad (4.17)$$

where  $\delta_{ij}$  is the Kronecker delta and each  $\vec{\chi}$  is the solution to a cell problem that can be expressed in the weak form

$$(a(\nabla \vec{\chi} + \vec{e}_j), \nabla \varphi_j) = 0, \quad (4.18)$$

for all 1-periodic test functions  $\varphi_j$ ; where  $\vec{e}_j$  is a unit vector in  $j$  direction.

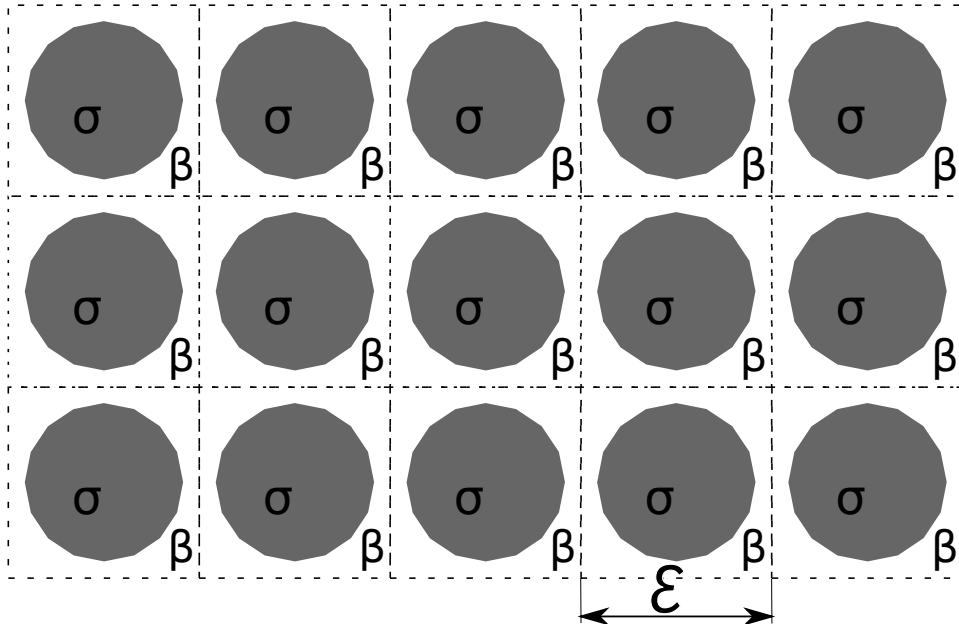


Figure 4.3: A domain consisting of repeated periodic structure of grains. Adapted from Paper B.

### 4.3.2 Summary of homogenization derivation of Darcy's law

If we consider an example of flow in porous media on an even finer scale, we would arrive at Navier-Stokes-type flow between individual grains, see Section 2.4.2. Similarly to the previous example we assume that the fine scale is periodic. An example of a periodic domain is given in Figure 4.3, where  $\beta$  corresponds to the subdomain occupied with fluid, while  $\sigma$  is the solid-matrix part. We assume that the flow is governed by steady-state Navier-Stokes equations (2.31) with no-flow boundary conditions on the contact with solid:

$$\begin{cases} \varepsilon \nabla \cdot \vec{u}^\varepsilon = 0, & \text{in } \beta, \\ \varepsilon^\gamma \rho \vec{u}^\varepsilon \cdot \nabla \vec{u}^\varepsilon + \nabla p^\varepsilon - \varepsilon^2 \mu \Delta \vec{u}^\varepsilon = 0, & \text{in } \beta, \\ \vec{u}^\varepsilon = 0, & \text{in } \sigma, \end{cases} \quad (4.19)$$

where the original variables are replaced with multi-scale variables with superscript  $\varepsilon$ . Note, that some terms in (4.19) have been scaled with  $\varepsilon$  to represent rescaling of the variables compared to the Darcy's scale.

Taking  $\gamma \geq 2$  in (4.19) is a choice that is physically correct for most flow regimes observed in porous media. In the derivations below we only consider this choice to simplify the homogenization procedure. Following the same homogenization procedure as in the previous subsection, we rewrite the equations (4.19) using a multiscale expansion. The momentum equation yields

$$0 = \varepsilon^{-1} [\nabla_y p_0] \quad (4.20)$$

$$+ \varepsilon^0 [\nabla_y p_1 + \nabla_x p_0 - \mu \Delta_y \vec{u}_0] \quad (4.21)$$

$$+ \varepsilon^1 [...].$$

The continuity equation results in

$$0 = \varepsilon^0 [\nabla_y \cdot \vec{u}_0] \quad (4.22)$$

$$\begin{aligned} &+ \varepsilon^1 [\nabla_y \cdot \vec{u}_1 + \nabla_x \cdot \vec{u}_0] \\ &+ \varepsilon^2 [...]. \end{aligned} \quad (4.23)$$

We follow the steps similar to the example in the previous subsection:

$\varepsilon^{-1}$ : From equation (4.20) we deduce that the pressure  $p_0$  is independent of the fine-scale variable:

$$p_0(x, y) = p_0(x) \quad (4.24)$$

$\varepsilon^0$ : Equations (4.21) and (4.22) yield a cell problem that resembles the original equation but is solved on a unit cell:

$$\begin{aligned} \nabla_y \cdot \vec{u}_0(x, y) &= 0, && \text{in } \beta, \\ \nabla_y p_1(x, y) - \mu \Delta_y \vec{u}_0(x, y) &= -\nabla_x p_0(x), && \text{in } \beta, \\ \vec{u}_0(x, y) &= 0, && \text{in } \sigma. \end{aligned} \quad (4.25)$$

As in the previous example the cell problem solution is linear in the coarse pressure gradient  $\nabla_x p_0$  and can therefore be rewritten as:

$$\vec{u}_0(x, y) = \underline{\underline{\chi}}(y) \nabla_x p_0(x), \quad (4.26)$$

where  $\underline{\underline{\chi}}(y)$  is a matrix-valued function.

$\varepsilon^1$ : Finally, we integrate (4.23) over the unit cell to average out fine-scale effects:

$$0 = \int_Y \nabla_y \cdot \vec{u}_1 + \nabla_x \cdot \vec{u}_0 dy \quad (4.27)$$

$$= \int_Y \nabla_y \cdot \vec{u}_1 dy + \nabla_x \cdot \int_Y \vec{u}_0 dy = I + II. \quad (4.28)$$

After applying the divergence theorem, the integral  $I$  vanishes due to the boundary conditions: periodicity on the outer boundary and zero flow on the inner boundary. The remaining term  $II$  represents a continuity equation for the coarse-scale velocity. Notice that unlike the previous example, the coarse-scale velocity is different from  $\vec{u}_0$ . It is actually equal to  $\vec{u}_c$ , that is the average of the velocity in the unit cell  $\vec{u}_c = \int_Y \vec{u}_0 dy$ .

This steps can be summarized into a Darcy's law described in section 2.4.1 [47]:

**Proposition 2** *For  $\gamma > 1$ , the two-scale problem (4.19) is equivalent to Darcy's law:*

$$\vec{u}_c = -\frac{\underline{\underline{K}}_c}{\mu} \nabla p, \quad (4.29)$$

$$\nabla \cdot \vec{u}_c = 0, \quad (4.30)$$



Figure 4.4: Schematics of the HMM.

where  $\vec{u}_c$  is the velocity averaged over the unit cell, and permeability  $\underline{\underline{K}}_c$  is defined by

$$\frac{\underline{\underline{K}}_c}{\mu} = \int_Y \underline{\underline{\chi}}(y) dy, \quad (4.31)$$

where  $\underline{\underline{\chi}}$  is the auxiliary matrix valued function defined by (4.26). The closed form solution for  $\underline{\underline{\chi}}(y)$  can be found by substituting (4.26) into the cell problem (4.25).

## 4.4 Heterogenous multiscale methods

Heterogeneous multiscale methods (HMM) were introduced in [33] as a generic framework for multiscale simulations (see Figure 4.1) where resolving the full fine scale is not viable.

In comparison to more traditional multiscale methods [13, 48, 49, 54], it allows to solve problems where both equations and grids are completely different between the scales. In this section we will loosely follow the description of HMM presented in [32].

As mentioned before, HMM is most useful for problems where one is interested in computing the coarse-scale solution without having a closed-form coarse-scale model. Instead, the fine-scale model (with corresponding fine-scale variables  $u_f$ ) is available and can be formally written as

$$F_f(u_f, D_f) = 0, \quad (4.32)$$

where  $D_f$  is data needed for the set-up of a fine-scale problem. Even though the coarse-scale problem may not be explicitly known, it is assumed to exist and have a well-defined parametrization, i.e. coarse variables  $u_c$ . Then, the coarse-scale problem can be written in general form:

$$F_c(u_c, D_c) = 0, \quad (4.33)$$

where  $D_c$  is the unknown data needed for the closure of the coarse-scale model. The complete method attempts to solve the coarse-scale problem while reconstructing parts of it as necessary by performing local fine-scale computations on cell problems.

The scheme of an HMM method is presented in Figure 4.4. The basic building blocks of the multiscale method are as follows.

1. A macroscopic solver that is based on available information. It assumes some form of the macro-scale model and a parametrization, see (4.33).
2. A procedure for estimating the missing information  $D_c$  needed for the closure of the macro-scale problem. It can be split into three sub-steps:
  - (a) Constraint operator, which provides the data needed for fine-scale problems:

$$D_f = D_f(u_c), \quad (4.34)$$

where the data should be consistent with the current state of the coarse-scale solution  $u_c$ .

- (b) Local micro-scale solvers, which solve problem (4.32) locally.
- (c) Data processing or data estimator that extracts the data needed from the local fine-scale solution to substitute missing information on the coarse scale

$$D_c = D_c(u_f, u_c). \quad (4.35)$$

In addition to data mapping, one can consider the so-called compression and reconstruction operators. They correspond to upscaling and downscaling of the solution, so that:

$$Qu_f = u_c, \quad (4.36)$$

$$Ru_c = u_f. \quad (4.37)$$

While the downscaling is not unique [67], it should be consistent with upscaling:

$$QRu = u. \quad (4.38)$$

Compression and reconstruction operators are not always required for HMM, hence plotted as dashed lines in Figure 4.4. At the same time, the reconstruction operator would provide the initial conditions to local fine-scale problem. Therefore, it can be seen as a part of the constraint operator.

In many cases, the HMM can be perceived as a discrete approximation of homogenization, see e.g. [8, 10]. At the same time, the methodology extends seamlessly beyond regimes where homogenization is possible [8, 35], as we also demonstrate in Paper B.

### Control volume HMM for non-Darcy flows in porous medium

To demonstrate an example of the construction of an HMM method, we briefly present a simpler version of the method considered in Paper B. For the coarse-scale solver we choose the control volume method described in Section 3.1 and call the resulting method accordingly: control volume heterogeneous multiscale method (CVHMM). The solver based on the control volume method ensures the physically-sound mass conservation on the coarse scale, hence defining the coarse scale problem:

$$F_c(p_c, D_c) = 0, \quad (4.39)$$

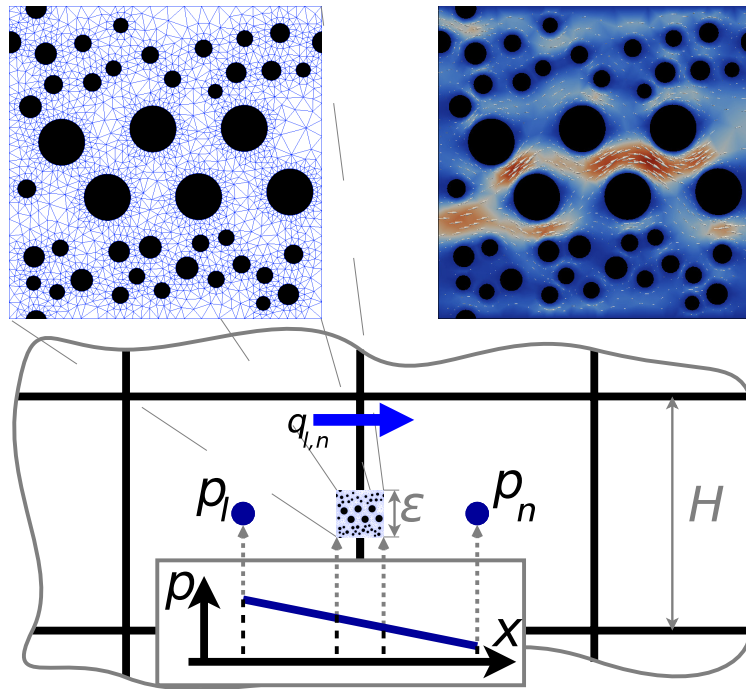


Figure 4.5: Building blocks of the HMM from Paper B. The figure shows schematics of constraint operator providing pressure boundary conditions to the fine-scale problem. The zoomed-in portion shows a finite-element triangulation of the fine scale and an example of flow solution.

where  $p_c$  is the coarse pressure variables in the cell centers. For the closure of the system we need to estimate the pressure-flux relationship ( $D_c$  in (4.39)). Instead of using a closed-form Darcy's law, we estimate it from local pore scale problems in an HMM fashion (see Figure 4.5 for illustration):

1. Project the pressure linearly from the coarse-scale to the fine-scale cell problem to form its boundary conditions.
2. Solve the steady-state Navier-Stokes equations on pore geometry for given pressure boundary conditions and assuming periodicity of the flow solution.
3. Estimate the flux on the coarse scale by integrating the flow velocity across the unit cell and scaling it to match the size of the cell boundary.

These sub-steps are repeated whenever we lack information needed to reconstruct the Jacobian of the coarse-scale problem and until the solver converges.

In Paper B we demonstrate that CVHMM formulation converges to the Darcy's law solution of the problem for the linear case (i.e. when the non-linear term is dropped from the Navier-Stokes equation as shown in Section 4.3). At the same time the methodology allows us to analyze a larger set of problems with non-linear dynamics as described in the included papers A, B and C.

## 4.5 Self-similarity analysis

As it was discussed in the previous section, for a problem to be solvable by an HMM it is required to have well-defined coarse variables. Defining them requires a certain notion of scale separation. A large class of problems (Class D in Figure 4.2) has continuous variability of scales. Consequently, one cannot explicitly define micro- and macroscopic variables for this class, thus rendering HMM concepts inapplicable.

A general technique to address this class of problems is to perform an analytical study of the corresponding self-similar solutions. In our terminology, this is a multi-scale modeling approach, see Figure 4.1.

Multiscale problems of Class D have self-similarities that require solving an eigenvalue problem [20]. By definition of self-similarity such an eigenvalue problem can be formulated as

$$\mathcal{L}_* u = \lambda u, \quad (4.40)$$

where  $\lambda$  is an eigenvalue,  $u$  is a solution shape-function (eigen-function), and  $\mathcal{L}_*$  is an operator (possibly non-linear) that advances the shape-function through the scales. The definition of the shape-function and the operator is problem-specific and comes from dimensional analysis and other physical considerations.

### Self similarity analysis of structures in freezing brine

In Paper D we apply this technique to a problem of rapid freezing in brine, see Section 5.2. Addressing eigenvalue problem (4.40) specific to the model analytically and numerically one can identify and simulate two freezing regimes:

- with compact ice formation, see Figure 4.6 (a),
- with fractal ice formation caused by secondary nucleation, see Figure 4.6 (b).

Furthermore, based on the analysis of the two regimes, we formulate a semi-analytical heuristic model that is able to predict properties of ice for other regimes. For example, we can consider a rapid freezing with the temperature governed by a logistic function, which does not have scaling required for self-similarity regimes.<sup>2</sup> Nevertheless, under these conditions the heuristic estimate give a good approximation to the properties of the formed ice, see Figure 4.6 (c). Thus, self-similarity analysis proves itself as a generic tool for multiscale problems of Class D. Discussion of the analysis results is summarized in Section 5.2 and technical details are presented in Paper D itself.

---

<sup>2</sup> To be more precise, the model from Paper D is controlled by the critical salinity and not temperature directly, see (2.37). Temperature is a monotone function of critical salinity (2.36) and might be slightly different from the logistic function.

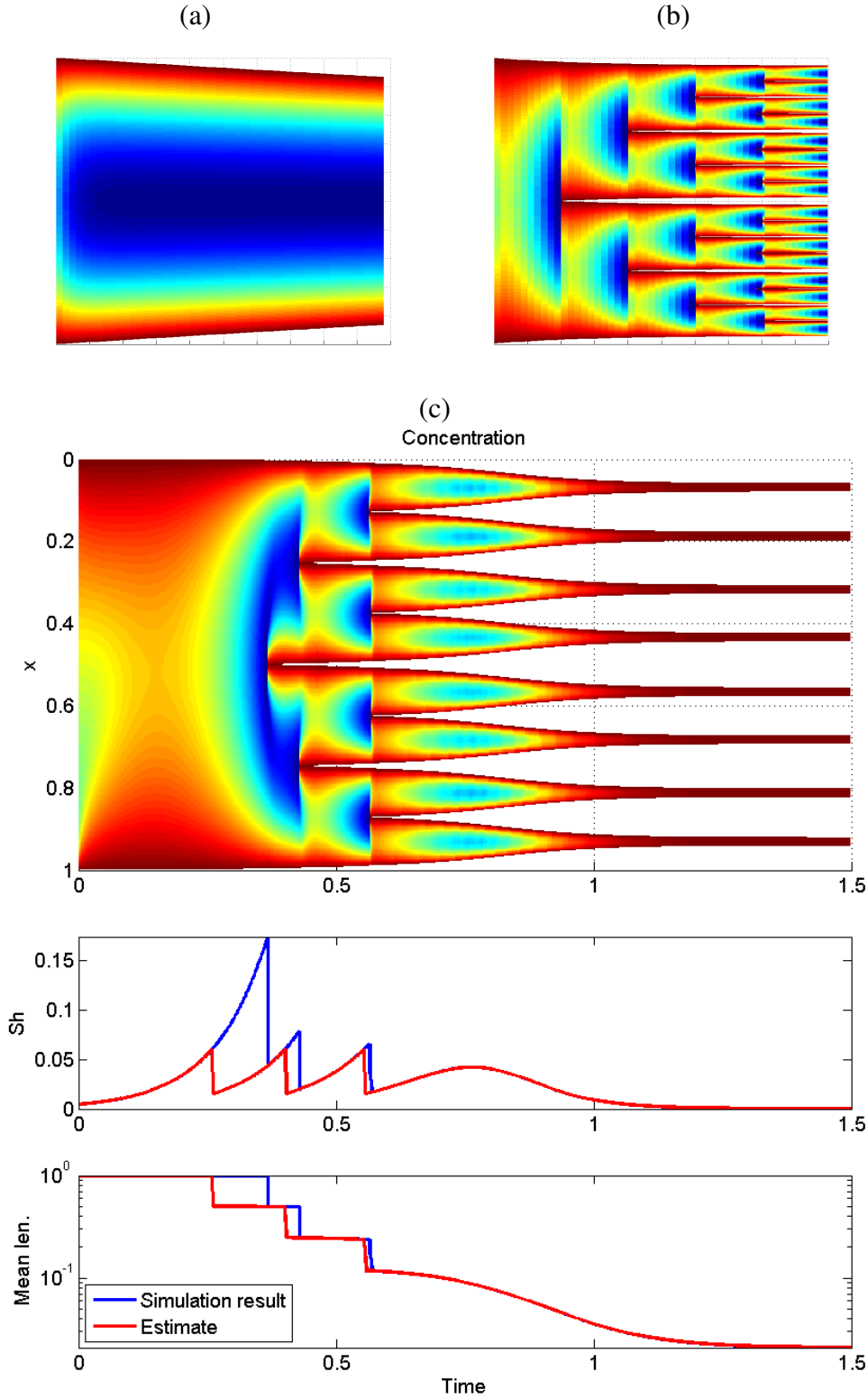


Figure 4.6: Plots showing ice structure as a function of time in 1D. The colored areas represent domains filled with brine, while white spaces represent ice inclusions. Color differs depending on the dimensionless salinity. (a) and (b) show self-similar solutions corresponding to compact and fractal ice formation regimes respectively. (c) shows numerical solution during rapid freezing modeled by a logistic function. (c) also provides comparison between the simulated and the heuristically-estimated solutions in terms of their characteristic parameters (Sherwood number [Paper D] and mean length of brine domains).

# Chapter 5

## Discussion of included papers

This result is too beautiful to be false; it is more important to have beauty in ones equations than to have them fit experiment.

---

Paul Dirac

In this chapter, we present an overview of the results that are presented in the included papers (Chapter 6). We put the results in the context of the frontiers of knowledge in the area of multiscale methods.

This work bridges some specific, but important gaps between multiscale modeling and simulation for several specific problems of fluid dynamics. The methods developed in the thesis are substantially different from each other since they are built as fit-for-purpose models. At the same time they all address the difficulty of reproducing behavior of complex systems by understanding and modeling the structure of sub-scale dynamics. With this in mind it is natural to group them based on the physical problem that they address. Papers A, B and C address a problem of fast non-linear flows in porous medium where fluid flows around solid. The Paper D studies a simplified problem of ice growth in brine, where the concentration of solid (ice) increases with time until a porous medium is formed. Finally, Paper E studies a free fluid flow with presence of particles covered with flocculant which can create agglomerates due to viscous bridging.

### 5.1 Control volume heterogeneous multiscale methods for non-linear flows in porous media

As it was shown in Section 2.4, flow in porous medium definitely is a multiscale phenomenon. Traditionally, the flow in porous medium was approximated by Darcy's law, derived by Henry Darcy in the 19th century from a 1D experiment in homogeneous sand [58]. This simple relationship has been exploited and extended over time to increase its domain of applicability, sometimes compromising the underlying physical principles, see e.g. [44].

It is known that this classical relation fails when the flow velocity becomes large enough for the inertia effects to come into play [70, 85]. In those cases the pore scale

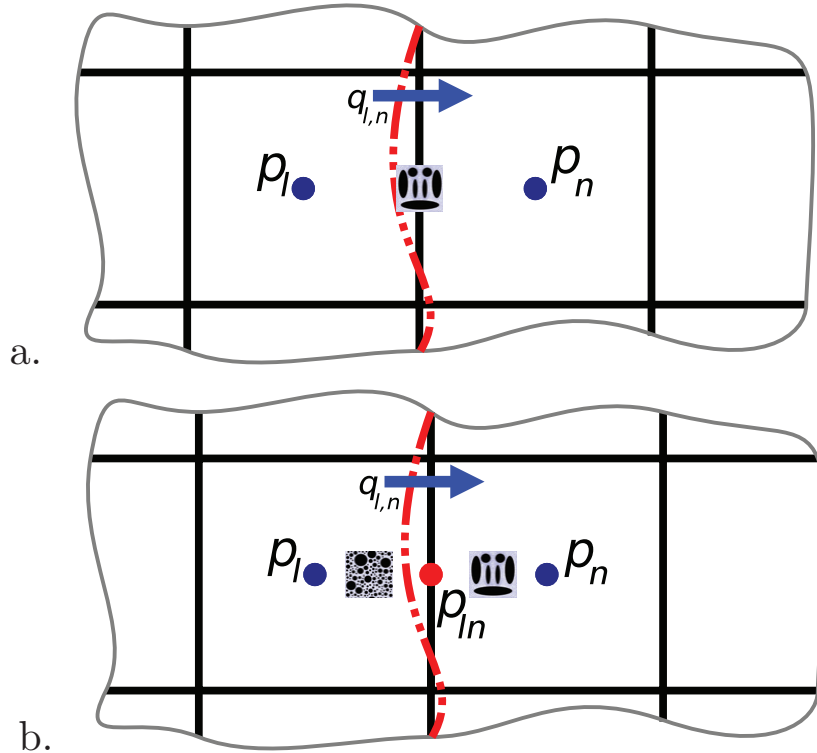


Figure 5.1: Treatment of discontinuities (dashed red lines) by one point (a) and two point (b) quadrature rules. Adapted from Paper B.

dynamics cannot be decoupled from the Darcy scale due to non-linearity. In papers A, B and C we have approached this challenging regime by developing a framework for multiscale simulation that operates on the Darcy-scale and local pore-scale simultaneously. The framework, that we call the control volume heterogeneous multiscale method (CVHMM) follows the HMM philosophy. A CVHMM only assumes mass conservation on the coarse scale but replaces Darcy's law approximation of the flux with data estimation from a finer scale. To do so, it couples a control volume method with an on-demand reconstruction of pressure-flow relationship obtained from local solutions of pore-scale problems. In this work the fine-scale problems are modeled by Navier-Stokes equations. They are solved on pore geometries locally by a mixed finite-element method with Taylor-Hood elements. The full method is summarized in Section 4.4.

A non-matching formulation of the fine and the coarse scales distinguishes our method from "classical multiscale" methods for flow in porous media, such as [54, 64], and earlier HMM-based methods, such as [6, 46]. Our methodology complements the approach that was proposed earlier [29] where pore network model was used for fine-scale. Formulating the fine scale problems directly on pore pore geometries allows us to omit the stage of creating the pore network based on MRI.

The following subsections summarize the specific results obtained in each of papers A, B and C, which, respectively, introduce, analyze and extend the CVHMM. At the end of the section we discuss current and suggested future directions of HMM effort for systems that couple pore-scale and Darcy-scale.

### 5.1.1 Summary of Paper A

CVHMM for non-linear flows in porous media is originally introduced in Paper A. While control volume finite difference HMM formulations have been used before (in e.g. [11]), the new method differs in two major aspects. Firstly, our methodology admits and emphasizes independent problem formulations on fine and coarse scales. Secondly, instead of using a straightforward one-point quadrature the method in Paper A is a multiscale extension of a more robust control volume method with two-point flux approximation (TPFA). The comparison of the two approaches was presented in Figure 3.2.

TPFA as a single-scale method that is known to preserve mathematically sound harmonic averages of the permeability [1]. TPFA-based HMM is therefore expected to inherit consistency when the discontinuities are resolved by the coarse grid. Figure 5.1 shows a coarse grid that roughly follows the discontinuity. TPFA quadrature has sampling points, where fine-scale problems are formulated, away from the coarse-cell boundaries (see Figure 5.1b) and, therefore, is less affected by sampling errors.

Specific to Paper A is handling of both incompressible and weakly compressible fluids for both linear (Stokes) and non-linear (Navier-Stokes) regimes on the pore scale. In this paper, compressible flows are handled by a Class E method (see Section 4.2) which assumes instantaneous equilibration of density on the fine scale.

We perform a quarter of the 5-point well test numerically and demonstrate that the multiscale solution converges to the reference solution on the coarse scale for the linear case as fine-scale grid is refined. This corresponds to improving the approximation of permeability in Darcy's law. The second order convergence for simple pore geometry is the expected fine-scale error for Tailor-Hood elements [81] that in this case propagates with same rate to the coarse-scale solution.

In the other numerical example we observe that the non-linearity of the system influences not only the near-well regions, but also the regions with high flow that is induced by heterogeneity of the medium. In the transient regime of weakly compressible flow the discrepancy between the linear and the non-linear solutions increases with the rate of injection while exhibiting latency effects. These effects slowly disappear when the injection is continued with a fixed rate.

### 5.1.2 Summary of Paper B

Paper B focuses on the convergence analysis of CVHMM. In the paper we have considered both the finite volume element method (FVEM, see Section 3.2.1) and the two-point flux (see Section 3.1.1) version of CVHMM. Other works (e.g. [29]) have also presented FVEM-based HMM methods, however these use a distinctly different fine-scale solver. We kept the TPFA-based method from Paper A due to its desirable properties discussed earlier.

The analysis of the method is performed using the mathematical toolkit of FVEM [28]. At the same time, we show that two coarse-scale approximations can be associated with two choices of quadrature rules in the multiscale method, see Figure 5.1. This allows to extend all the estimates to the complete CVHMM framework.

We assume that typical applications of this method are from Class C (see Section 4.2), which focuses on approximating the coarse-scale solution while automati-

cally parametrizing the fine-scale dynamics. Therefore, we carry out the analysis of convergence for the  $H^1$ -norm of the coarse scale solution in pressure.  $H^1$  norm implies convergence of the pressure as well as its derivatives [12, 23]. For an elliptic problem that implies convergence of the fluxes.

The errors are estimated with respect to the homogenization solution of the Stokes problem (see proposition 2 from Section 4.3.2). Following [6, 7, 35] we split the error into components using the triangle inequality. However the presented analysis differs from most earlier works due to the fact that the method uses different formulations on different scales and is specifically tailored to the FVEM setting. We prove that the error between the homogenization solution  $p_0$  and the fully discrete coarse solution obtained from the CVHMM,  $p_{MS}^{H,h}$  for the weakly linear case can be represented as follows:

$$\begin{aligned} \|p_0 - p_{MS}^{H,h}\|_{\mathcal{H}^1} &\leq I + II + III \\ &\leq C \left[ \eta + \left(\frac{h}{\varepsilon}\right)^\alpha + H \right], \end{aligned} \quad (5.1)$$

where

- I. **Modeling error** is the error from substituting the correct cell problem equations with an approximate model.
- II. **Propagation of fine-scale error** is the error from solving cell problems numerically on a grid with cell sizes  $h/\varepsilon$ .
- III. **Coarse scale error** is the error from solving the coarse problem numerically on a grid with cell size  $H$ .

Even though we follow the naming convention for the terms introduced in [7], in our analysis the term II is treated in the continuous setting, before the coarse-scale discretization has been introduced. This choice allows us to carry out proofs in a continuous setting, which can be advantageous for more complex problems.

Under the assumption of periodicity and coarse grid alignment, the modeling error I vanishes for the linear regime: when CVHMM uses Stokes approximation on the fine scale. Even though the formal estimate becomes weaker under non-linearity, for realistic scenarios when  $\varepsilon \not\rightarrow 0$  the HMM approximation is supposed to better capture solution dynamics.

The convergence estimates presented in the paper are supported by numerical convergence tests. The numerical convergence results emphasize the importance in both fine and coarse-scale solutions. As in Paper A, we estimate a fine-scale-geometry-dependent constant in term II and get:  $\alpha = 2$ . The fine and the coarse-scale errors are of order  $(\frac{h}{\varepsilon})^2$  and  $H^2$  respectively. Additional numerical tests try to cover and quantify other properties of CVHMM: modeling error of two-point methods, comparison of FVEM and TPFA quadrature rules and extension of the analysis to fully non-linear solutions.

A convergence test with random alignment of fine-scale structure demonstrates that ignoring anisotropy, which is implied by two-point methods, introduces consistency errors that are not reduced under refinement. Even though this behavior is inherited from the standard TPFA [3], the context of HMM where the anisotropy is estimated

as an online computation and not known a priori highlights new challenges for the technique that remains popular in reservoir simulation [62].

In the analysis, the estimate for TPFA-based HMM is derived from the FVEM-based estimate. To demonstrate benefits of using the new method, we compare quadrature approximations numerically. Numerical results indicate that while the methods has same convergence rates (as expected from the analysis), the TPFA is superior when the coarse grid approximates the discontinuities.

Paper B also discusses an extension of the estimate (5.1) to the fully non-linear case for which steady-state Navier-Stokes equation with different scaling results in Dupuit-Forchheimer-Ergun law as its homogenization solution [47]. While the rigorous proof is not provided, the self-convergence example indicates convergence rates that coincide with numerical results for the Darcy's regime.

### 5.1.3 Summary of Paper C

While Paper B is dedicated to an in-depth analysis of the method, Paper C focuses on an extension of CVHMM to improve the method's robustness. To distinguish the new method we will abbreviate it rCVHMM ('r' for robust). The rCVHMM is an HMM extension of multi-point flux approximation (MPFA). Among MPFA methods we chose the L-method (discussed in Section 3.1.2) as the coarse-scale solver (equivalently CVHMM quadrature). The choice is motivated by the properties of single-scale L-method. As such, it preserves continuity of reconstructed pressures [4] and reliably handles hanging nodes for polygonal grids with adaptive refinement [42]. This choice of coarse-scale approximation enables the rCVHMM to handle anisotropic media with arbitrary alignments and a large class of general polygonal grids on its coarse scale, which significantly extends the method's applicability. This is especially important in the context of an HMM where coarse-scale quantities such as permeability are not known a priori and the tuning of coarse discretization needed for two-point methods to be consistent [1, 42] cannot be applied. The numerical examples presented in the paper confirm that the more robust coarse-scale solver increases the domain of validity of CVHMM without worsening the convergence properties.

The suggested applications of rCVHMM are flows in porous media where non-linear behavior not captured by standard one-scale models is observed. Our method is therefore complementary to e.g. [78] that also challenges representation of physics complexity for two-phase flow on the coarse scale through multiscale simulation. Equipped with our robust method the paper addresses synthetic problems inspired by the non-linear problems: near-well flow where the pore geometry can be estimated by MRI core analysis, and industrial porous media with control over pore geometry.

The numerical experiments show that, for permeable pore geometry, the near-well flow calls for a non-linear extension of Darcy's law. The typical non-linear extension used in reservoir modeling is the Forchheimer's law [70]:

$$(\underline{\underline{A}}^{-1} + \beta |\vec{u}_c|) \vec{u}_c = -\nabla p_c, \quad (5.2)$$

which adds an additional inertia term to Darcy's relation. In (5.2),  $\underline{\underline{A}}$  is the matrix-valued Darcy's coefficient related to permeability, and  $\beta$  is a scalar-valued Forchheimer coefficient that is estimated experimentally. We compare our pressure-velocity relationship that is automatically obtained in the HMM fashion to the Forchheimer's law. The

comparison shows that, by tweaking the constant  $\beta$ , the latter can give qualitatively similar results to the multiscale formulation where the full complexity of sub-scale model is resolved. At the same time, the Forchheimer approximation cannot give one-to-one correspondence to the automatically up-scaled values even for random porous medium.

We also consider near-well flows in a tighter formation which should not show non-linear behavior. The flow still exhibits a sufficient non-linearity in the presence of a single simulated fracture which commonly occurs in near-well regions. The non-linear effects are not completely localized near the fracture due to the elliptic character of the problem, but do decay rapidly away from the fracture and the well perforation where the simulated flow source is located. This example especially highlights that the rCVHMM automatically adapts itself and spends most of the computational effort in the part of the domain where the non-linearity has influence.

Finally, with an artificial porous medium we show that flow can show non-reversibility effects. These effects are not captured by standard models, even by Forchheimer law. At the same time, this type of behavior is handled seamlessly by rCVHMM.

#### 5.1.4 Further directions

After CVHMM was introduced in Paper A in 2012, the field of HMMs for flows in porous media that take into account sub-Darcy scale has received a lot of attention. There were numerous parallel developments that addressed different aspects in the field some of which might have been inspired by the work presented in this thesis. While it is a challenging task to give a complete review of the rapidly expanding field, a short overview of the most related works is required to formulate possible further directions.

A further analysis of HMMs for sub-Darcy scale formulations is conducted in [9, 10] in a finite element setting. While using linear Stokes equations for the fine scale, the papers address a sub-scale structures that slowly vary within the coarse computational domain. The authors present convergence estimates for the resulting multiscale method which takes into account such aspects as non-matching periodicity of the cell problems, and continuously varying sub-scale structure. They also formulate a reduced basis HMM [10] that uses the structure of the problem to increase computational efficiency of the multiscale method for the described setting. This contrasts with our studies, where we focus on problems with heterogeneities that are well approximated by the coarse grid.

The analysis of further, more complex extensions of CVHMM becomes inherently more difficult. This is one of the reasons that convergence estimates are not included in Paper C. Based on the experience with CVHMM it seems that a good strategy for developing multiscale methods in the future is similar to benchmarking of single scale methods in the past. Analysis is vital for ensuring the convergence and, most importantly, consistency of an HMM. At the same time, in most cases it is more viable to carry out the analysis in a simplified setting as a benchmark. One can thereafter extend the range of problems where the method can be applied without breaking the fundamental assumptions required in the simplified analysis. These speculations demonstrate that the developments of CVHMM provide an additional insight into future developments of other multiscale simulation techniques. The experience presented in this thesis can

provide a basis for filling other knowledge gaps in the field of multiscale methods.

Following [29], Chu et. al. continued to explore the possibility of the pore network model on the fine scale to include additional physics. The original paper [29] contained an example of a simple model where pore throats were varying in time, resembling elasticity. In [30] they present an HMM that is capable of handling pore networks with non-linear model of conductivity and a two-phase flow. The paper demonstrates that the pore network formulation also allows to create non-local pore channels (resembling fractures) that can be treated within the framework. This concludes that the pore network model on the fine scale gives superior flexibility to include additional effects. At the same time, special care should be taken to ensure that the fine-scale physics is consistently translated into a graph-like pore network formulation.

CVHMM inherits modularity typical to HMM. Its modularity first and foremost allows for applying different types of fine-scale methods both in terms of discretization and sub-scale model formulation. In [45] the authors applied the CVHMM methodology combining it with a different fine-scale solver: smoothed particle hydrodynamics, that is formulated within Lagrangian frame of reference. The application of pore network models has been already explored in parallel development [29, 30]. As of now, the unexploited possibility lies in combining the flexibility of CVHMM with statistical representation of the fine-scale model. A statistical formulation may be specifically interesting for reservoir simulation. It would make it possible to combine available core samples to set up fine-scale models. At the same time, some kind of population modeling with uncertainty can be used to predict the sub-scale geometry at the locations where standard single-scale approximation is insufficient. At this point it is difficult to foresee the best formulation of fine-scale model, but a mixture of resolving the pore geometry and pore network models seems to be a viable alternative for such a method.

Finally, now more than ever CVHMM can make its way to industrial applications. With the continuous improvements in technology for imaging and design of porous media the presented computational framework offers an attractive tool for multiscale simulations, where it can smartly adapt to varying flow conditions with no user interactions.

## 5.2 Multiscale analysis of freezing in brine

The sea-ice formation and, more generally, freezing in brine is an interesting problem for the transitional regime between free flow of fluid and a porous medium. The initial intention of this study was to formulate a homogenization problem for the transient regime of ice creation and growth applying the techniques from [26, 71, 80]. This would bring a mathematical basis to mushy layer models [50, 86, 87] and create a foundation for HMM-type methods on the continuum scale of the problem.

The complexity of the complete problem motivated handling it in a simplified setting to better understand the mathematical properties of ice formation. Earlier attempts approximated ice growth by the Ginzburg-Landau reaction-diffusion equations, with a phase field function replacing the notion of ice-brine fronts [56]. In contrast, we treated the ice fronts explicitly, prohibiting transport of salt in the solid domain. The complete set of chosen simplifications (see Section 2.4.3) resulted in a fractal-type multiscale problem (Class D from Section 4.2), which cannot be handled by a typi-

cal two-scale method. An application-driven study led to applying non-standard fractal techniques that allowed us to reveal distinct regimes of the model behavior. The study of the problem from both analytical and numerical perspectives led to development of a semi-analytical method to quantify the structural properties of the ice.

The following subsection summarizes the results presented in Paper D. We also dedicate a separate subsection to highlight the alternations that were made to the control volume method to handle this problem with moving boundary and verify numerically that the method gives a convergent approximation. The section is concluded by directions of further work.

### 5.2.1 Summary of Paper D

Paper D presents a mathematical model for ice formation in brine on the continuum scale that is finer than the scale used in mushy layer approximation, as shown in Section 2.4.3. An explicit treatment is given to micro-scale diffusion of salt and the phase transition due to the secondary nucleation. We study the process under idealized conditions: the temperature constant in space and no flow of fluid. A similar setting can be reproduced in 1D column and 2D thin slit experiments. Specific to the presented model, is addressing an onset of secondary nucleation within the fluid domain that may occur due to over-cooling. Even though we are not aware of experiments that mimic the conditions of the presented mathematical problem, secondary nucleation (ahead of the freezing front) has been observed in Hele-Shaw cell experiments reported in [69].

In our model we assume that the concentration threshold triggering secondary nucleation is related linearly to the freezing concentration for every given temperature, see (2.45):

$$S_{\text{nucl}}(T) = \nu S_{\text{freez}}(T), \quad (5.3)$$

where  $\nu$  is the nucleation multiplier. The linearity assumption means that during the secondary nucleation the ratio between the minimum and the maximum of salinity profile for a solution is fixed. We extend this argument by assuming that the shape of the solution at each sub-domain is self-similar after the nucleation. This allows to analyze the problem using fractal techniques similar to [20].

The analysis performed for a one-dimensional case demonstrates that the interplay between the salt expulsion from ice and its diffusion away from the ice boundary can produce two types of freezing regimes depending on the external cooling rate:

- sub-critical homogeneous (consolidated) ice growth for which nucleation never occurs;
- super-critical regime that gives rise to emerging fractal patterns.

Paper D explicitly identifies the critical cooling rate that separates the two regimes. Under the critical cooling rate, the problem exhibits a self similar solution stable in time. Furthermore, the paper presents a closed-form analytical solution to the critical ice growth. This solution is used extensively in the paper and serves two purposes. Firstly, it benchmarks the non-standard control volume method derived specifically for the problem with varying boundary, that is used in the paper to compliment the analysis of the problem, see Section 5.2.2. Secondly, it provides a foundation for analysis of the solution properties under generalized freezing conditions.

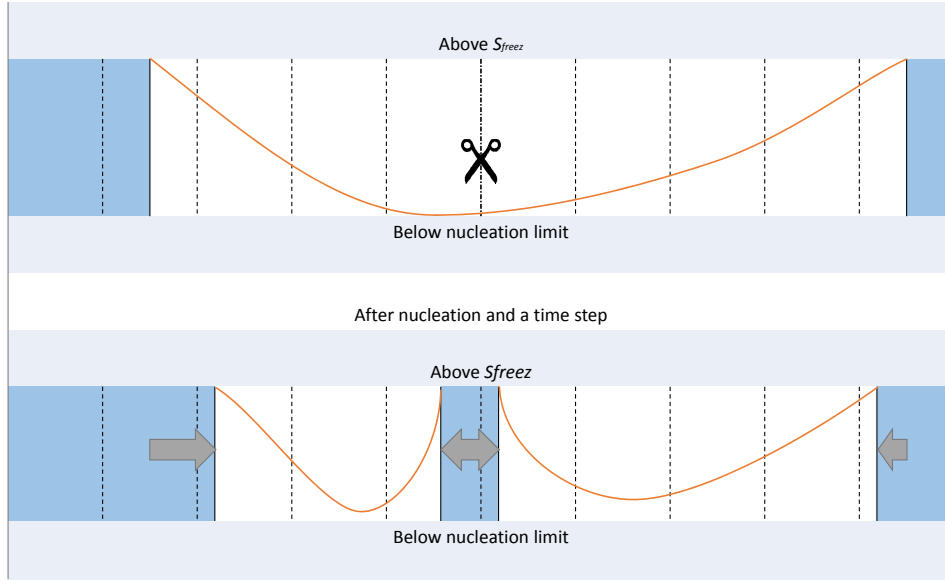


Figure 5.2: Illustration of finite difference method with occurrence of spontaneous nucleation. Dashed lines represent the boundaries of grid cells, sub-domains occupied by solid are filled, scissors indicate the place where splitting occurs due to nucleation, and arrows show how ice domain has expanded. Adapted from Paper D.

While it is not possible to obtain a closed-form solution in the nucleation-dominated super-critical regime, our problem-specific numerical method reproduces the expected nucleation process, resembling Cantor sets. The fractal structures resulting from numerical modeling provide an additional understanding of the transition between brine and porous ice that augment the averaged mushy layer approaches. The robustness of the discussed fractal patterns with respect to initial conditions is also verified numerically.

In addition to verifying the fractal self-similar behavior in super-critical regimes, we propose a heuristic method for estimating the typical length scale of fluid-ice structures for general freezing conditions. The estimates of length scales can be seen as basis for deriving structural properties of porous ice: porosity, permeability and rigidity.

### 5.2.2 Discussion of control volume approximation of ice growth

To produce an approximation of ice growth, Paper D utilizes a control volume method. There is no standard approximation of moving boundaries for control volume methods. In this subsection we provide a detailed description of a specific variation of the control volume method that was used in Paper D. This also includes a verification of the method in the critical regime where the analytical solution is known.

The conservation equations for salinity are solved by a standard control volume method (see Section 3.1) on a static uniform grid, which is bundled with the explicit Euler method for time stepping. This standard approximation ensures consistency of the solution in terms of mass conservation in each continuous fluid sub-domain. Since ice inclusions act as barriers, without any loss of generality it is possible to formulate the scheme for a single fluid sub-domain and apply it consequently to each sub-domain when required. Therefore, the non-standard part of the method is the treatment of flux

approximation between the cells and handling secondary nucleation. While the flux approximation is discussed in more detail later, the secondary nucleation is handled in a more direct manner. Before every time step, the algorithm performs a check: if the solution has crossed the nucleation threshold, the domain is split in two. The splitting is performed at the boundary between the cells closest to where the nucleation limit has been reached, see Figure 5.2. All further time steps treat the resulting two sub-domains separately.

Figure 5.2 illustrates how the numerical method handles a time step where propagation of the boundary occurs. There are three local scenarios that need to be accounted for:

1. Away from the boundaries, the flux is approximated by the standard finite difference equation:

$$\vec{q}_{i+1/2} = -D \frac{S_{i+1} - S_i}{\Delta x}, \quad (5.4)$$

where  $\vec{q}_{i+1/2}$  is the flux of salt<sup>1</sup> between cells  $i$  and  $i + 1$ ;  $S_i$  is the discrete concentration in cell  $i$  and  $\Delta x$  is the cell size.

2. In the cell closest to the boundary, the boundary conditions should be satisfied. For definiteness, let us consider the left boundary, i.e. cell  $i$  is on the boundary while  $i + 1$  is not. It is necessary to resolve the motion of the boundary on a sub-grid scale. For the boundary cell  $i$  we introduce an additional variable  $\eta_i$ , representing the fraction of cell occupied by ice. The equation for the flux from the boundary cell is solved explicitly as in case 1:

$$\vec{q}_{i+1/2} = -D \frac{S_{i+1} - S_i}{\frac{1}{2}\Delta x + \frac{1-\eta_i}{2}\Delta x}, \quad (5.5)$$

where  $t_0$  is the time corresponding to the previous time step and the denominator is adjusted to account for the shifted center of the cell due to the portion occupied by the ice. The boundary condition for the freezing problem requires that the concentration at the boundary is equal to the externally defined freezing concentration:

$$S_i(t) = S_{\text{freez}}(t), \quad (5.6)$$

where we assume that the salinity value is constant in the whole boundary cell. Due to secondary nucleation, the condition (5.6) might not be satisfied in the beginning of a time step. It is however enforced by adjusting the ice fraction in the cell during each time step. The new ice fraction in the boundary cell  $\eta_i(t_0 + \Delta t)$  is found so that both the Rankin-Hugoniot condition (2.44) and the condition on salinity 5.6 are satisfied in the discrete sense

$$[S_{\text{freez}}(t_0 + \Delta t) \cdot (1 - \eta_i(t_0 + \Delta t)) - S_i(t_0) \cdot (1 - \eta_i(t_0))] \Delta x = \vec{q}_{i+1/2} \Delta t, \quad (5.7)$$

where  $\Delta t$  is the time step.

3. The case when the ice boundary crosses a cell boundary (see the left boundary in Figure 5.2) requires a special treatment, since the equation (5.7) is no longer

---

<sup>1</sup> In this section we drop original indexes of  $\vec{q}_{fna}$  and  $S_f$  to improve readability.

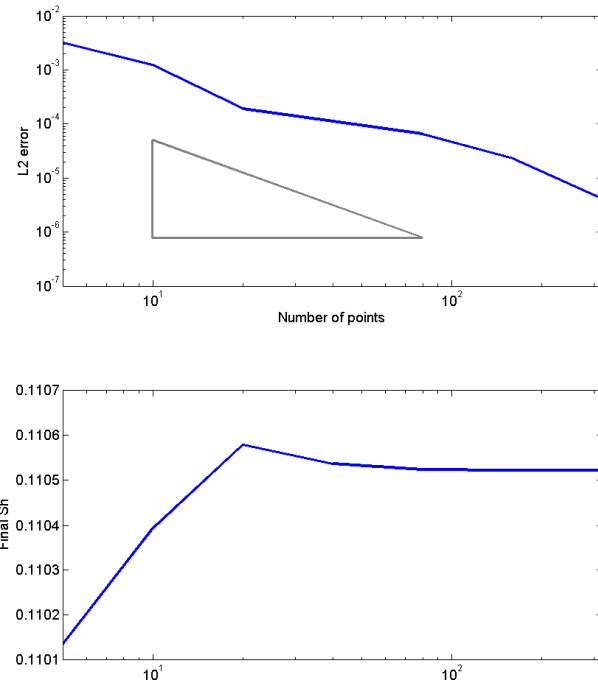


Figure 5.3: The convergence of the critical solution to the exact solution.

well-defined. In our method we choose to merge the cell on the boundary ( $i$ ) and its neighbor ( $i + 1$ ), and therefore obtaining formulation similar to the case 2. The salinity of the merged cell  $S_{i+1}^*$  is derived by redistribution of salt mass

$$S_{i+1}^*(t_0) \cdot (\eta_i(t_0) + 1)\Delta x = S_{\text{freez}}(t_0)\eta_i(t_0)\Delta x + S_{i+1}(t_0)\Delta x. \quad (5.8)$$

Consequently, the equations for the flux  $\vec{q}_{i+3/2}$  become

$$\vec{q}_{i+1/2} = -D \frac{S_{i+2} - S_{i+1}^*}{\frac{1}{2}\Delta x + \frac{1+\eta_i}{2}\Delta x}. \quad (5.9)$$

The fraction of ice in the merged cell is deduced analogously to (5.7) and is afterwards used to compute  $\eta_{i+1}$ . By ensuring sufficiently small steps propagation of the boundary over multiple steps can be avoided.

To verify that the method described above provides a convergent approximation we benchmark it against the analytical solution derived in Paper D:

$$\frac{S(t, x)}{S_{\text{freez}}(t)} = \frac{\cosh(\text{Sh}^{\frac{1}{2}}(\left[\frac{x-x_0(t)}{l(t)}\right] - \frac{1}{2}))}{\cosh(\frac{1}{2}\text{Sh}^{\frac{1}{2}})}, \quad (5.10)$$

where  $x_0(t)$  and  $l(t)$  are the time dependent position of the left boundary of the domain and the size of the domain respectively. Equation (5.10) provides a one-parametric class of solutions. The parameter Sh is the Sherwood number that varies depending on initial conditions.

Using the class of self-similar solutions (5.10), we study convergence of the numerical scheme with respect to the refinement of the spatial discretization with the following procedure. We start with a single interval  $[0, 1]$  as the fluid domain and initialize the method with a convex function

$$S(0, x) = 0.01|x - 0.5| + 0.995. \quad (5.11)$$

After that, we run the method until a stable self-similar solution is achieved in the sense of (5.10).

Figure 5.3 shows that the numerical solution tends to an analytical solution. Observe that since the initial conditions (5.11) are approximated on a control volume grid, it is expected that the stable mode of the numerical solution might have a Sherwood number that varies depending on the discretization. The "correct" Sherwood number cannot be determined, since the analytical solution does not account for time-dependent dynamics. Importantly, the second plot in Figure 5.3 indicates that the value of the Sherwood number also converges as the mesh is refined.

### 5.2.3 Further directions

The further directions related to studies of the super-critical freezing of brine in light of the presented paper can be addressed from two points of view: physical and computational.

The model presented in Paper D includes a number of assumptions about the physics of the problem that enabled a deeper mathematical analysis. In the absence of experiments, it is difficult to judge how reasonable these assumptions are. Therefore, it is of scientific interest to set up an experiment that resembles the conditions proposed in the model. While the experiment in [69] identified a regime with nucleation ahead of the ice front, it is interesting to see if the rapid freezing in a thin strip produces self-similar fractal structures due to secondary nucleation. Even though the analysis in Paper D is limited to 1D, the presented model remains valid in two dimensions. Further experimental studies can verify that the analysis results extend to a two-dimensional setting.

The two-dimensional setting also presents an interesting extension from the computational point of view. This requires a control volume method that is capable of treating moving boundaries and singularities associated to secondary nucleation in multiple dimensions. Developing such a method raises questions about the rules of proposition of the moving boundary that would involve several neighboring cells. Another distinct difference is that in 2D the nucleation would not separate the domain. The implication is that the method would be likely required to work on a larger computational grid. Additionally, an unconstrained domain means that the marginal ice expansion can force fluid to move which introduces requirements for more complex approximation of salt fluxes. The severity of the fluid movement due to ice expansion can be estimated by envisioned numerical method.

Finally, the study of time-dependent self-similar solutions specific to the problem of rapid freezing in brine revealed an interesting mathematical perspective on the problem. Finding a solution that is self-similar with a period poses a non-trivial mathematical problem

$$\tilde{u}(x, t) = \tilde{u}(x, t + \delta t), \quad (5.12)$$

where  $\tilde{u}$  is an unknown dimensionless solution function and  $\delta t$  is the period. Unlike the classical theory of self-similar solutions, the solution is continuously changing but the structure of the change creates a self-similar pattern. In the absence of the analytical form, finding such solution requires solving an eigenvalue problem that is discrete and is likely to be non-linear

$$\mathcal{L}_{\Delta x}(u(x,t), \delta t) = \lambda u(x, t + \delta t), \quad (5.13)$$

where  $\mathcal{L}_{\Delta x}$  is the numerical approximation of differential operator that performs numerical time integration, mapping the input function  $u(x, t)$  to the solution at time  $t + \delta t$  and  $\lambda$  is an eigenvalue. Obtaining the initial conditions for a self-similar fractal solution required solving such an eigenvalue problem with a fixed eigenvalue  $\lambda$  and time interval  $\delta t$  which were derived from the analysis. The fact that the discrete operator was formulated in the setting with moving boundary posed an additional challenge. While in Paper D the solution was obtained by a simple iteration developing more sophisticated and robust methods opens interesting research possibilities.

### 5.3 Semi-analytical solution for micro-mechanics of agglomeration forced by capillary bridging

The main objective of this thesis is analysis of problems in fluid dynamics. Paper E studies interaction of solid particles and is more oriented towards physics, hence, it is independent from our main objective. At the same time, the motivation for studying such particle interactions comes from multiscale problem of suspended particle flows in fluid streams. The latter presents a strong example of current utilization of multiscale methods in fluid dynamics and as such directly relates to the scope of the thesis.

#### 5.3.1 Summary of Paper E

The Paper E considers collision of particles affected by liquid bridging described in Section 2.4.4. The collisions of particles are analyzed pair-wise, each consisting of three stages:

1. Formation of the bridge and approach of the particles;
2. Mechanical contact;
3. Separation of particles with further breakage of the bridge.

While the mechanical contact is well described by the classical hard-sphere collision model, this work tries to close the knowledge gap related to dynamics during liquid bridging between particles and provide understanding for when agglomeration of particles will occur. On top of capillary and viscous forces, common to modeling of liquid bridging, the paper considers an additional external force that can be used to mimic the influence from the flow dynamics on coarser scale. The paper provides a numerical solution to the formulated problem validated against experiments from [66].

In the absence of external forces, which is common to the problem, applying typical assumption for geometry of the bridge [17, 66] allows to derive an approximate analytical solution for loss of momentum during approach and separation. Equipped with a numerical model we verify the validity of the derived approximation.

Importantly, the analysis gives rise to a reliable agglomeration criterion. We foresee the use of this criterion for estimation of the probability of agglomeration in statistical models.

At the same time when agglomeration does not take place, the analysis yields a semi-analytical expression that gives a reliable estimate for the velocities of the particles after the bridge breakage. The expression can be used in Eulerian-Lagrangian computational fluid dynamics' models to substitute expensive numerical solvers of fine-scale dynamics, drastically reducing the total computational cost.

### 5.3.2 Paper E in the context of multiscale simulation

Following the development of the fine-scale semi-analytical model for particle intention from Paper E, it has been applied in a multiscale setting. In [19], the authors present a multiscale computational fluid dynamics model that couples the fine-scale semi-analytical solution in a Lagrangian framework from Paper E with an Eulerian flow model on the coarse scale. Utilization of the analytical approximation rather than a numerical model for the fine scale enables the technique to be viable for industrial applications in many areas. The resulting multiscale simulation is capable of improving prediction of agglomeration of particles in the flow as well as interaction of particles with walls and flow start-up effects. The multiscale model validated by experiments was furthermore used to study the problem of probability of agglomeration in the granular flow [18].

Eulerian-Lagrangian models used in computational fluid dynamics can be seen as a special case of HMM. In definitions of Section 4.4 the constrain operator formulates the local discrete problems while data estimation provides feedback in terms of forces and momenta arising from the local particle interactions. Earlier we have mentioned a model formulated in the CVHMM framework that also connects Lagrangian and Eulerian models [45]. With this in mind, it seems natural that further unification of toolboxes developed across disciplines would constitute better multiscale methods. A unified toolbox would take advantage of thorough analysis common to mathematics, experimental verification common to physics and more advanced algorithms common to computer science.

The developments in [18, 19] demonstrate that cross-disciplinary adoption of problem-driven multiscale methods is becoming reality.

# Bibliography

- [1] AAVATSMARK, I. An introduction to multipoint flux approximations for quadrilateral grids. *Computational Geosciences* (2002), 405–432.
- [2] AAVATSMARK, I. *Bevarlesesmetoder for elliptiske differensialligninger*. University of Bergen, Bergen, 2007.
- [3] AAVATSMARK, I. Interpretation of a two-point flux stencil for skew parallelogram grids. *Computational Geosciences* 11, 3 (feb 2007), 199–206, doi: 10.1007/s10596-007-9042-1.
- [4] AAVATSMARK, I. Multipoint flux approximation methods for quadrilateral grids. *The 9th International Forum on Reservoir Simulation*, December (2007), 9–13.
- [5] AAVATSMARK, I., EIGESTAD, G. T., MALLISON, B. T., AND NORDBOTTEN, J. M. A compact multipoint flux approximation method with improved robustness. *Numerical Methods for Partial Differential Equations* 24 (2008), 1329–1360, doi: 10.1002/num.20320.
- [6] ABDULLE, A. On A Priori Error Analysis of Fully Discrete Heterogeneous Multiscale FEM. *Multiscale Modeling & Simulation* 4, 2 (2005), 447, doi: 10.1137/040607137.
- [7] ABDULLE, A. The finite element heterogeneous multiscale method: a computational strategy for multiscale PDEs. *Multiple scales problems in biomathematics, mechanics, physics and numerics* 31 (2009), 133–181.
- [8] ABDULLE, A. A priori and a posteriori error analysis for numerical homogenization: A unified framework. *Ser. Contemp. Appl. Math. CAM* (2011).
- [9] ABDULLE, A., AND BUDÁČ, O. An adaptive finite element heterogeneous multiscale method for Stokes flow in porous media. *Multiscale Modeling & Simulation* 13, 1 (2015), 256–290.
- [10] ABDULLE, A., AND BUDÁČ, O. A reduced basis finite element heterogeneous multiscale method for Stokes flow in porous media. *Computer Methods in Applied Mechanics and Engineering* 307 (2016), 1–31.
- [11] ABDULLE, A., AND E, W. Finite difference heterogeneous multi-scale method for homogenization problems. *Journal of Computational Physics* 191, 1 (oct 2003), 18–39, doi: 10.1016/S0021-9991(03)00303-6.

- [12] ADAMS, R. A., AND FOURNIER, J. J. *Sobolev spaces*, vol. 140. Academic press, 2003.
- [13] ALYAEV, S. *Adaptive Multiscale Methods Based on A Posteriori Error Estimates*. Master's Thesis, University of Bergen, Bergen, 2010.
- [14] ARBOGAST, T. Numerical subgrid upscaling of two-phase flow in porous media. In *Numerical treatment of multiphase flows in porous media*. Springer, 2000, pp. 35–49.
- [15] ARBOGAST, T. Mixed multiscale methods for heterogeneous elliptic problems. In *Numerical Analysis of Multiscale Problems*. Springer, 2012, pp. 243–283.
- [16] BALAKIN, B. V., HOFFMANN, A. C., AND KOSINSKI, P. Population balance model for nucleation, growth, aggregation, and breakage of hydrate particles in turbulent flow. *AICHE Journal* 56, 8 (2010), 2052–2062, doi: 10.1002/aic.12122.
- [17] BALAKIN, B. V., HOFFMANN, A. C., AND KOSINSKI, P. The collision efficiency in a shear flow. *Chemical engineering science* 68, 1 (2012), 305–312.
- [18] BALAKIN, B. V., KUTSENKO, K. V., LAVRUKHIN, A. A., AND KOSINSKI, P. The collision efficiency of liquid bridge agglomeration. *Chemical Engineering Science* 137 (2015), 590–600, doi: 10.1016/j.ces.2015.07.002.
- [19] BALAKIN, B. V., SHAMSUTDINOVA, G., AND KOSINSKI, P. Agglomeration of solid particles by liquid bridge flocculants: Pragmatic modelling. *Chemical Engineering Science* 122 (2014), 173–181, doi: 10.1016/j.ces.2014.09.003.
- [20] BARENBLATT, G. I. *Scaling, self-similarity, and intermediate asymptotics: dimensional analysis and intermediate asymptotics*, vol. 14. Cambridge University Press, 1996.
- [21] BATCHELOR, G. K. *An introduction to fluid dynamics*. Cambridge university press, 2000.
- [22] BEAR, J. *Dynamics of Fluids in Porous Media*. Courier Corporation, 1972.
- [23] BRAESS, D. *Finite elements: Theory, fast solvers, and applications in solid mechanics*. Cambridge University Press, 2007.
- [24] BRANDT, A. Multiscale scientific computation: review 2001. In *Multiscale and multiresolution methods*, vol. 20 of *Lect. Notes Comput. Sci. Eng.* Springer, Berlin, 2002, pp. 3–95.
- [25] BRIGGS, W. L., MCCORMICK, S. F., ET AL. *A multigrid tutorial*. Siam, 2000.
- [26] BRINGEDAL, C., BERRE, I., POP, I. S., AND RADU, F. A. A model for non-isothermal flow and mineral precipitation and dissolution in a thin strip. *Journal of Computational and Applied Mathematics* 289 (2015), 346–355, doi: 10.1016/j.cam.2014.12.009.

- [27] CAI, X.-C., AND KEYES, D. E. Nonlinearly Preconditioned Inexact Newton Algorithms. *SIAM Journal on Scientific Computing* 24, 1 (jan 2002), 183–200, doi: 10.1137/S106482750037620X.
- [28] CAI, Z., MANDEL, J., AND MCCORMICK, S. The finite volume element method for diffusion equations on general triangulations. *SIAM Journal on Numerical Analysis* 180, 2 (1991), 392–402.
- [29] CHU, J., ENGQUIST, B., PRODANOVIC, M., AND TSAI, R. A multiscale method coupling network and continuum models in porous media I: steady-state single phase flow. *Multiscale Modeling & Simulation* 10, 2 (2012), 515–549, doi: 10.1137/110836201.
- [30] CHU, J., ENGQUIST, B., PRODANOVIC, M., AND TSAI, R. A Multiscale Method Coupling Network and Continuum Models in Porous Media II - Single- and Two-Phase Flows. In *Advances in Applied Mathematics, Modeling, and Computational Science*, R. Melnik and I. S. Kotsireas, Eds., vol. 66 of *Fields Institute Communications*. Springer US, Boston, MA, 2013, pp. 161–185.
- [31] CROWE, C. T., SCHWARZKOPF, J. D., SOMMERFELD, M., AND TSUJI, Y. *Multiphase flows with droplets and particles*. CRC press, 2011.
- [32] E, W. *Principles of Multiscale Modeling*. Cambridge University Press, 2011.
- [33] E, W., AND ENGQUIST, B. The Heterogeneous Multiscale Methods. *Comm. Math. Sci.* 1, 1 (2003), 87–132.
- [34] E, W., ENGQUIST, B., LI, X., REN, W., AND VANDEN-EIJNDEN, E. Heterogeneous Multiscale Methods : A Review. *Communications in Computational Physics* 2, 3 (2007), 367–450.
- [35] E, W., MING, P., AND ZHANG, P. Analysis of The Heterogeneous Multiscale Method for Elliptic Homogenization Problems. *Journal of the American Mathematical Society* 18, 1 (2005), 121–156.
- [36] EFENDIEV, Y., AND GALVIS, J. Coarse-grid multiscale model reduction techniques for flows in heterogeneous media and applications. *LNCSE In Numerical Analysis of Multiscale Problems* 83, September (2011).
- [37] EFENDIEV, Y., AND HOU, T. Multiscale finite element methods for porous media flows and their applications. *Applied Numerical Mathematics* 57, 5-7 (may 2007), 577–596, doi: 10.1016/j.apnum.2006.07.009.
- [38] EICKEN, H. From the microscopic, to the macroscopic, to the regional scale: growth, microstructure and properties of sea ice. In *Sea ice: An introduction to its physics, chemistry, biology and geology*. Blackwell: Oxford, UK, pp. 22–81.
- [39] ERN, A., AND GUERMOND, J.-L. *Theory and practice of finite elements*, vol. 159. Springer Science & Business Media, 2013.
- [40] EWALD, W. *From Kant to Hilbert: a source book in the foundations of mathematics*, vol. II. Oxford University Press, 2005.

- [41] EYMARD, R., AND HÉRARD, J.-M. *Finite volumes for complex applications*. John Wiley & Sons, 2008.
- [42] FAIGLE, B., HELMIG, R., AAVATSMARK, I., AND FLEMISCH, B. Efficient multiphysics modelling with adaptive grid refinement using a MPFA method. *Computational Geosciences* (2014), 625–636, doi: 10.1007/s10596-014-9407-1.
- [43] GRAHAM, I. G., HOU, T. Y., LAKKIS, O., AND SCHEICHL, R. *Numerical analysis of multiscale problems*, vol. 83. Springer Science & Business Media, 2012.
- [44] HASSANIZADEH, S. M., AND GRAY, W. G. Thermodynamic basis of capillary pressure in porous media. *Water Resources Research* 29, 10 (oct 1993), 3389, doi: 10.1029/93WR01495.
- [45] HASSARD, P. C., TURNER, I., FARRELL, T., AND LESTER, D. Simulation of micro-scale porous flow using smoothed particle hydrodynamics. *ANZIAM Journal* 56 (2016), 463–480.
- [46] HENNING, P., AND OHLBURGER, M. The heterogeneous multiscale finite element method for elliptic homogenization problems in perforated domains. *Numerische Mathematik* 113, 4 (jul 2009), 601–629, doi: 10.1007/s00211-009-0244-4.
- [47] HORNUNG, U. *Homogenization and porous media*, vol. 6. Springer Verlag, 1997.
- [48] HOU, T. Y., AND WU, X.-H. A Multiscale Finite Element Method for Elliptic Problems in Composite Materials and Porous Media. *Journal of Computational Physics* 134, 1 (jun 1997), 169–189, doi: 10.1006/jcph.1997.5682.
- [49] HUGHES, T. J., FEIJÓO, G. R., MAZZEI, L., AND QUINCY, J.-B. The variational multiscale method: a paradigm for computational mechanics. *Computer methods in applied mechanics and engineering* 166, 1 (1998), 3–24.
- [50] HUNKE, E. C., NOTZ, D., TURNER, A. K., AND VANCOPPENOLLE, M. The multiphase physics of sea ice: a review for model developers. *The Cryosphere* 5, 4 (nov 2011), 989–1009, doi: 10.5194/tc-5-989-2011.
- [51] JIANGUO, H., AND SHITONG, X. On the Finite Volume Element Method for General Self-Adjoint Elliptic Problems. *SIAM journal on numerical analysis* 35, 5 (1998), 1762–1774.
- [52] JONES, J., CAI, Z., MCCORMICK, S., AND RUSSELL, T. Control-volume mixed finite element methods. *Computational Geosciences MIX*, 97 (1997).
- [53] KEILEGAVLEN, E. *Robust control volume methods for reservoir simulation on challenging grids*. PhD thesis, 2010.
- [54] KIPPE, V., AARNES, J. E., AND LIE, K.-A. A comparison of multiscale methods for elliptic problems in porous media flow. *Computational Geosciences* 12, 3 (sep 2008), 377–398.

- [55] KLÖFKORN, R., KVASHCHUK, A., AND NOLTE, M. Comparison of linear reconstructions for second order finite volume schemes on polyhedral grids. In *ECMOR XIV-15th European Conference on the Mathematics of Oil Recovery* (2016).
- [56] KUTCHAN, B., MORAWETZ, K., AND GEMMING, S. Modeling the morphogenesis of brine channels in sea ice. *Physical Review E* 81, 3 (mar 2010), 036106, doi: 10.1103/PhysRevE.81.036106.
- [57] LARSON, M. G., AND MÅLQVIST, A. Adaptive variational multiscale methods based on a posteriori error estimation: energy norm estimates for elliptic problems. *Computer methods in applied mechanics and engineering* 196, 21 (2007), 2313–2324.
- [58] LARSON, R. G. Derivation of generalized Darcy equations for creeping flow in porous media. *Industrial & Engineering Chemistry Fundamentals* (1981), 132–137.
- [59] LEPPÄRANTA, M. *The drift of sea ice*. Springer, Berlin, Heidelberg, 2011.
- [60] LEVEQUE, R. J. *Finite Difference Methods for Differential Equations*, amath 585- ed. University of Washington, 2005.
- [61] LIE, K., MØYNER, O., NATVIG, J., KOZLOVA, A., BRATVEDT, K., WATANABE, S., AND LI, Z. Successful application of multiscale methods in a real reservoir simulator environment. In *ECMOR XIV-15th European Conference on the Mathematics of Oil Recovery* (2016).
- [62] LIE, K.-A. *An introduction to reservoir simulation using Matlab*. SINTEF ICT, 2014.
- [63] LOGG, A., MARDAL, K., AND WELLS, G. *Automated solution of differential equations by the finite element method*, vol. 84 of *Lecture Notes in Computational Science and Engineering*. Springer Berlin Heidelberg, Berlin, Heidelberg, 2012.
- [64] LUNATI, I., AND JENNY, P. Multiscale finite-volume method for compressible multiphase flow in porous media. *Journal of Computational Physics* 216, 2 (aug 2006), 616–636, doi: 10.1016/j.jcp.2006.01.001.
- [65] MANDELBROT, B. B. *The fractal geometry of nature*, vol. 173. Macmillan, 1983.
- [66] MAZZONE, D., TARDOS, G., AND PFEFFER, R. The behavior of liquid bridges between two relatively moving particles. *Powder technology* 51, 1 (1987), 71–83.
- [67] NORDBOTTEN, J. M., AND CELIA, M. A. *Geological storage of CO<sub>2</sub>: modeling approaches for large-scale simulation*. John Wiley & Sons, 2011.
- [68] PAVLIOTIS, G. A., AND STUART, A. *Multiscale methods: averaging and homogenization*. Springer Science & Business Media, 2008.
- [69] PEPPIN, S. S. L., HUPPERT, H. E., AND WORSTER, M. G. Steady-state solidification of aqueous ammonium chloride. *Journal of Fluid Mechanics* 599 (2008), 465–476, doi: 10.1017/S0022112008000219.

- [70] PESZYNSKA, M., TRYKOZKO, A., AND SOBIESKI, W. Forchheimer law in computational and experimental studies of flow through porous media at porescale and mesoscale. *Mathematical Sciences and Applications* 32 (2010), 463–482.
- [71] RAY, N., VAN NOORDEN, T., RADU, F. A., FRIESS, W., AND KNABNER, P. Drug release from collagen matrices including an evolving microstructure. *Z. Angew. Math. Mech.* (2013), 1–12, doi: 10.1002/zamm.201200196.
- [72] RINGROSE, P., AND BENTLEY, M. *Reservoir model design*. Springer, 2015.
- [73] SANDVE, T. H. *Multiscale simulation of flow and heat transport in fractured geothermal reservoirs*. PhD thesis, 2013.
- [74] SCHEIBE, T. D., MURPHY, E. M., CHEN, X., RICE, A. K., CARROLL, K. C., PALMER, B. J., TARTAKOVSKY, A. M., BATTIATO, I., AND WOOD, B. D. An analysis platform for multiscale hydrogeologic modeling with emphasis on hybrid multiscale methods. *Groundwater* 53, 1 (2015), 38–56, doi: 10.1111/gwat.12179.
- [75] SKOGESTAD, J. O., KEILEGAVLEN, E., AND NORDBOTTEN, J. M. Two-scale preconditioning for two-phase nonlinear flows in porous media. *Transport in Porous Media* (2015), 1–19.
- [76] SMITH, B., BJORSTAD, P., AND GROPP, W. *Domain decomposition: parallel multilevel methods for elliptic partial differential equations*. Cambridge university press, 2004.
- [77] THOMS, S., KUTCHAN, B., AND MORAWETZ, K. Phase-field theory of brine entrapment in sea ice: Short-time frozen microstructures. *arXiv preprint arXiv:1405.0304* (2014).
- [78] TOMIN, P., AND LUNATI, I. Investigating Darcy-scale assumptions by means of a multiphysics algorithm. *Advances in Water Resources* (2015).
- [79] VAN DUIJN, C., KNABNER, P., AND SCHOTTING, R. An analysis of crystal dissolution fronts in flows through porous media part 2: incompatible boundary conditions. *Advances in Water Resources* 22, 1 (sep 1998), 1–16, doi: 10.1016/S0309-1708(97)00038-9.
- [80] VAN NOORDEN, T. L. Crystal precipitation and dissolution in a porous medium: effective equations and numerical experiments. *Multiscale Modeling & Simulation* 7, 3 (jan 2009), 1220–1236, doi: 10.1137/080722096.
- [81] VERFÜRTH, R. Error estimates for a mixed finite element approximation of the Stokes equations. *RAIRO. Analyse numérique* 18, 2 (1984), 175–182.
- [82] VOLLMER, V. R., SWENSON, J. B., AND PAOLA, C. An analytical solution for a Stefan problem with variable latent heat. *International Journal of Heat and Mass Transfer* 47, 24 (2004), 5387–5390, doi: 10.1016/j.ijheatmasstransfer.2004.07.007.
- [83] WENDT, J. *Computational fluid dynamics: An introduction*. Springer Science & Business Media, 2008.

- [84] WHITAKER, S. Advances in theory of fluid motion in porous media. *Industrial & Engineering Chemistry* 61, 12 (dec 1969), 14–28, doi: 10.1021/ie50720a004.
- [85] WHITAKER, S. The forchheimer equation: A theoretical development. *Transport in Porous Media* 25 (1996), 27–61.
- [86] WORSTER, M. G. The dynamics of mushy layers. In *Interactive Dynamics of Convection and Solidification*, S. H. Davis, H. E. Huppert, U. Muller, and M. G. Worster, Eds. Kluwer Academic Publishers, 1992, pp. 113–138.
- [87] WORSTER, M. G. Convection in mushy layers. *Annual Review Of Fluid Mechanics* 29 (1997), 91–122, doi: 10.1146/annurev.fluid.29.1.91.
- [88] WU, H., AND LI, R. Error estimates for finite volume element methods for general second-order elliptic problems. *Numerical Methods for Partial Differential Equations* 19, 6 (nov 2003), 693–708, doi: 10.1002/num.10068.
- [89] ZAITSEV, V., AND POLYANIN, A. *Handbook of exact solutions for ordinary differential equations*. CRC Press, 2002.
- [90] ZARBA, R. L., BOULOUTAS, E., AND CELIA, M. General mass-conservative numerical solution for the unsaturated flow equation. *Water Resources Research WRERAQ* 26, 7 (1990), 1483–1496.



# **Chapter 6**

## **Included papers**



# Paper A

## 6.1 Multiscale simulation of non-Darcy flows

S. ALYAEV, E. KEILEGAVLEN, AND J.M. NORDBOTTEN

In *Proceedings of the XIX Computational Methods in Water Resources, CMWR 2012* (University of Illinois at Urbana-Champaign, June 17 - 21, 2012).



## MULTISCALE SIMULATION OF NON-DARCY FLOWS

Sergey Alyaev<sup>\*†</sup>, Eirik Keilegavlen\* and Jan M. Nordbotten\*

<sup>\*</sup>University of Bergen  
 Department of Mathematics  
 Postboks 7803, 5020 Bergen, Norway  
 web page: <http://www.uib.no/math/en>  
<sup>†</sup>e-mail: Sergey.Alyaev@math.uib.no

**Key words:** multiscale modelling, pore scale, control volume method, Navier-Stokes

**Summary.** In this work we present control volume multiscale methods which address problems on the interaction between pore scale and Darcy scale. For the case when linear equations govern the flow on the pore scale our solution converges to semi-analytical solution. Moreover, the method also extends to non-linear problems governed by Navier-Stokes equations. We show numerical results illustrating the applicability of the method.

### 1 INTRODUCTION

The standard way of modelling flow in porous media includes applying Darcy's law. Initially, this constitutive equation was phenomenologically derived in the middle of 19th century. In the 20th century it was also shown that under particular assumptions one can derive it from the Stokes equations on porous geometry<sup>2</sup>. Stokes equations, however, rely on several assumptions and are just a linear simplification of full physical problem on the fine scale. If non-linear Navier-Stokes terms are introduced on the pore scale, Darcy's law is amended with non-linear terms. The applications where we can come across such effects are flows that may occur near wells and in fractured regions in subsurface. Moreover, those flows are common for industrial and near-surface porous media.

To obtain the flux expression on Darcy (coarse) scale a multiscale modelling can be applied. The traditional derivations of Darcy type relations on the coarse scale achieve this by homogenization. From the above discussion, we understand that this approach relies on a priory assumptions of the nature of the fine scale flow. Furthermore, since homogenization yields a one-way upscaling, possible feedback from the coarse scale to the fine scale cannot be captured.

As an alternative, we present a multiscale method that for the coarse scale assumes only mass conservation on control volumes, that is, no phenomenological relationships are assumed a priory. The method is designed in the framework of the Heterogeneous Multiscale Methods (HMM) proposed by E and Engquist<sup>4</sup>. Additional information needed, such as a relationship between coarse scale pressure and fluxes, is obtained by locally

---

Sergey Alyaev, Eirik Keilegavlen and Jan M. Nordbotten

---

solving continuum mechanics' equations on the pore scale. While the fine scale solver accounts for non-linear effects of the pore scale, the coarse solver takes care of slowly varying effective parameters.

The advantage of our HMM is that it converges to the correct upscaled solution derived by homogenization when the equations are essentially linear. Moreover, it gives flexibility of solving a wider range of problems, for which we cannot access the exact solution, without any need of additional user participation. As our method extends naturally to this variety of problems and, hence, should give a reasonable approximation that is better than a solution for a simplified model.

HMMs of such kind were considered previously; in particular, a control volume HMM formulation was considered by Abdulle and E<sup>1</sup>. Our method, however, is different not only in the fine scale problem but also in that it treats discontinuities more consistently as it is described in Sect. 3.2.

This paper presents an HMM for the problems of interaction between pore scale and Darcy scale. Our HMM is formulated on the coarse scale as a control volume method consistent with two-point flux approximation. The paper sketches the method algorithm and describes possible ways to optimize it.

Our numerical results test the algorithm for various aspects:

- convergence to semi-analytical homogenisation solution for linear flow regime;
- handling of heterogeneous porous media with discontinuities;
- difference of the presented method to linearised problems for non-linear regimes.

## 2 MODEL PROBLEM

The goal of our work is to investigate how the HMM framework can produce a solution to the coarse scale problem that accounts for the interplay between the coarse and the fine scale. As a model problems we choose an artificial pore structure that is periodic on macro subdomains. For simplicity only 2D porous media are considered, and the upscaled permeability is assumed to be aligned with the coarse grid.

For the coarse scale we only use the (physically justified) continuity equation that provides mass conservation. We consider both problems with incompressible flow,

$$\nabla \cdot \vec{u} = f, \quad (1a)$$

and weakly compressible flow on the form

$$\begin{aligned} \phi p_t + \nabla \cdot \vec{u} &= f, \\ \rho_p &= c\rho. \end{aligned} \quad (1b)$$

In the equations above  $\vec{u}$  is flux density vector,  $f$  is the mass source,  $p$  is the pressure,  $\rho$  is density,  $\phi$  is the porosity, and  $c$  is compressibility.

Sergey Alyaev, Eirik Keilegavlen and Jan M. Nordbotten

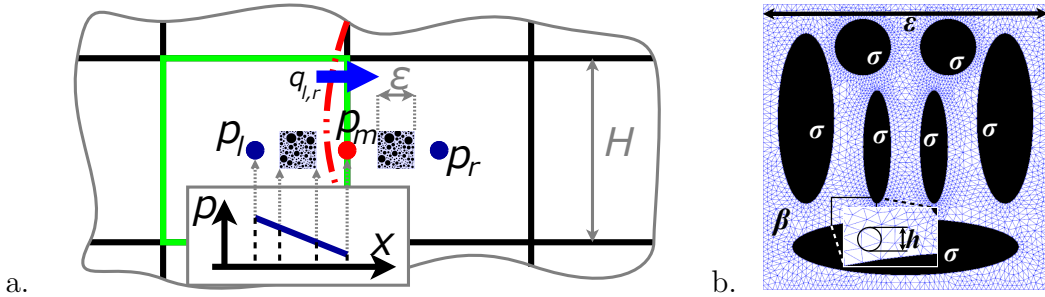


Figure 1: Building blocks of the multiscale method from the coarse grid perspective (a) and an example of a fine scale cell problem with triangulation (b).

As for the fine scale we study the Navier-Stokes equations on porous geometries like on Fig. 1b. The governing equations in this case are (1a) and

$$\rho \vec{u} \cdot \nabla \vec{u} = -\nabla p + \mu \Delta \vec{u} + \vec{g}, \quad (2)$$

where  $\mu$  is viscosity,  $\vec{u}$  is velocity and  $\vec{g}$  represents body forces. Time dependent terms are omitted from the equations (1a,2) since we will only consider fine scale sub-problems that equilibrate much faster than the typical time scale of the coarse problem. For analysis purposes we will also consider Stokes equation, which is obtained by setting  $\rho \vec{u} \cdot \nabla \vec{u} = 0$  in (2).

### 3 DESCRIPTION OF THE MULTISCALE METHOD

The method is formulated within the HMM framework<sup>4</sup>. To describe the method one should choose a fine scale method, a coarse method and operators to project information between the two. This section describes our choice of method's components.

#### 3.1 The coarse scale control volume method

The coarse scale equation is discretized by a two-point-flux-style control volume method. The unknowns are pressures in the cell centers denoted  $p_l$  and  $p_r$  on Fig. 1a. Along with the cell center pressures, auxiliary variables  $q_{l,r}$  denoting fluxes between neighbouring cells are considered. The method ensures local mass conservation, in other words for each cell it satisfies

$$\frac{d}{dt} \int_{\tau_l} \rho_l \phi dx + \oint_{\partial \tau_l} \rho \vec{u} \cdot \vec{n} ds = \int_{\tau_l} f dx, \quad (3)$$

where  $\partial \tau_l$  is the border of the cell  $\tau_l$  and  $\vec{n}$  is an outgoing unit normal. As we are using the simplified continuity equations (1) the method will ensure that the corresponding equation is satisfied locally in the integral sense instead; for (1b) it takes the form:

$$\frac{d}{dt} \int_{\tau_l} p_l \phi dx + \oint_{\partial \tau_l} \vec{u} \cdot \vec{n} ds = \int_{\tau_l} f dx. \quad (4)$$

The second term is nothing more than a sum of fluxes (such as  $q_{l,r}$ ) over all edges of  $\tau_l$ .

As previously mentioned the constitutive relationship between primary pressure variable and fluxes are not known a priori. The fluxes  $q_{l,r}$  can be found from a formal relationship

$$q_{l,r} = F(\vec{x}_l, \vec{x}_r, p_l, p_r, \rho_l, \rho_r) \quad (5)$$

by interpolating information from fine scale problems. Here,  $\vec{x}$  is the coordinate and subscripts denote the cells.

Before projecting coarse scale pressures to the fine scale, an auxiliary pressure  $p_m$  is introduced on all edges. Then we interpolate linearly between  $p_l$  and  $p_m$  and project the pressure values to form boundary conditions of the fine scale problem at point  $(\vec{x}_m + \vec{x}_l)/2$  as shown on Fig. 1a. After solving the fine scale problem (see remark 1) we integrate the component of the velocity that is parallel to the flow direction  $(\vec{x}_m - \vec{x}_l)$  across the cell and obtain  $q_{l,m}$  by scaling the result (see also remark 2).

In order to omit  $p_m$  and hence obtain  $q_{l,r}$  we solve the equation  $q_{l,m} = q_{l,r} = q_{m,r}$ , that is coupled naturally to the two fine scale problems associated with the coarse edge; see Fig. 1a. This equation is true under the assumption that for this local coarse problem the flow is only happening between the cells  $l$  and  $r$  driven by the corresponding pressures and  $\rho$  is constant, i.e. (1a) is valid.

Equipped with flux expressions on each edge, one can perform coarse scale time stepping, discretizing equation in time by backward Euler or solve the system by the Newton method for the stationary case.

**Remark 1 : Fine scale.** *We define our fine scale problem as a PDE on a domain, that for simplicity is taken to be a square. The size of this square is equal to the period of the porous media  $\varepsilon$ , and it is positioned around the coarse sampling point. In homogenization, this fine scale problem is referred to as a cell problem.*

*The boundary conditions for velocity are: no flow in the solid grains  $\sigma$  and on their boundaries, and periodicity on the square edges; see Fig. 1b. Pressure is also periodically transversal to the flow and has a jump of a given  $\Delta p$  in the direction of the flow. This boundary value problem is consistent with the homogenization cell problem for Stokes flow (see Sect. 4.1 for more details).*

*To solve the fine scale problem we use the lowest order Taylor-Hood finite element method on a triangular grid (see Fig. 1b) as implemented in FEniCs<sup>5</sup>.*

---

Sergey Alyaev, Eirik Keilegavlen and Jan M. Nordbotten

---

**Remark 2 : Optimization of the algorithm.** *In order to reduce the total computational time we reuse fine scale computations if possible. If for a given cell problem  $\alpha$  and pressure drop  $p$  we have computed  $F_\alpha(p_0)$  and  $F_\alpha(p_1)$ , such that  $p_0 \leq p \leq p_1$  and  $|F_\alpha(p_1) - F_\alpha(p_0)| < \delta$  then we approximate  $F_\alpha(p)$  by linear interpolation between the two values. In the case where no information is available an on-demand solver is invoked for the fine scale problem and the resulting flux is stored for future use.*

We can also reduce the computational cost by reformulating half of the original problem (5)  $F(\vec{x}_l, p_l, \rho_l)$  to a one parametric dimensionless problem  $F_\alpha(\tilde{p})$  where  $\alpha$  corresponds to geometry in point  $\vec{x}_l$ . The resulting problem can be solved by techniques described in this remark.

### 3.2 Handling discontinuities

The method proposed in this paper differs from the control volume HMM proposed earlier, e.g. by Abdulle and E<sup>1</sup>, in how the coarse scale sampling is performed. In<sup>1</sup>, the sampling domains are located in the middle of the border between coarse cells. In contrast, we use two domains, one in each cell, between the center of the cell and the center of the considered border. The old approach resembles control volume finite elements, whereas our approach coincides with two-point flux approximation.

For problems with continuous parameter fields both methods perform similarly, and our method tends to be slower due to more sampling points. The extra sampling points are however necessary to get a proper coarse flux expression for porous media with discontinuities.

It is natural to assume that the discontinuities can be resolved by the coarse grid in average (see the red line on Fig. 1a). A perturbation of order  $\varepsilon \ll H$  in the interface can cause the old method to give an arbitrary wrong sample. For the problems where the scale of discontinuities is small (of order  $l$ ) or where the grid is non-uniform the old approach will give an error of order  $H/l$ . Our approach however will give an error that is only proportional to the  $\varepsilon$  perturbation of discontinuity; thus this sampling strategy is superior to using a single point only.

## 4 NUMERICAL EXPERIMENTS

Numerical experiments presented below show applicability of the discussed method. In Sect. 4.1 it is shown that our method converges to homogenization solution for Stokes flow. In Sect. 4.2 we show full flexibility of the proposed method on a heterogeneous domain with discontinuity using realistic parameters. The final example demonstrates the importance of using a non-linear approximation on the fine scale and relates it to various applications.

### 4.1 Verification of convergence for the Stokes flow

For method validation, it is of interest to verify that the multiscale method gives correct result to problems with a well known solution. In the paper Alyaev et al<sup>3</sup>, an a priori error

Sergey Alyaev, Eirik Keilegavlen and Jan M. Nordbotten

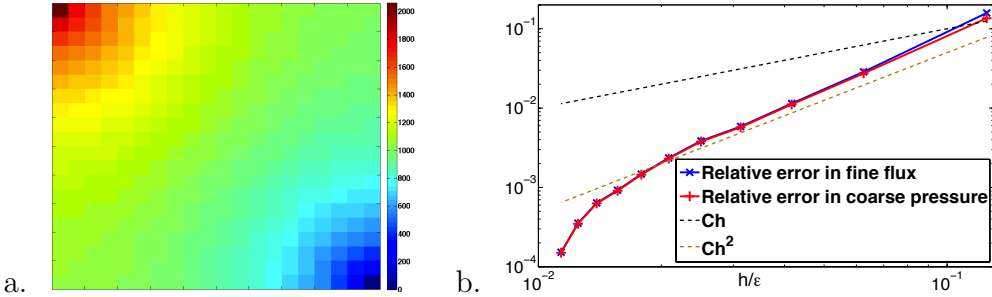


Figure 2: A coarse scale pressure solution to a linear problem (a) and convergence of solution to the reference (b).

estimate for the HMM described here is proved for the case of incompressible Stokes-type flow. The error between the homogenization solution<sup>2</sup> and the fully discrete solution has the form

$$\left\| p - p_{MS}^{H,h} \right\|_{L^2} \leq C \left( \left( \frac{h}{\varepsilon} \right)^\alpha + H \right), \quad (6)$$

where the terms represent the propagation of the fine scale error and the coarse scale error respectively. The sizes involved in (6) are shown on Figures 1a and 1b:  $H$  is the coarse cell size,  $\varepsilon$  is the period of the porous medium and  $h$  is the fine grid size. The parameter  $1 \leq \alpha < 2$  comes from the estimate for Taylor-Hood elements for Stokes problem and depends on the cell geometry<sup>6</sup>. The analysis<sup>3</sup> shows that the coarse scale error in the pressure is proportional to the fine scale error in velocity that is  $C(h/\varepsilon)^\alpha$ . The coarse scale error is the error of the two-point flux approximation, which is well analysed and verified in the literature.

Here we present a verification of the propagation of the fine scale error specific for this method. We consider a quarter of a 5-well problem and look for a coarse scale solution in a square domain with no-flow Neumann boundary conditions except for the right-bottom cell that has zero Dirichlet condition (Fig. 2a). In the top-left corner cell the forcing term is introduced. The fine scale structure is taken from Fig. 1b. For the comparison  $H$  and  $\varepsilon$  are fixed. We consider the relative error between solution on  $h$  grid and a reference grid with very small cells. Figure 2b shows that the  $L^2$  error in coarse scale pressure is indeed proportional to the error in the coarse flux and the rate of convergence is not lower than expected ( $\alpha \approx 2$  for our geometry Fig. 1b).

## 4.2 Non-linear compressible flow in heterogeneous media

This numerical example shows the full potential of the HMM described in this paper. We consider weakly compressible non-Darcy flow of water in the domain consisting of 2 regions: a low permeable region with anisotropic porous structure as on Fig. 1b in the middle and an isotropic high permeable region made of circular grains in the square

Sergey Alyaev, Eirik Keilegavlen and Jan M. Nordbotten

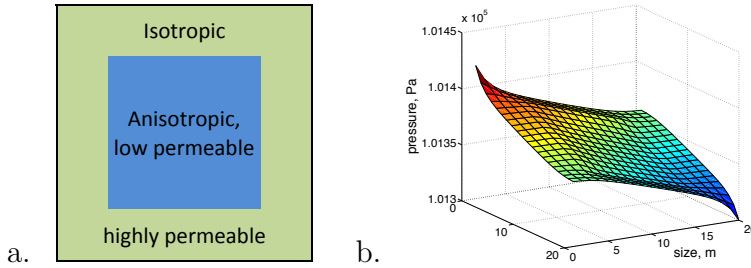


Figure 3: Permeability field structure (a) and a solution after a number of time steps (b) for the heterogeneous problem.

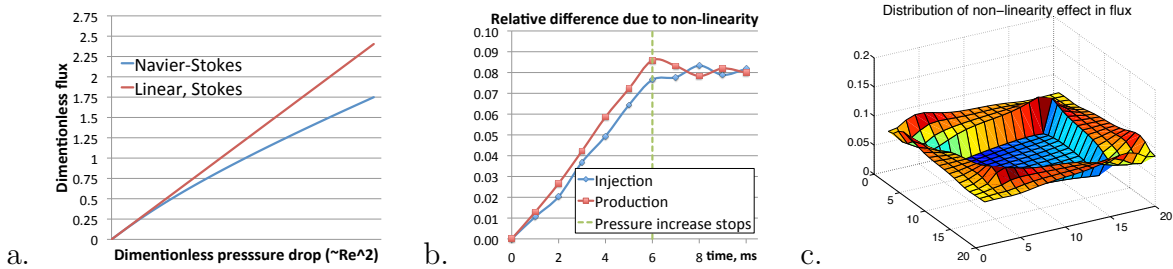


Figure 4: Comparison of linear and non-linear fluxes for the cell problem on Fig. 1b (a), dynamics of injection and production error in time for the linear approximation (b) and spatial distribution of relative non-linearity effect in flux for the heterogeneous example (c).

arrangement forming a frame; see Fig. 3a. In analogy to the previous example we place an injector in one corner and a producer in the opposite corner. The pressure in the producer increases linearly in time for a number of steps and then remains constant.

Figure 3b shows a solution before injection stops. There are 3 noticeable features of the solution: fast decrease of pressure around the injector before the low permeable region (forming a peak) with a little build-up on the border of it; almost linear variation within the low-permeable region; and a smaller (due to compressibility) negative peak in the production point.

To investigate the importance of non-linearities on the fine scale, we first consider the coarse flux as a function of the pressure drop over a single edge when the pore geometry is as shown in Fig. 1b. Figure 4a shows the dependency of the non-dimensional mean flux to the non-dimensional pressure drop, that can be interpreted as a scaled Reynolds number squared. As seen from the figure the difference between the linear approximation and the true flux reaches 35% even in the non-turbulent stationary regime.

Next, let us consider again the problem from Fig. 3 and compare it to the same problem but with linear flux approximation. Fig. 4b shows how the deviation in the injection and production will evolve in time. As expected higher pressure drop results in higher influence of the non-linear flow on the fine scale, and which persists after the solution reaches steady-state. For this problem the linear constitutive law overestimates the production by almost

10% which can be crucial for applications such as oil recovery.

Finally, we consider the spatial distribution of the error when using a linear flux relation for the heterogeneous example. Fig. 4c shows the relative magnitude of the difference between a linear approximation and the true flux. As expected, the non-linear effects are largest near the injection and production wells, where the pressure drop is highest. Predictably, error is also significant throughout high permeable channels forming the outer part of the domain, in particular there are large errors close to the boundary between the two permeability regions. Comparing with Fig. 3, we see that non-linear flux effects can be important not only in regions with large pressure drops, but also close to material discontinuities, where flow focusing may occur. The small error in the low permeable region was to be expected, since the pressure drop is much smaller there.

## 5 CONCLUSIONS

We have presented a new control volume multiscale method for handling effects on the pore and Darcy scale. The method utilizes either Stokes or Navier-Stokes formulations of the fine scale problem, coupled with an incompressible or weakly compressible conservation law on the coarse scale. The coarse-scale fluxes are treated by a multi-scale extension of the standard two-point flux approximation, and this makes the scheme capable of handling discontinuities that are resolved by the coarse grid.

Our numerical results verify analytically obtained convergence estimates of the method for problems where a homogenized coarse-scale formulation is known. Furthermore, we illustrate the applicability of the method to non-linear flows on heterogeneous domains, observing that non-linear flow formulations may be of importance not only near wells, but also in regions where high flow rates are induced by material heterogeneities.

## REFERENCES

- [1] A. Abdulle and W. E. Finite difference heterogeneous multi-scale method for homogenization problems. *Journal of Computational Physics*, 191(1):18–39, Oct. 2003.
- [2] G. Allaire. One-Phase Newtonian Flow. In U. Hornung, editor, *Homogenization and Porous Media*, chapter 3, pages 45–68. Springer, New York, 1996.
- [3] S. Alyaev, J. M. Nordbotten, and E. Keilegavlen. Convergence analysis of HMM for single phase flow in porous media. *In preparation*.
- [4] W. E and B. Engquist. The Heterogeneous Multiscale Methods. *Comm. Math. Sci.*, 1(1):87–132, 2003.
- [5] A. Logg, K.-A. Mardal, G. N. Wells, et al. *Automated Solution of Differential Equations by the Finite Element Method*. Springer, 2012.
- [6] R. Verfürth. Error estimates for a mixed finite element approximation of the Stokes equations. *RAIRO. Analyse numérique*, 18(2):175–182, 1984.

# Paper B

## 6.2 Analysis of control volume heterogeneous multiscale methods for single phase flow in porous media

S. ALYAEV, E. KEILEGAVLEN, AND J.M. NORDBOTTEN

*Multiscale Modeling & Simulation* 12, 1 (2014), 335–363.<sup>1</sup>

doi: 10.1137/120885541

---

<sup>1</sup>First published in *Multiscale Modeling & Simulation* in volume 12 issue 1, published by the Society for Industrial and Applied Mathematics (SIAM). ©2014 Society for Industrial and Applied Mathematics.



**ANALYSIS OF CONTROL VOLUME HETEROGENEOUS MULTISCALE METHODS FOR SINGLE PHASE FLOW IN POROUS MEDIA\***SERGEY ALYAEV<sup>†</sup>, EIRIK KEILEGAVLEN<sup>†</sup>, AND JAN MARTIN NORDBOTTEN<sup>†</sup>

**Abstract.** The standard approximation for the flow-pressure relationship in porous media is Darcy’s law that was originally derived for infiltration of water in fine homogeneous sands. Ever since there have been numerous attempts to generalize it for handling more complex flows. Those include upscaling of standard continuum mechanics flow equations from the fine scale. In this work we present a heterogeneous multiscale method that utilizes fine scale information directly to solve problems for general single phase flow on the Darcy scale. On the coarse scale it only assumes mathematically justified conservation of mass on control volumes, that is, no phenomenological Darcy-type relationship for velocity is presumed. The fluid fluxes are instead provided by a fine scale Navier–Stokes mixed finite element solver. This work also considers several choices of quadrature for data estimation in the multiscale method and compares them. We prove that for an essentially linear regime, when the fine scale is governed by Stokes flow, our method converges to a rigorously derived homogenization solution—Darcy’s law. Moreover the method gives the flexibility to solve problems with faster nonlinear flow regimes that is important in a number of applications, such as flows that may occur near wells and in fractured regions in subsurface. Those flows are also common for industrial and near surface porous media. The numerical examples presented in the paper verify the estimate and emphasize the importance of good data estimation.

**Key words.** control volume method, heterogeneous multiscale method, a priori estimate**AMS subject classifications.** 76S05, 34E13, 35B45, 65N08, 74Q05, 74Q15**DOI.** 10.1137/120885541

**1. Introduction.** Flow in porous media models several physical phenomena of great practical importance, spanning flow in natural geological systems to anthropogenic materials such as fuel cells or human tissue. At the same time, the rigorous description of the continuum scale equations, here referring to the scale where the porous structure is not resolved, has remained elusive for all but the simplest systems. Spanning research from the engineering to applied sciences, it remains one of the fundamentally unresolved cross-disciplinary challenges.

At the porous scale, the governing equations are well understood as those of fluids and solids with appropriate interface conditions. In this setting, one may allow for multiple fluid phases, as well as deformation of the porous material. However, the challenging geometry of the pore space coupled with the large length scales required by applications prohibits the use of direct numerical simulation on this scale.

The first continuum scale description was brought by the experimental result known as Darcy’s law valid for slow single phase flows in homogeneous media. In the theoretical setting, a long history of works have set out to establish continuum

---

\*Received by the editors July 23, 2012; accepted for publication (in revised form) November 26, 2013; published electronically March 18, 2014. This work has been done as a result of the Special Semester on Multiscale Simulation and Analysis in Energy and the Environment (October 3–December 16, 2011) organized by RICAM (Johann Radon Institute for Computational and Applied Mathematics, Austrian Academy of Science) Linz, Austria. The research of the authors receives financial support from The Research Council of Norway under grant 180679.

<http://www.siam.org/journals/mms/12-1/88554.html>

<sup>†</sup>University of Bergen, Department of Mathematics, Postboks 7803, NO-5020 Bergen (Sergey.Alyaev@math.uib.no, Eirik.Keilegavlen@uib.no, Jan.Nordbotten@math.uib.no).

relationships based on derivations from the pore scale which validated and extended Darcy's law (see, e.g., [27, 11, 36, 25, 26, 14]). While in all these works the derivation of the continuum conservation principles is relatively straightforward, the closure relationships almost uniformly lack analytical treatment. Furthermore, as one considers more complex flows, the derivations become largely untenable and for some cases it is not possible to achieve full decoupling [26].

This has led to a situation where two scale models have gained increased attention as a way to handle potentially complex porous media systems. To some extent, this can be seen in the development of general frameworks for two-level couplings (see, e.g., [10, 20, 29, 13, 18]), but also particular implementations tailored to porous media (see, e.g., [37, 22, 32, 28, 16, 8, 15]). Of particular interest to us is the work related to implementation of the heterogeneous multiscale method (HMM) framework (such as [5, 16, 8, 15]).

In this communication, we give a more thorough description of a new way to implement the HMM framework in the setting of control volume discretizations for the continuum conservation equation that was introduced in [8], that we refer to as control volume heterogeneous multiscale method (CVHMM). Our approach takes advantage of the mathematically justified continuity equation on the coarse scale and uses the full solution of the Navier–Stokes equations on perforated domains at the pore scale to recover constitutive relations. Such design makes the method capable of handling single-phase flow in porous media for arbitrary flow rates, thus extending beyond the validity of Darcy's law. Of importance, in the limit of low flow rates, the classical results are recovered.

An alternative approach is discussed in the work of Chu et al. [16] (and [15] that extends it) where for local computation, pore network modeling is performed. Instead of having an extra procedure of deriving a pore network possessing the same properties as the actual pore structure we do simulations directly on the porous geometry, hence, avoiding errors caused by network reconstruction but paying the price of more expensive fine scale computations. For problems where the details of the pore geometry become important, e.g., for nonlinear flows or more general problems involving deformation of the porous geometry, the direct treatment of the pore space as presented herein will be more accurate than the idealized network approaches.

In this work we propose two choices of the quadrature points. The first one follows [6, 16] and mimics control volume finite element methods. The second novel choice is more in the spirit of classical flux approximation schemes, wherein it preserves harmonic averages at the coarse scale, and thus is more robust to material discontinuities.

We complement the new method with a priori convergence analysis for the essentially linear flows. Our analysis follows the layout suggested by E, Ming, and Zhang in [21] and later developed for a fully discrete finite element framework by Abdulle [4, 5]. Here it is specifically adapted to the particular setting of finite volume discretization, such as presented in [12]. Furthermore, our analysis departs from Abdulle in the particular grouping of error terms. The analysis also differs from most of the previous work since in our case we have different problem formulations on different scales.

The remainder of the paper is structured as follows: In the next section, the model problem is established. In section 3, we define the method. After putting some additional assumptions on the method in section 4, the proof of an a priori estimate for the linear regime is presented in section 5, followed by section 6 containing observations regarding extensions of the analysis to nonlinear cases. After numerical examples in section 7 the paper is concluded by section 8.

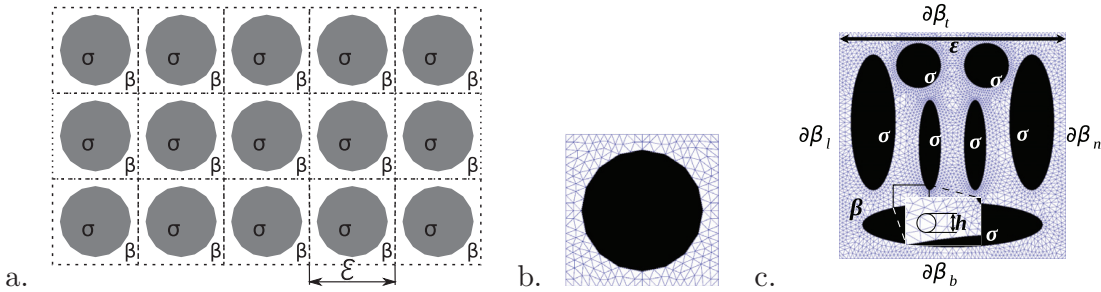


FIG. 1. A simple periodic structure forming a coarse scale domain (a) and triangulation of a simple (b) and a more complex (c) cell problem.

**2. Model problem.** The focus of this paper is the interplay between pore scale and Darcy scale. In this section we introduce model equations and briefly review a relation between the scales that can be derived by homogenization.

**2.1. Model equations.** On the pore scale the motion of fluids is governed by Navier–Stokes equations which for the incompressible case look as follows:

$$(2.1a) \quad \nabla \cdot \vec{v}^\varepsilon = 0,$$

$$(2.1b) \quad \rho \left( \frac{\partial \vec{v}^\varepsilon}{\partial t} + \vec{v}^\varepsilon \cdot \nabla \vec{v}^\varepsilon \right) = -\nabla p^\varepsilon + \mu \nabla^2 \vec{v}^\varepsilon + \vec{f}.$$

Here  $\vec{v}^\varepsilon$  is fluid velocity,  $p^\varepsilon$  is the pressure associated with the fine scale ( $\varepsilon$  indicates the exact solution of the full fine scale problem),  $\rho$  is the constant fluid density,  $\mu$  is viscosity,  $t$  is time and  $\vec{f}$  is volumetric forces. These equations are valid in the pore volume inside the pore geometry the example of which is shown on Figure 1 and marked by  $\beta$ . Darker areas on Figure 1, marked by  $\sigma$ , represent the solid impermeable grains; in those areas and on their boundary there is no flow or

$$(2.2) \quad \vec{v}^\varepsilon = \vec{0}.$$

It is convenient to picture porous media as being combined of the “cells” of size  $\varepsilon$  as on Figure 1.

The coarse scale flux density  $\vec{v}$  (defined as integrated velocity) is assumed to fulfill the continuity equation

$$(2.3) \quad \nabla \cdot \vec{v} = f,$$

where  $f$  is a source/sink term. Furthermore, we assume a relationship between the coarse pressure and flux density of the form

$$(2.4) \quad \vec{v}(\vec{x}) = \vec{F}(\nabla p(\vec{x}), \vec{x}).$$

We note that this formulation includes the well-known linear relation between the flux and the pressure gradient referred to as Darcy’s law,

$$(2.5) \quad \vec{v} = -\frac{K}{\mu} \nabla p,$$

where the resistivity coefficient  $K$  is called the permeability. However the expression for  $\vec{F}$  is more general as it also includes the cases of nonlinear relationships such as the Dupuit–Forchheimer–Ergun law.

**2.2. Homogenization solution of the fine scale problem.** Using homogenization theory, the Darcy relationship (2.5) can be rigorously derived from the fine scale equations (2.1) under the assumptions of scale separation and essential linearity. Consider a Navier–Stokes problem with scaling of the terms suitable for homogenization and numerical upscaling in porous media:

$$(2.6) \quad \begin{cases} \varepsilon^\gamma \vec{v}^\varepsilon \cdot \nabla \vec{v}^\varepsilon + \nabla p^\varepsilon - \varepsilon^2 \mu \Delta \vec{v}^\varepsilon = \vec{f} & \text{in } \Omega^\varepsilon, \\ \nabla \cdot \vec{v}^\varepsilon = 0 & \text{in } \Omega^\varepsilon, \\ \vec{v}^\varepsilon = 0 & \text{on } \partial \Omega^\varepsilon, \end{cases}$$

where  $\Omega^\varepsilon$  is the coarse domain  $\Omega$  without the solid part. The parameter  $\gamma$  determines the strength of nonlinearity, smaller  $\gamma$  corresponds to larger nonlinearity. So, for  $\gamma = \infty$  the equation is reduced to Stokes equation.

In [7, Thm. 1.1, p. 46; Thm. 2.4, p. 59; Thm. 2.5, p. 60] the following theorems are proved.

**THEOREM 2.1.** *For  $\gamma > 1$  and  $\varepsilon \rightarrow 0$  there exists a homogenized solution for (2.6)*

$$(2.7a) \quad \begin{cases} \vec{v} = \frac{1}{\mu} K (\vec{f} - \nabla p) & \text{in } \Omega, \\ \nabla \cdot \vec{v} = 0 & \text{in } \Omega, \\ \vec{v} \cdot \vec{n} = 0 & \text{on } \partial \Omega, \end{cases}$$

$$(2.7b) \quad K_{ij} = \int_\beta \nabla \vec{u}_i \cdot \nabla \vec{u}_j dy,$$

$$(2.7c) \quad \begin{cases} \nabla \pi_i - \Delta \vec{u}_i = \vec{e}_i & \text{in } \beta, \\ \nabla \cdot \vec{u}_i = 0 & \text{in } \beta, \\ \vec{u}_i = 0 & \text{in } \bar{\sigma}, \\ \pi_i, \vec{u}_i, & y\text{-periodic,} \end{cases}$$

where  $\beta$  is the porous part of the unit square domain where the fluid can flow, and  $\sigma$  is solid.  $\beta \cup \bar{\sigma}$  forms the periodic unit cell scaled to a unit square; see Figure 1. Scaling introduced in (2.6) results in  $K$  in (2.7) being the nondimensional permeability (see, e.g., [34]).

**THEOREM 2.2.** *For  $\gamma = 1$  and  $\varepsilon \rightarrow 0$  there exists a homogenized solution for (2.6):*

$$(2.8a) \quad \nabla_y p_1 + \vec{v}_0 \cdot \nabla_y v_0 - \mu \nabla_y^2 \vec{v}_0 = \vec{f}(\vec{x}) - \nabla p(\vec{x}) \quad \text{in } \beta \times \Omega,$$

$$(2.8b) \quad \nabla_y \cdot \vec{v}_0 = 0 \quad \text{in } \beta \times \Omega,$$

$$(2.8c) \quad \nabla_x \cdot \vec{v} = 0 \quad \text{in } \Omega,$$

$$(2.8d) \quad \vec{v} \cdot \vec{n} = 0 \quad \text{on } \partial \Omega,$$

$$(2.8e) \quad \vec{v}_0, p_1, \quad y\text{-periodic,}$$

$$(2.8f) \quad \vec{v} = \int_\beta \vec{v}_0 dy,$$

where notation from Theorem 2.1 is used; in addition,  $y$  represents the fast periodic variable and  $\vec{v}_0$  and  $p_1$  are auxiliary variables that for this truly nonlinear case cannot be decoupled.

In the next section we will introduce a numerical method that can handle cases without separation of scales and nonperiodic media. The above theorems will serve as a useful benchmark for this numerical scheme when the corresponding assumptions are satisfied.

**3. Method description.** In this section we describe a method to compute the flux expression (2.4) by using multiscale techniques. The method is formulated in the framework of the HMM [19] to which we first give a brief introduction.

**3.1. The HMM.** An HMM for a two scale problem considers two sets of equations:

- coarse scale:  $F(\mathbf{U}, \mathbf{D}) = 0$ ;
- fine scale:  $f(\mathbf{u}, b) = 0$ .

Here  $\mathbf{U}$  and  $\mathbf{u}$  are the functions that we are seeking the solution for, while  $\mathbf{D}$  and  $b$  are data. Unknown quantities are marked as bold and, crucially, the coarse scale equation contains unknown data  $\mathbf{D}$ . In the HMM framework the aim is to solve the coarse equation, and to obtain necessary information on  $\mathbf{D}$  by solving localized fine scale problems. Thus together with the equations one should specify operators to transfer information between the two scales. This involves both constraints to formulate local fine scale problems based on the coarse state and data estimation to recover coarse scale data from the solution of the fine scale problem.

**3.2. The HMM for flow in porous media.** To apply HMM to the problem outlined in section 2, discretization must be specified on both the coarse and the fine scale, as well as transfer operators between the scales.

**3.2.1. Coarse scale discretization.** To preserve conservation of mass the coarse continuity equation is discretized by a control volume method. For convenience of proofs in this paper we choose a control volume finite element formulation, although the methodology can be applied to more general control volume methods. Thus the coarse problem can be formulated as the following.

PROBLEM 3.1. Consider a problem on a coarse domain  $\Omega$ . Find  $p$ , such that for all Lipschitz subdomains  $\tau \subset \Omega$

$$(3.1) \quad \int_{\partial\tau} \vec{F}(\nabla p, \vec{x}) \cdot \vec{n} ds = \int_{\tau} f dx,$$

where  $\vec{n}$  is the outward pointing normal and  $f$  is the function that represents the volumetric source density inside  $\tau$ .

The operator  $\vec{F}$  in terms of HMM is the data estimation operator.

To proceed to a numerical method we introduce a triangulation (with no loss of generality we describe the two-dimensional (2D) version of the algorithm); see Figure 2. The pressure is represented by a linear function on each triangle, and it can thus be represented by its value in the vertexes. The control volume grid is the Voronoi diagram that is dual to the triangulation (marked by red on Figure 2). We require that (3.1) is satisfied for all triangles in the grid (replacing  $\tau$ ). However instead of computing  $\vec{F}(\nabla p, \vec{x})$  purely on the coarse scale by introducing, e.g., a Darcy relationship between the flux and the pressure gradient, the flux is estimated by solving a fine scale problem around a quadrature point on an edge of the triangle. To define this fine scale problem, we must first define a projection of the coarse pressure onto the fine scale.

**3.2.2. Transfer from coarse to fine scale problem.** Since the coarse scale flux is driven by pressure differences, as indicated by the functional form  $\vec{F}(\nabla p, \vec{x})$ , the fine scale problem should be formulated to account for this pressure difference. A natural way of projecting the coarse pressure difference onto the fine scale is to adjust the fine scale boundary conditions. Consider a local crop of the coarse scale grid as

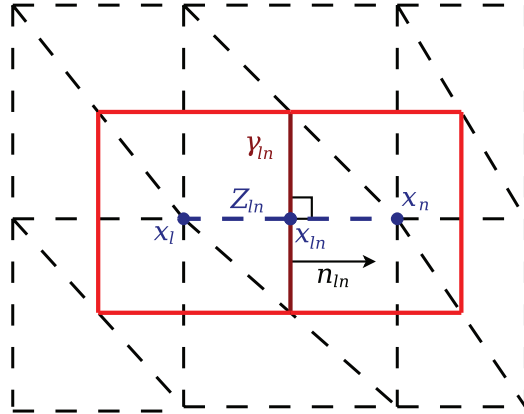


FIG. 2. The structure of finite element grid (dashed lines) and the Voronoi finite volume grid dual to it (solid lines).

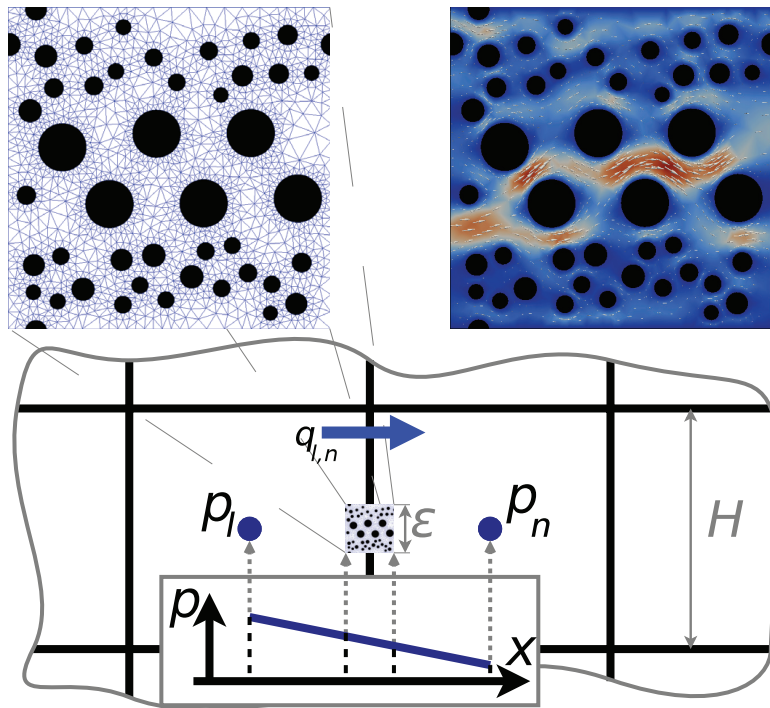


FIG. 3. Building blocks of the multiscale method from the coarse grid perspective, zoom in to fine scale grid, and an example of flow solution on the fine grid.

shown on Figure 2. We will describe how to set up the fine scale problem to estimate the flux between  $\vec{x}_l$  and  $\vec{x}_n$ . By assumption 2 in section 4.1, as our grid is aligned with the axes, flow over a coarse edge will only be driven by the pressure difference between the two adjacent cells. Therefore the fine scale boundary conditions can be defined based on only  $p_l$  and  $p_n$ . To form boundary conditions for a local problem of the type (2.1) we project pressure to the fine scale problem defined on  $\beta(\vec{x}_{ln})$  as it is shown on Figure 3:

$$(3.2) \quad p(\vec{x}) = \tilde{p}_l, \quad \vec{x} \in \partial\beta_l,$$

$$(3.3) \quad p(\vec{x}) = \tilde{p}_n, \quad \vec{x} \in \partial\beta_n,$$

where  $\tilde{p}_l$  and  $\tilde{p}_n$  are linear projections of  $p_l$  and  $p_n$  on the domain boundary as shown on Figure 3;  $\beta$  is the fine cell (see Definition 4.2);  $\partial\beta_\xi$  ( $\xi \in l, n, t, b$ ) are the corresponding parts of the external boundary of a fine cell; see Figure 1(c).

**3.2.3. Fine scale discretization.** The pressure projection described above defines some of the boundary conditions needed to solve the fine scale Stokes problem. For desirable cases where we can identify a periodic cell, for the top and bottom boundary the pressure is set to be periodic.<sup>1</sup> Moreover, the velocity is set as periodic on both the top-bottom and the left-right boundaries. On the internal boundaries, no-flow conditions are assigned. As it is shown later those boundary conditions are consistent with homogenization results.

Since the typical time scale of a fine scale cell problem is much smaller than one of the coarse scale it is fair to assume that in (2.1b)  $\frac{\partial \vec{v}^\varepsilon}{\partial t} = \vec{0}$ . Taking into account this assumption the fine scale problem can be summarized as follows.

PROBLEM 3.2. *The fine scale cell problem takes the following form:*

$$(3.4a) \quad [\vec{v} \cdot \nabla \vec{v}] + \nabla p - \mu \Delta \vec{v} = 0,$$

$$(3.4b) \quad \nabla \cdot \vec{v} = 0,$$

with the boundary conditions

$$(3.4c) \quad p(\vec{x}) = \tilde{p}_l, \quad \vec{x} \in \partial\beta_l,$$

$$(3.4d) \quad p(\vec{x}) = \tilde{p}_n, \quad \vec{x} \in \partial\beta_n,$$

$$(3.4e) \quad \vec{v}(\vec{x}) = \vec{0}, \quad \vec{x} \in \bar{\sigma},$$

$$(3.4f) \quad p, \vec{v} \text{—periodic on the square elsewhere,}$$

following the notation from Figure 1(c). Neglecting the term in the brackets in (3.4a) results in a linear problem that is analyzed in most of the paper.

In our HMM we will solve Problem 3.2 numerically. To this end we introduce a triangulation as illustrated on Figure 1(c) and discretize the problem by Taylor–Hood elements using FEniCs [31]. The possibility of having different solvers on different scales is one of the key features of the HMM framework that is also utilized in the method described in our paper where mixed finite elements are used on the fine scale and control volumes are used for the coarse scale. For convenience the fine local problem is rescaled to a unit square domain  $\beta$ . This results in the full fine scale problem being scaled as (2.6).

*Remark 3.3.* The methodology described in this paper is not limited by the periodicity assumptions and can be applied on general representative elementary volumes with different boundary conditions, such as zero Dirichlet on top-bottom and Neumann on left-right. For the latter case on general geometries the proofs cannot be conducted and hence it is not described in more detail. The interested reader may find a discussion about effects of boundary conditions for similar upscaling problems in, e.g., [17].

**3.2.4. Computation of coarse scale flux.** The coarse flux density is computed by integrating the horizontal component of the velocity in the fine scale problem from top to bottom and dividing it by the cell size  $\varepsilon$ . Incompressibility of the fine scale

---

<sup>1</sup>For general geometry different possible boundary conditions are described in Remark 3.3.

problem allows us to perform this procedure in any cross section of the fine scale cell problem.

*Remark 3.4.* It is important to note that in practice, to save computational effort, one can perform computations in the call-by-need manner, meaning that for a given geometry we store previous computations and reuse these result in future. For the linear problem with periodic media this means that the total computational effort on the fine scale would be solving only one local problem, which is equivalent to the effort spent in traditional upscaling methods.

**3.2.5. Summary of the algorithm.** The algorithm to solve for the coarse scale pressure and fluxes can be summarized as follows.

1. Start with a guess of the coarse pressure in all cells.
2. Estimate the flux over the coarse edges from the pressure drop over the edge.  
If a flux for a similar pressure drop and grain structure is available from a previous calculation, use this. If not, invoke the fine scale solver.
3. Compute the residual from the new fluxes equal to the difference between sources and total outflow in each coarse cell. If this is sufficiently small, the solution is found. If not, update the coarse pressure by an iterative method based on the residual and go to point 1 (in our implementation for simplicity we use a Newton-type method that converges in a few iterations for flow regimes we have tested the method on).

**3.3. Location of quadrature points.** The method described in section 3.2 is a straightforward generalization of the control volume finite element method (CVFEM) to the HMM framework. The straightforward quadrature approximation introduced in the description of the method in section 3.2.2 can be formally expressed as

$$(3.5) \quad \vec{F}_q^{FE}(\vec{x}_{ln}, p_l, p_n) = \vec{F}\left(\frac{p_l - p_n}{|Z_{ln}|}, \vec{x}_{ln}\right) = \vec{F}(\nabla p_H(\vec{x}_{ln}), \vec{x}_{ln}),$$

where index  $q$  stands for quadrature approximation and  $FE$  indicates it mimics CVFEM behavior;  $\frac{p_n - p_l}{|Z_{ln}|}$  is a finite element (FE) approximation to the gradient parallel component and  $p_H$  is a notation for the finite element approximation of the pressure.

However, for media with high permeability contrasts that are roughly resolved by the control volumes (see Figure 4), CVFEM gives a poor approximation of the pressure drop, and thus the flux. The reason is that a linear pressure interpolation between cell centers cannot capture the discontinuity in the pressure gradient associated with the jump in the permeability. Therefore, the flux computed by the CVFEM-based HMM method will be highly dependent on the location of the quadrature point; see Figure 4(a).

A control volume method commonly used to simulate porous media flow is the so-called two point flux approximation (TPFA) that is derived as a mass conservative finite difference method. In TPFA an auxiliary pressure is introduced at the interface between the control volumes, and using this TPFA will correctly compute an interface transmissivity equal to the harmonic mean. Thus for heterogeneous media, it is of interest to consider control volume HMM based on TPFA. To do so an auxiliary pressure variable is introduced at a point  $\vec{x}_{ln}$  on the interface between two control volumes; see Figure 4(b). This splits the local problem between point  $\vec{x}_l$  and  $\vec{x}_n$  into two. We again assume pressure varies linearly between each two neighboring points and hence perform the same interpolation as in section 3.2 on both sides from  $\vec{x}_{ln}$ ; see

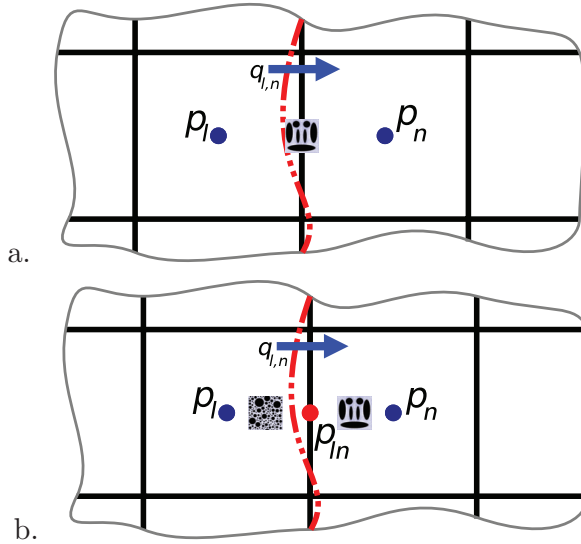


FIG. 4. Handling of discontinuity roughly resolved by coarse grid by methods utilizing two types of quadrature approximation: CVFEM style (a) and TPFA style (b).

Figure 3. After integrating the results from the auxiliary problems,  $p_{ln}$  is eliminated. As the problem is local the continuity equation implies that the flux between the two cells will be the same in all cross sections along  $Z_{ln}$ . This means that for the linear problem the permeability computed in such a way will be equal to the harmonic mean and hence this choice of quadrature will mimic the TPFA. This can be more formally written in a way similar to (3.5),

$$(3.6) \quad F_{q\parallel}^{TPFA}(\vec{x}_{ln}, p_l, p_n) = \left( \frac{|\vec{x}_{ln} - \vec{x}_l|}{|Z_{ln}|} \left[ F_{\parallel} \left( \nabla p_H(\vec{x}_{ln}), \frac{\vec{x}_{ln} + \vec{x}_l}{2} \right) \right]^{-1} + \frac{|\vec{x}_{ln} - \vec{x}_n|}{|Z_{ln}|} \left[ F_{\parallel} \left( \nabla p_H(\vec{x}_{ln}), \frac{\vec{x}_{ln} + \vec{x}_n}{2} \right) \right]^{-1} \right)^{-1},$$

where  $\parallel$  indicates that this is a component parallel to the flow and the right-hand side is the harmonic mean.

The TPFA-based approximation also introduced earlier in [8] differs significantly from older publications that consider control volume multiscale methods and only use a one point approximation, such as [6]. The error introduced by using different quadrature approximations is estimated in Remark 5.12. The practical applicability of choices of quadrature points is considered in the numerical experiments in section 7.2.

**4. Assumptions.** In this paper we will limit ourselves to 2D problems. Moreover, in order to carry out proofs in this paper some assumptions to both the coarse and the fine problem should be introduced.

#### 4.1. Fine scale assumptions.

1. On the fine scale it is assumed that porous geometry is known and periodic with period  $\varepsilon$  within large subdomains.
2. The pore structure is assumed to be aligned with the coarse grid, in the sense that flow normal to the coarse edges is only driven by the corresponding

normal component of the coarse pressure gradient. For Darcy's law this means that the permeability tensor  $K$  in (2.5) is diagonal in the coordinate system of the grid (for Cartesian grids).

3. Furthermore we introduce some simplifications to (2.1b):

- There are no volumetric forces;  $\vec{f} = \vec{0}$ .
  - The velocities are small so that the nonlinear term  $\vec{v}^\varepsilon \cdot \nabla \vec{v}^\varepsilon$  is negligible.
- In most of the paper we assume it is exactly zero.

*Remark 4.1.* The simplifications concerning (2.1b) introduced in assumption 3 will be used in proofs in section 5. Section 6, however will weaken them and present the sketches of the proofs for weakly nonlinear fine scale problem and discuss applicability of the framework to fully nonlinear flow.

**4.2. Coarse scale assumptions.** The convergence proof for the coarse pressure assumes that the solution  $p$  lies in the space

$$(4.1) \quad p \in \mathcal{H}_0^{(2)}(\Omega) \equiv \mathcal{H}_0^1(\Omega) \cap \mathcal{H}^2(\Omega),$$

where  $\Omega$  is the coarse domain of the problem. According to Cai, Mandel, and McCormick [12] sufficient requirements on the problem to possess property (4.1) are

1. the components of permeability tensor  $K_{ii}$  are continuous;
2. the source term  $f \in L_2(\Omega)$ ;
3. the domain  $\Omega$  is convex.

Requirement 1 relies on the fine scale. In order to fulfill it we define the flux function  $F(\nabla p, \vec{x})$  described in (2.4) to be a solution to the fine scale problem on a square domain  $\beta^\varepsilon$  around  $\vec{x}$  defined as

$$(4.2) \quad \beta^\varepsilon = \left[ \vec{x}_1 - \frac{\varepsilon}{2}, \vec{x}_1 + \frac{\varepsilon}{2} \right] \times \left[ \vec{x}_2 - \frac{\varepsilon}{2}, \vec{x}_2 + \frac{\varepsilon}{2} \right].$$

Perturbations in  $\vec{x}$  on a scale much smaller than  $\varepsilon$  will result in small perturbations of the local fine scale domain configuration and hence the solution, that for the linear case means continuous permeability.

Further on in the paper we will need a slightly different definition of local fine scale domain.

**DEFINITION 4.2.** *The fine cell domain  $\beta$  is the fluid part of  $\beta^\varepsilon$  defined by (4.2) scaled to the unit square.*

**5. An a priori error estimate.** In this subsection we will estimate the  $\mathcal{H}^1$  norm of the difference in pressure between the HMM solution and the real solution. We start by explaining the error contributors and later prove the estimate for each of them separately.

By repeated application of the triangle inequality, the difference between the true averaged solution  $p$  and the fully discrete coarse solution obtained from HMM,  $p_{MS}^{H,h}$ , can be expressed as in [5],

$$(5.1) \quad \|p_0 - p_{MS}^{H,h}\|_{\mathcal{H}^1} \leq \|p_0 - p_{MS}^{0,0}\|_{\mathcal{H}^1}$$

$$(5.2) \quad + \|p_{MS}^{0,0} - p_{MS}^{0,h}\|_{\mathcal{H}^1}$$

$$(5.3) \quad + \|p_{MS}^{0,h} - p_{MS}^{H,h}\|_{\mathcal{H}^1}$$

$$(5.4) \quad \leq C \left( \eta + \left( \frac{h}{\varepsilon} \right)^\alpha + H \right).$$

The auxiliary terms in (5.1)–(5.3) have the following meaning:

- $p_0$ : The exact solution of the homogenized problem when  $\varepsilon \rightarrow 0$ ;
- $p_{MS}^{0,0}$ : The solution by the multiscale method when both scales are solved exactly;
- $p_{MS}^{0,h}$ : The solution by the multiscale method when the coarse scale is solved exactly, but the fine scale is solved on the  $h$ -size grid;
- $p_{MS}^{H,h}$ : The solution by the fully discrete multiscale method (with  $H$  and  $h$  grids).

With this in mind we identify the terms in (5.1)–(5.3) in the following way.

- (5.1) *Modeling error.* The error from substituting the correct cell problem with an approximate one.
- (5.2) *Propagation of fine scale error.* The error due to solving cell problem numerically on a grid with cell sizes  $h/\varepsilon$ .
- (5.3) *Coarse scale error.* The error due to solving the coarse problem numerically on a grid with cell size  $H$  and using quadrature approximation for the flux term.

*Remark 5.1* (nonlinear modeling error  $C\eta$ ). In (5.4) the modeling error (5.1) is estimated to be proportional to  $\eta$  which is a measure of nonlinearity, that is a more general statement than is proven in this section. In this section the fine scale problem is assumed to be linear and hence  $\eta = 0$ . This is proven in Theorem 5.6.

For a weakly nonlinear flow,  $\eta$  describes the deviation of the flux from linear (6.1). More general estimates, for the case when  $\eta > 0$ , are discussed in section 6.1.

*Remark 5.2* (different ways of treating the propagation of fine scale error). In most previous works, in which analysis of HMMs is carried out (e.g., [4, 5]), the splitting into error terms was done differently. Namely, in the chain of triangle inequalities the fine scale discretization error was introduced after the coarse scale error. In the analysis phase this leads to analyzing  $\|p_{MS}^{H,0} - p_{MS}^{H,h}\|_{\mathcal{H}^1}$  rather than  $\|p_{MS}^{0,0} - p_{MS}^{0,h}\|_{\mathcal{H}^1}$  in our case. While both approaches are valid the one used in this paper allows proofs to be carried out in a continuous setting that can be more convenient, for example, for nonlinearly driven problems.

Equation (5.4) is the summary of the error terms following the estimates formulated in the rest of the section as theorems.

**5.1. Modeling error.** In this subsection we prove that for linear problem on the fine scale, our HMM represents a method of numerical upscaling consistent with homogenization solutions. The proof is split into several lemmas and it is summarized in Theorem 5.6.

**5.1.1. Equivalence on the fine scale.** We start by proving the equivalence of cell problem formulations in our multiscale method and in homogenization

LEMMA 5.3. *The velocity solution  $\vec{u}$  of the homogenization cell problem given by (2.7c) is equivalent to the solution of the fine scale problem in the HMM (3.4) with the following scaling*

$$(5.5) \quad \vec{u}_i = \frac{\mu}{\delta p_1} \vec{v}_i,$$

where  $\delta p_1$  is defined as pressure drop between the boundary conditions (3.4c), (3.4d)  $\delta p_1 = \tilde{p}_n - \tilde{p}_l$ .

*Proof.* The weak formulation of (2.7c) can be written in a weak form [33, Chapter 9].

PROBLEM 5.4. Find  $\vec{u} \in \mathcal{H}_{per,div0}^1$  such that for all  $\vec{w} \in \mathcal{H}_{per,div0}^1$

$$(5.6) \quad \int_{\beta} \nabla \vec{u}_i : \nabla \vec{w} = \int_{\beta} \vec{f} \cdot \vec{w},$$

where for the considered case the force  $\vec{f} = \vec{e}_i$ . Index  $div0$  means that it is a subspace of divergence free functions.

The formulation (5.6) gives the unique solution for velocity  $\vec{u}_i$  for (2.7c). The absence of pressure in (5.6) implies that the pressure is an auxiliary variable in the Stokes equations and does not influence  $\vec{u}_i$ .

If  $\vec{f} = \nabla \psi$  is a potential vector field then (5.6) can be further rewritten, using the properties of  $\vec{w}$ ,

$$(5.7) \quad \int_{\beta} \nabla \vec{u}_i : \nabla \vec{w} = \int_{\beta} \nabla \psi \cdot \vec{w} = \int_{\partial\beta} \psi \vec{n} \cdot \vec{w} - \int_{\beta} \psi \nabla \cdot \vec{w} = \int_{\partial\beta} \psi \vec{n} \cdot \vec{w},$$

that also implies that  $\psi$  can be replaced by any other function that has the same values on the boundary.

A potential corresponding to the force in our case is  $\psi = x_i + c$ , where  $x_i$  is the  $i$ th coordinate and  $c$  is an arbitrary constant. To achieve our goal we choose  $c$  such that  $\psi = \tilde{p}_l/\delta p_1$  on  $\partial\beta_l$  implying the right boundary condition  $\psi = \tilde{p}_l/\delta p_1 + 1$  on  $\partial D_l$ . The boundary conditions on the remaining sides of the domain can be set to  $\psi = x_i + c$  or even simply forced to be periodic since it will not change the behavior of the right-hand side integral in (5.7).

After those modifications the differences between HMM fine scale problem and homogenization cell problem are the viscosity factor  $\mu$  in front of  $\vec{v}^\varepsilon$  and the factor in the boundary conditions  $\delta p_1$ . Due to linearity the two solutions are equivalent with the scaling given by (5.5).  $\square$

**5.1.2. Equivalence in data estimation.** Second, we should prove that for the linear case the data estimation operator  $\vec{F}(\vec{x}, \nabla p)$  is equivalent to the averaging done in homogenization to compute the flux density in (2.7a) and (2.7b). By the assumptions in section 4.1 the flow is driven only by a difference in the pressure and hence in (2.7a)  $\vec{f} = 0$ .

We start by proving an auxiliary lemma interpreting equation (2.7b).

LEMMA 5.5. *The integration in (2.7b) to compute  $K_{ii}$  is equivalent to integration of the  $i$ th velocity component across the cell perpendicular to  $\vec{e}_i$ ,*

$$(5.8) \quad K_{ii} = \int_{\beta} \nabla \vec{u}_i : \nabla \vec{u}_i dx = \int_{\beta_i(x_i)} \vec{u}_i \cdot \vec{n}_i ds,$$

where  $\beta_i(x_i)$  is a plane perpendicular to  $\vec{e}_i$  at point with coordinate  $x_i$ .

*Proof.* Choosing the test function in Problem (5.4) as  $\vec{u}_i$  gives a simplified expression for  $K_{ii}$ ,

$$(5.9) \quad K_{ii} = \int_{\beta} \nabla \vec{u}_i : \nabla \vec{u}_i dx = \int_{\beta} \vec{e}_i \cdot \vec{u}_i dx.$$

Periodic boundary conditions provide mass conservation along  $e_i$  meaning that the integral flux in the direction of  $e_i$  over each perpendicular cross section is constant

with respect to the normal spatial direction. Thus

$$\begin{aligned} \int_{\beta} \vec{e}_i \cdot \vec{u}_i dx &= \int_0^1 \int_{\beta_i(x_i^0)} \vec{u}_i(x_i) \cdot \vec{n}_i ds dx_i \\ &= \int_0^1 1 dx_i \int_{\beta_i(x_i)} \vec{u}_i(x_i) \cdot \vec{n}_i ds = \int_{\beta_i(x_i)} \vec{u}_i(x_i) \cdot \vec{n}_i ds \end{aligned}$$

that is by (5.9) the coefficient  $K_{ii}$ , concluding the lemma.  $\square$

The equivalence in data estimation is summarized in the following theorem.

**THEOREM 5.6.** *The homogenized solution is equivalent to the HMM problem when both the fine scale problem and the coarse scale problem are solved exactly and hence*

$$(5.10) \quad \left\| p^0 - p_{MS}^{0,0} \right\|_{\mathcal{H}^1} = 0.$$

*Proof.* To show the equivalence let us compare the data estimation expressions obtained by the HMM and homogenization.

The expression for the parallel component of the flux density  $\vec{v}$  in the HMM as it is described in section 3.2.4 takes the form

$$\begin{aligned} \vec{v}_i^{HMM} &= \frac{1}{\varepsilon} \int_{\beta_i} \vec{v}_i^\varepsilon \cdot \vec{n}_i = \frac{\delta p_1}{\mu \varepsilon} \int_{\beta_i} \vec{u}_i \cdot \vec{n}_i = -\frac{\varepsilon}{\mu \varepsilon} \frac{\partial p}{\partial x_i} \int_{\beta_i} \vec{u}_i \cdot \vec{n}_i \\ (5.11) \quad &= -\frac{K_{ii}}{\mu} \frac{\partial p}{\partial x_i} - \frac{K_{ij}}{\mu} \frac{\partial p}{\partial x_j} = \vec{v}_i^{Hom}. \end{aligned}$$

To carry out the chain of inequalities to achieve (5.11) we have used (5.5) from Lemma 5.3, the definition from (3.4d), the assumption that permeability is aligned with the grid, and the homogenized equation (2.7a).

The equality in (5.11) implies that for the linear case the HMM solved exactly coincides with the homogenization solution, meaning that the solutions are also the same and hence proving (5.10).  $\square$

**5.2. Propagation of the fine scale error.** The fine scale error (5.2) in our approximation is the combination of two multiplicative parts:

- the actual error induced by the approximate solution of the fine scale equations by a numerical method;
- the propagation of this error to the coarse solution.

We will consider here these two building blocks.

**5.2.1. Fine scale error from finite element solution of the Stokes problem.** The analysis of Taylor–Hood elements (see [24, Chapter II, 4.2] or [35]) gives the following estimate of the fine scale error,

$$(5.12) \quad \|\vec{v}_{i0}^\varepsilon - \vec{v}_{ih}^\varepsilon\|_{L^2(\beta)} \leq C_i \left( \frac{h}{\varepsilon} \right)^\alpha,$$

where  $\vec{v}_{i0}^\varepsilon$  is exact solution to the Stokes problem and  $\vec{v}_{ih}^\varepsilon$  is a numerical solution with Taylor–Hood elements on a grid with size  $h/\varepsilon$ . We note that the size  $h/\varepsilon$  is relative to the coarse grid, in the actual simulation the cell problem is scaled to the unit square and, hence, the estimate is of order  $h$  instead.

In (5.12)  $\alpha$  depends on the fine cell geometry, i.e., the largest internal angles  $1 \leq \alpha \leq 2$ , where  $\alpha = 2$  on convex domains and decreases with increase of internal angles over  $\pi$  [35]. For the cases of interest in this paper, where the grains are assumed to be polygons which are close to discs and hence have angles  $\varphi \gtrsim \pi$ , the parameter  $\alpha$  is close to 2.

**5.2.2. Propagation of the fine scale error.** The approximation of the fine scale velocity from (5.12) is integrated as it is described in section 5.1 to form the parameter field of the coarse scale problem. From (5.12) together with (5.9) and the Sobolev embedding theorem it follows that at each point in space

$$|K_{ii} - K_{ii}^h| \leq \left| \vec{e}_i \cdot \int_{\beta} (\bar{v}_{i0}^\varepsilon - \bar{v}_{ih}^\varepsilon) dx \right| \leq \|\bar{v}_{i0}^\varepsilon - \bar{v}_{ih}^\varepsilon\|_{L_1(\beta)} \leq C_i \left( \frac{h}{\varepsilon} \right)^\alpha.$$

Taking the 2-norm of the matrix  $K$  we end up with

$$(5.13) \quad \max_{\Omega} \|K - K^h\|_2 \leq C \left( \frac{h}{\varepsilon} \right)^\alpha.$$

Prior to proving the theorem providing the estimate let us introduce an important lemma that shows how the perturbation in data influences the error in the solution to an elliptic PDE in the weak form. Up till now we have been using a formulation of the PDE in the integral conservation form (Problem 3.1). However, for simplicity of proofs, it is more convenient to use the weak formulation of our problem, since the two formulations are equivalent when  $f \in L^2$ .

LEMMA 5.7. *Consider a PDE in the weak form*

$$(5.14) \quad a_\kappa(p, v) \equiv \int_{\Omega} \kappa \nabla p \cdot \nabla v dx = \int_{\Omega} f v dx.$$

*Given two continuous parameter sets for the problem  $\kappa = A$  and  $\kappa = \tilde{A}$ , such that both lead to an elliptic problem with the ellipticity constant  $\gamma$ ,*

$$(5.15) \quad a_\kappa(v, v) \geq \gamma \|v\|_{\mathcal{H}^1(\Omega)}^2.$$

*If these parameter sets further satisfy*

$$(5.16) \quad \max_{\Omega} \|A - \tilde{A}\|_2 \leq \lambda$$

*then the corresponding solutions  $p$  and  $\tilde{p}$  can be bounded in the sense*

$$(5.17) \quad \|p - \tilde{p}\|_{\mathcal{H}^1} \leq C \lambda \|\nabla \tilde{p}\|_{L_2},$$

*where  $C$  is independent of  $A$  and  $\tilde{A}$ .*

The proof of the lemma follows from [21, Lemma 1.8] The result of the lemma can be interpreted as the following.

COROLLARY 5.8. *If two problems of the form (5.14) with the restrictions (5.15) have solutions bounded in  $\mathcal{H}^1$  norm*

$$(5.18) \quad p, \tilde{p} \in \mathcal{H}^1$$

*and the parameter fields are lying close in the sense of (5.16), then the solutions of those problems are close in the  $\mathcal{H}^1$  norm*

$$(5.19) \quad \|p - \tilde{p}\|_{\mathcal{H}^1} \leq C \lambda.$$

*Proof.* The result follows from Lemma 5.7 by using the boundedness assumption (5.17).  $\square$

The following theorem gives the error estimate due to propagation of the fine scale error to the coarse scale.

**THEOREM 5.9.** *The propagation of the fine scale error onto the coarse scale is bounded as*

$$(5.20) \quad \left\| p_{MS}^{0,0} - p_{MS}^{0,h} \right\|_{\mathcal{H}^1} \leq C \left( \frac{h}{\varepsilon} \right)^\alpha.$$

*Proof.* Since both  $p_{MS}^{0,0}$  and  $p_{MS}^{0,h}$  are solutions to continuous problems the proof can be carried out in the set up of the weak formulation. Moreover the solutions are in  $\mathcal{H}^1$  by assumptions of the paper (see section 4.2). Applying Corollary 5.8 with  $\lambda = C(\frac{h}{\varepsilon})^\alpha$  gives the result of the theorem.  $\square$

**5.3. Coarse scale error from finite volume approximation.** In order to prove the estimate on the coarse scale we will follow the proof in [12], and introduce the quadrature approximation whenever needed. For convenience of notation let us omit unused indexes

$$(5.21) \quad p_{MS}^{\xi,h} \equiv p^\xi;$$

let us also introduce the notation for the equation coefficient to replace the fraction

$$(5.22) \quad A^\xi = \frac{K^\xi}{\mu}.$$

Since the flow is assumed to be linear, the flux achieved from the fine scale computation will correspond to the Darcy relation (2.5) with an appropriate permeability field as is shown in section 5.1, and the solution approaches of the method on the two scales decouples. Moreover, this permeability and hence the parameter field  $A$  are essentially smooth.

The CVFEM is defined as follows [12].

**PROBLEM 5.10.** *Find  $\tilde{p}^H \in S_0^H$  (the space of piecewise-linear finite elements), such that for all grid cells  $\tau^H$  the equality below is satisfied:*

$$(5.23) \quad - \int_{\partial\tau^H} (A \nabla \tilde{p}^H) \cdot \vec{n} ds = \int_{\tau^H} f dx,$$

where  $A$  is a continuous parameter field on the coarse scale. In other words,  $\tilde{p}^H$  is a finite element solution to the problem where no quadrature is introduced.

Let us also define a linear operator  $B : S_0^H + \mathcal{H}_0^{(2)} \rightarrow \mathcal{R}^n$  associated with the left-hand side of the equation above:

$$(5.24) \quad b_{ln}(v) = - \int_{\gamma_{ln}} (A \nabla v) \cdot \vec{n}_{ln} ds,$$

$$(5.25) \quad Bv = \left( \sum_{n \in \omega_l} b_{ln} v \right)_{l \in I} = \left( - \int_{\partial\tau_l} (A \nabla v) \cdot \vec{n} ds \right)_{l \in I},$$

where  $\gamma_{ln}$  is the boundary between control volumes around  $l$  and  $n$  (see Figure 2),  $\omega_l$  is the set of vertices adjacent to  $l$ , and  $I$  is the index set for all vertices in the finite element space. We will also consider the continuous problem analogous to Problem 3.1,

$$(5.26) \quad - \int_{\partial V} (A \nabla p^0) \cdot \vec{n} ds = \int_V f dx,$$

where  $V$  is any Lipschitz subdomain of  $\Omega$ .

Finally, we will consider the discrete problem

$$(5.27) \quad - \int_{\partial\tau^H} (A^H \nabla p^H) \cdot \vec{n} ds = \int_{\tau^H} f dx,$$

where  $A^H$  is chosen, such that the quadrature rule is satisfied,

$$(5.28) \quad F_{q\parallel}(\nabla q^H)|_{ln} = \int_{\gamma_{ln}} (A^H \nabla q^H) \cdot \vec{n} ds,$$

where  $F_{q\parallel}(\nabla q^H)$  is the discrete approximation to the flux function made by our multiscale method and  $q^H \in S_0^H$ . We choose  $A^H$  to be a sufficiently smooth function that satisfies (5.28). If we want it to be continuous it can be chosen from the second order polynomials on the edges and interpolated appropriately inside the domain.

**LEMMA 5.11.** *There exists an  $A^H$  sufficiently smooth and strictly positive definite such that (5.28) is satisfied, which is sufficiently close to the given  $A$*

$$(5.29) \quad \max_{x \in \Omega} \|A^H - A\|_2 \leq CH.$$

*Proof.* We give an algorithm to construct such an  $A^H$ . First let us define a quadrature value of  $A$  on every edge that we denote by  $A_q$ ,

$$(5.30) \quad |\gamma_{ln}| \vec{n}_{ln} \cdot A_q^{ln} \vec{e}_k = \vec{F}_{q\parallel}(\vec{e}_k)|_{ln},$$

where unit vector  $\vec{e}_k$  replaces the pressure gradient and superscript  $ln$  indicates the edge between control volume  $l$  and  $n$  in the grid. From here we follow three steps to construct  $A^H$  on entities of the grid.

1. On the vertices of the control volume grid we set

$$A^H(x) = \min_{\forall i_1 i_2, x \in \gamma_{i_1 i_2}} (A_q^{i_1 i_2}).$$

2. On the edges of the control volume grid  $A^H$  is approximated by a polynomial that satisfies step 1 and respects the quadrature rule (5.28) in terms of (5.30),

$$(5.31) \quad \int_{\gamma_{ln}} \vec{n} \cdot A^H \vec{e}_k ds = |\gamma_{ln}| \vec{n}_{ln} \cdot A_q \vec{e}_k = \vec{F}_{q\parallel}(\vec{e}_k)|_{ln}.$$

3. Elsewhere  $A^H$  is interpolated smoothly, e.g., by a harmonic function respecting steps 1 and 2.

The minima of  $A^H$  defined by the steps above are guaranteed to be located in the vertices of the control volume grid and the positive definiteness of  $A^H$  is guaranteed by positive definiteness of  $A_q$  that follows from properties of fine scale.

Due to continuity, the derivative is bounded and hence  $A^H$  approximates  $A_q$  that is extended to a piecewise constant around quadrature points as

$$(5.32) \quad \max \|A_q - A^H\|_2 \leq CH$$

by construction. For the quadrature choices of this paper, a piecewise constant approximation of  $A_q$  also gives  $\max \|A - A_q\|_2 \leq CH$  (see Remark 5.12 below), hence proving the lemma.  $\square$

*Remark 5.12* (specific choices of quadrature rules). If the permeability function  $A$  is in  $W_\infty^1$  or, in other words, has its derivative's variation limited in the weak sense then for a finite volume approximation given by (3.5) we have

$$(5.33) \quad \|A - A_q^{FE}\|_2 \leq CH,$$

since  $A_q$  along the edge is equal to its value in the midpoint.

For the case of TPFA for which it is expressed in terms of the harmonic mean (3.6) the result is obtained by use of the triangle inequality once more. In the worst scenario

$$(5.34) \quad \|A - A_q^{TPFA}\|_2 \leq CH + \max(\|A(\vec{x}_{ln}) - A(\vec{x}_l)\|_2, \|A(\vec{x}_{ln}) - A(\vec{x}_n)\|_2) \leq 2CH.$$

The latter result (5.34) gives the same asymptotic rate as (5.33), but has a worse constant. It should be noted that in applications, the assumption on continuity of the permeability is too strong; in practice material discontinuities that are approximately resolved by the coarse grid are as common. In such cases the TPFA quadrature produces more accurate results as illustrated by a numerical example in section 7.2.

With results for the quadrature approximation at hand we can proceed to estimating the norm of the coarse scale error. We construct finite elements for our CVFEM as triangles with degrees of freedom corresponding to potential lying on the mesh corners as was discussed in section 3.2.1. For the case when the control volumes are rectangles the triangles would be right angled and there will be no flow along the hypotenuse due to orthogonality (the length of the dual grid's side is equal to 0; see Figure 2).

We want to estimate the error in the discrete seminorm

$$(5.35) \quad |p|_{1,\bar{\Omega}^H} = \sqrt{\sum_{l,n} (p(x_l) - p(x_n))^2 \frac{|\gamma_{ln}|}{|Z_{ln}|}},$$

where  $\gamma_{ln}$  and  $Z_{ln}$  are illustrated on Figure 2.

The goal is to achieve a bound for the error between the correct solution of the problem  $p^0$  and the CVFE solution on the  $H$ -sized grid using quadrature integration  $p^H$ . Using the triangle inequality a norm of the error can be split,

$$(5.36) \quad \|p^0 - p^H\|_{\mathcal{H}^1} \leq \|p^0 - \tilde{p}^H\|_{\mathcal{H}^1} + \|\tilde{p}^H - p^H\|_{\mathcal{H}^1},$$

where  $\|p^0 - \tilde{p}^H\|_{\mathcal{H}^1}$  is the error due to the finite element approximation and  $\|\tilde{p}^H - p^H\|_{\mathcal{H}^1}$  is the error due to the quadrature approximation of  $A$  by  $A^H$ . In the paper by Cai, Mandel, and McCormick [12] the estimate for the first term is given in the sense of the seminorm from (5.35) in Theorem 1 from [12]:

$$(5.37) \quad |p^0 - \tilde{p}^H|_{1,\bar{\Omega}^H} \leq CH.$$

We need to estimate the second term  $|\tilde{p}^H - p^H|_{1,\bar{\Omega}^H}$ . The estimate is proved in the following lemma.

**LEMMA 5.13.** *The seminorm due to quadrature approximation on the coarse scale is limited by the coarse grid resolution  $H$ ,*

$$(5.38) \quad |e^q|_{1,\bar{\Omega}^H} \equiv |\tilde{p}^H - p^H|_{1,\bar{\Omega}^H} \leq CH.$$

*Proof.* In [12] it is proved that under our assumptions on the permeability tensor (orientation along the grid and continuity/smoothness) the operator  $B$  is uniformly elliptic on our finite element function space  $S_0^H$ ; see Lemma 2 in [12], or formally

$$(5.39) \quad \sum_{l \in I} v(x_l)(Bv)_l \geq \gamma |v|_{1,\tilde{\Omega}^H}^2$$

for all  $v$  in  $S_0^H$ . Let us use this inequality to do the following estimate,

$$(5.40) \quad \gamma |\tilde{p}^H - p^H|_{1,\bar{\Omega}^H}^2 \leq \sum_{l \in I} e^q(x_l) (Be^q)_l \\ = - \sum_{l \in I} e^q(x_l) \int_{\partial\tau_l} (A\nabla\tilde{p}^H - A\nabla p^H) \cdot \vec{n}_l ds \\ (5.41) \quad = - \sum_{l \in I} e^q(x_l) \left( \int_{\partial\tau_l} ((A^H - A)\nabla p^H) \cdot \vec{n}_l ds \right),$$

where we have combined (5.23) and (5.27) for all control volumes in the grid. By the properties of quadrature derived in Lemma 5.11 we have a bound of the form (5.29) for the difference between the correct and approximate permeability. Using the inequality (5.29) and the Cauchy–Schwarz inequality leads to

$$\begin{aligned} & - \sum_{l \in I} e^q(x_l) \left( \int_{\partial\tau_l} ((A^H - A)\nabla p^H) \cdot \vec{n}_l ds \right) \\ & \leq -CH \sum_{l \in I} e^q(x_l) \int_{\partial\tau_l} (\nabla p^H) \cdot \vec{n}_l ds \\ & = CH \sum_{l \in I} e^q(x_l) \sum_{n \in \omega_l} \int_{\gamma_{ln}} (\nabla p^H) \cdot \vec{n}_l ds \\ & = CH \sum_{\{l,n\} \in \omega} (e^q(x_n) - e^q(x_l)) \int_{\gamma_{ln}} (\nabla p^H) \cdot \vec{n}_l ds \\ & \leq CH |e^q|_{1,\bar{\Omega}^H} \left( \sum_{\{l,n\} \in \omega} \left( \int_{\gamma_{ln}} (\nabla p^H) \cdot \vec{n}_l ds \right)^2 \frac{|Z_{ln}|}{|\gamma_{ln}|} \right)^{\frac{1}{2}}. \end{aligned}$$

Division by  $|e^q|$  results in the inequality

$$(5.42) \quad |e^q|_{1,\bar{\Omega}^H} \leq CH \left[ \sum_{\{l,n\} \in \omega} \left( \int_{\gamma_{ln}} (\nabla p^H) \cdot \vec{n}_l ds \right)^2 \frac{|Z_{ln}|}{|\gamma_{ln}|} \right]^{\frac{1}{2}}.$$

We need to ensure that the expression in the brackets in (5.42) is bounded. Since the properties of  $A^H$  from Lemma 5.11 are no worse than the properties of the original  $A$  we can formulate a continuous problem similar to (3.1) replacing  $A$  by  $A^H$  in the data estimation function

$$(5.43) \quad - \int_{\partial\tau} (A^H \nabla \sigma^H) \cdot \vec{n} ds = \int_{\tau} f dx,$$

and  $\sigma^H$  will be the unique solution to the problem. Moreover functions  $p_{\delta x}^H$  (for which data estimation is fixed to  $H$  but the grid is further refined to  $\delta x$  and  $p_H^H \equiv p^H$  by our definition) will converge to this solution  $\sigma^H$  with refinement of  $\delta x$ ,

$$(5.44) \quad p_{\delta x}^H \rightarrow \sigma^H \text{ as } \delta x \rightarrow 0$$

as proven in [12, Theorem 1].

The exact solution to the approximate problem,  $\sigma^H$ , lies in the same space as  $p^H$  as its parameter field is no worse, meaning that it converges to  $p$  with refinements as  $A^H$  goes to  $A$  by Lemma 5.7:

$$(5.45) \quad \sigma^H \rightarrow p.$$

From (5.44) and (5.45) we conclude that  $p^H$  converges to  $p$  which means that it is also bounded in  $\mathcal{H}^1$  norm; and hence the right-hand side in (5.42) is bounded by  $CH$ , proving (5.38).  $\square$

COROLLARY 5.14. *The full coarse error is limited in the seminorm,*

$$(5.46) \quad |e^c|_{1,\bar{\Omega}^H} \equiv |p^0 - p^H|_{1,\bar{\Omega}^H} \leq CH.$$

*Proof.* The result follows directly from the theorem above and Theorem 1 from [12].  $\square$

To bring the results back to the norms we started out with, i.e.,  $\mathcal{H}^1$ , we first use interpolation from finite element space of piecewise constants for fluxes. Applying our assumption that there is no flow in the direction tangent to control volume boundaries for piecewise linear pressures we get

$$\begin{aligned} \|\nabla v\|_{L_2}^2 &= \int_{\Omega} (\nabla v)^2 dx \\ &= \sum_{l,n \in \omega} \int_{\gamma_{ln}} (\nabla v)^2 dx \\ &= \sum_{l,n \in \omega} \frac{1}{2} |\gamma_{ln}| |Z_{ln}| \left[ \left( \frac{v(x_n) - v(x_l)}{|Z_{ln}|} \right)^2 + \left( \frac{v(x_{\gamma_{ln}1}) - v(x_{\gamma_{ln}2})}{|\gamma_{ln}|} \right)^2 \right] \\ &= \sum_{l,n \in \omega} \frac{1}{2} \frac{|\gamma_{ln}|}{|Z_{ln}|} (v(x_n) - v(x_l))^2; \end{aligned}$$

the sizes  $|Z_{ln}|$  and  $|\gamma_{ln}|$  and points  $x_l$  and  $x_n$  are depicted on Figure 2,  $x_{\gamma_{ln}1}$  and  $x_{\gamma_{ln}2}$  are the endpoints of  $\gamma_{ln}$ ,  $\omega$  is the set of FE edges defining neighboring degrees of freedom. This expression is half of the square of our discrete norm introduced in (5.35). Since the solution to the continuous problem has continuous flux the integration in the derivation above is not exact and by the mean value theorem gives a value in some point in-between  $x_l$  and  $x_n$  so finally we have

$$\begin{aligned} \|\nabla v\|_{L_2} &\leq \sqrt{\sum_{l,n \in \omega} \frac{1}{2} |\gamma_{ln}| |Z_{ln}| \left( \frac{[v(x_n) - v(x_l)] + CH|Z_{ln}|}{|Z_{ln}|} \right)^2} \\ &\leq \sqrt{\sum_{l,n \in \omega} \frac{1}{2} |\gamma_{ln}| |Z_{ln}| \left( \frac{[v(x_n) - v(x_l)] + CH^2}{|Z_{ln}|} \right)^2} \\ &\leq \sqrt{\sum_{l,n \in \omega} \frac{1}{2} \frac{|\gamma_{ln}|}{|Z_{ln}|} [(v(x_n) - v(x_l))^2 + CH^4]} \\ &\leq C|v|_{1,\bar{\Omega}^H} + CH. \end{aligned}$$

The second part is to go the  $\mathcal{H}^1$  norm from the seminorm which can be accomplished whenever we have a finite domain with zero Dirichlet boundary condition on

354

S. ALYAEV, E. KEILEGAVLEN, AND J. M. NORDBOTTEN

a part of the boundary using Friedrich's inequality (see, e.g., [9, page 30])

$$(5.47) \quad \|p^0 - p^H\|_{\mathcal{H}^1} \leq C |p^0 - p^H|_{L_2} \leq C |p^0 - p^H|_{1, \bar{\Omega}^H} + CH \leq CH$$

by corollary 5.14 and the derivation above. This fact can be written as a theorem.

**THEOREM 5.15.** *The coarse scale error is limited*

$$(5.48) \quad \|p_{MS}^{0,h} - p_{MS}^{H,h}\|_{\mathcal{H}^1} \leq CH.$$

**6. Remarks on estimates for nonlinear flows.** Due to the overall ellipticity of the problem, the results obtained in section 5 can be extended to weakly nonlinear flow in the sense where nonlinear terms are sufficiently small compared to the linear terms. In this regime, the resulting analysis retains the same structure, but becomes more involved as the propagation of fine-scale nonlinearities to the coarse scale needs careful attention. Since no new mathematical ideas are required, we choose to not present the rigorous proof, but only comment on the main aspects in section 6.1.

For nonlinear Navier–Stokes flow on the fine scale it is possible to show consistency of our method with the rigorously derived Dupuit–Forchheimer–Ergun law (see, e.g., [26, section 3.2.2]) which we show in section 6.2. However the error analysis for the multiscale discretization in the case of fully nonlinear flow is out of the scope of this paper, as it requires analysis for nonlinear control volume methods on the coarse scale.

**6.1. Remark on an estimate for weakly nonlinear flows.** We refer to weakly nonlinear problems in the sense that

- the solution on the fine scale is bounded by

$$(6.1) \quad \left| \frac{\mu}{\delta p_1} \vec{v}_i^\epsilon - \vec{u}_i \right| \leq \eta$$

replacing (5.5) in the context of Lemma 5.3;

- the resulting problem maintains ellipticity properties as given in (5.39) and (5.15):

$$(6.2) \quad \tilde{B}v = \left( - \int_{\partial\tau_l} \vec{F}(\nabla v) \cdot \vec{n}_l ds \right)_{i \in I},$$

$$(6.3) \quad \sum_{l \in I} v(x_l) (\tilde{B}v)_l \geq \gamma |v|_{1, \tilde{\Omega}^H}^2.$$

The nonlinearity constant  $\eta$  will influence the constant  $C$  in (5.4) and make the modeling error term in it (5.1) nonzero.

**6.1.1. Changes in the proofs from section 5.** Because of the ellipticity assumption (5.39) the structure used for estimates (5.2), (5.3) (Lemmas 5.13 and 5.7) will still be applicable. However, the proofs for several lemmas will be more technical, as linearizations must be introduced in several places.

As a representative example, in Lemma 5.13 in (5.40) before doing a linear splitting, the expression must be linearized to account for (6.1). This results in an additional factor of  $(1 + \eta)$  in the right-hand side of (5.46). However, as we assume  $\eta$  to be small, the factor can be treated as part of the constant  $C$ .

**6.1.2. The modeling error for the case of weak nonlinearity.** The deviation  $\eta$  due to nonlinearity introduced in (6.1) results in the following nonzero estimate for the modeling error,

$$(6.4) \quad \|p_0 - p_{MS}^{0,0}\|_{\mathcal{H}^1} \leq C\eta.$$

Here we summarize how it is derived.

The changes in the modeling error are caused by replacing Lemma 5.3 by assumption (6.1). The consequence is that in Theorem 5.6 using the nonlinearity bound in (5.11) will result in

$$(6.5) \quad \max|\vec{v}_i^{Hom} - \vec{v}_i^{HMM}| \leq C\eta$$

replacing (6.1). This implies that in the worst case, if we linearize the problem in the HMM, the difference in data will be of order  $\eta$  and hence by the lemma analogous to 5.7 from the appendix the estimate for the modeling error takes the form of (6.4).

*Remark 6.1.* Even though for the nonlinear problem the estimate (6.4) becomes weaker than (5.1), it is important to remember that our benchmark solution obtained by homogenization is an approximation when  $\epsilon \rightarrow 0$ . For problems with finite  $\epsilon$ , the nonlinear behavior may be better captured by the HMM approach than by the homogenized solution.

**6.2. Consistency with Dupuit–Forchheimer–Ergun law of fully nonlinear flow.** In this section we highlight an additional result of our analysis with respect to fully nonlinear flow. In particular, the consistency of the method in terms of the homogenization result stated in Theorem 2.1 carries over to the homogenization result stated in Theorem 2.2. We directly infer that the method presented herein is consistent with the Dupuit–Forchheimer–Ergun law.

Here, refer back to the key components of the method and the homogenization result, recalling that the consistency of the method is preserved.

1. The only coarse scale equation in the system (2.8) (where fine scale is not present) is (2.8c). Coarse scale conservation for control volumes (3.1) is basically its conservative form with  $\vec{F} = \vec{v}$ .
2. As is shown in section 5.1.1 the pressure boundary conditions for our fine scale local problem are equivalent to imposing a pressure gradient as in (2.8a).
3. The fine scale part of DFE law ((2.8a) and (2.8b)) coincides with our fine scale cell problem (3.4).
4. Our data estimation operator  $\vec{F}$  coincides with integration of flow over the fine scale domain given by (2.8f) as is shown in section 5.1.2.

The verification steps provided above are not sufficient to prove convergence for fully nonlinear case. While the full analysis of convergence for the fully nonlinear case is out of scope of this paper, we provide a numerical verification of convergence in section 7.3.

**7. Numerical examples.** In this section we present numerical examples that validate the properties of the CVHMMs discussed in this paper. In sections 7.1 and 7.2 we first emphasize the novelties presented in the paper, namely, the error estimate and different quadrature approximations. Thereafter we provide examples that illustrate capabilities of the method for cases where the theory was not fully developed. We extend theoretical results further in section 7.3 by an example illustrating convergence of the nonlinear solution to itself, supporting the consistency of the method

for nonlinear flows as discussed in section 6.2. After that, in section 7.4 we present a typical configuration of a heterogeneous domain for which nonlinear flows arise in applications. In the final example given in section 7.5, we explore how the presented method could be applied to nonsymmetric porous structures that lead to an effective anisotropic permeability field with nonzero off-diagonal components. In this last example the consistency of the coarse discretization is broken.

**7.1. Comparison of error contributions.** This numerical example verifies the rates of convergence proven in the error estimate (5.4). As this paper focuses mainly on the linear regime the results presented in this example only consider Stokes flow. For this case the theory in section 5 indicates the dependency of the error on the coarse and the fine scale grid resolutions ( $H$  and  $h$ ) resulting from Theorems 5.15 and 5.9.

For our test we choose a simple problem on the unit square domain with zero Dirichlet boundary conditions and a forcing function with discontinuity, namely,

$$(7.1) \quad f = \begin{cases} \pi^2 \sin(\pi x) \sin(\pi y), & 0 \leq x \leq \frac{1}{2}, \quad 0 \leq y \leq 1, \\ 4 \sin(\pi y) + \frac{1}{2}(-4x^2 + 4x) \sin(\pi y) \pi^2, & \frac{1}{2} \leq x \leq 1, \quad 0 \leq y \leq 1. \end{cases}$$

The pore structure is chosen to be homogeneous and isotropic; it is formed by circular grains with relative radius 0.4 forming a square arrangement. In the multiscale method the grains are approximated by polygons as on Figures 1(a)–(b).

We aim to compare our method to an analytical solution for the problem. As we are not aware of analytical solutions to the Stokes problem on this pore geometry, we use data estimation  $a_{ap} = -F_{\parallel}(1)$  produced by our method on a very fine grid as a reference. With this approximation the problem will have a semianalytical homogenization solution of the form

$$(7.2) \quad \begin{cases} \frac{1}{2a_{ap}} \sin(\pi x) \sin(\pi y), & 0 \leq x \leq \frac{1}{2}, \quad 0 \leq y \leq 1, \\ \frac{1}{2a_{ap}} (-4x^2 + 4x) \sin(\pi y), & \frac{1}{2} \leq x \leq 1, \quad 0 \leq y \leq 1. \end{cases}$$

The discrete  $L_2$  norms and  $\mathcal{H}^1$  seminorms of error between the solution provided by the method and semianalytical solution (7.2) are plotted on Figure 5. The coarse unit square domain is initially a discretized regular grid with  $H = 0.25$  and the fine scale cell problem has an unstructured triangulation as shown on Figure 1(b);  $h$  and  $H$  refinements are then performed uniformly on both scales. We first take a look at convergence rates. The rates of convergence proven in section 5 all concern the  $\mathcal{H}^1$  norm.

Figure 5(c) indicate that the numerical solution converges in the  $\mathcal{H}^1$  norm with rate  $H^2$ . This rate is higher than the predicted linear convergence in the estimate (5.4). The observed convergence rate in  $L_2$  is also  $H^2$  with respect to the coarse scale refinement. The fact that the convergence rates in both  $\mathcal{H}^1$  and  $L_2$  exceed the theoretical bound is typical for control volume methods on smooth problems (see, e.g., [23]).

The error due to propagation of the fine scale error can be studied from Figures 5(b) and 5(d). The cutoff on the rightmost point of the plots is a result of approximation of refinements reaching the resolution on which  $a_{ap}$  is approximated. The figures indicate that for considered porous media the rate of convergence is approximately  $h^2$ . This means that, as was noted in section 5.2.1 for our domain,  $\alpha \approx 2$ .

ANALYSIS OF CVHMM FOR FLOW IN POROUS MEDIA

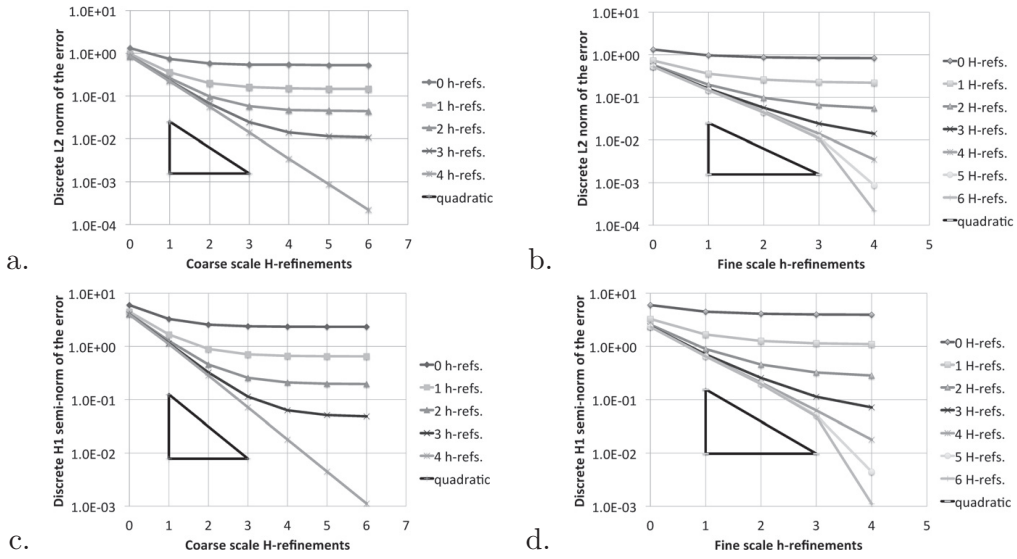


FIG. 5. Discrete error norms for solutions with different levels of refinements plotted against coarse (a), (c) and fine (b), (d) grid sizes. All refinements are uniform and split the edges in half.

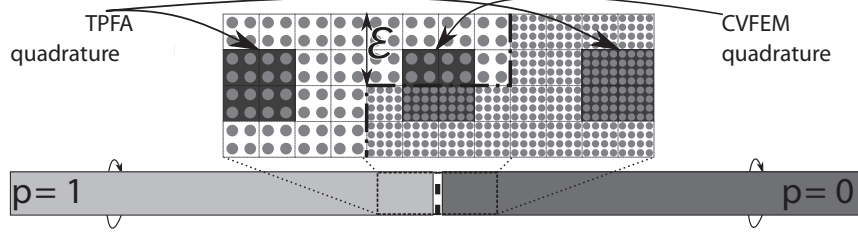


FIG. 6. The structure of the domain with discontinuity with locations of quadrature points.

The rate due to propagation of the fine scale error influences the errors in the  $H_1$  and  $L_2$  norms equivalently.

We conclude this example with emphasizing that no matter how fine either of the resolutions  $h$  or  $H$  is, the error may be governed by the other scale. The plateau on the upper plots on Figures 5 gives a good illustration. This fact is also important for single scale methods for which an effective parameter field is given: no matter how fine the resolution of the grid is, the real error may likely be dominated by the determination of the effective parameter.

**7.2. Domain with a jump.** In this example we address the issue discussed at the end of Remark 5.12. The industry standard for reservoir simulation is finite volume methods and the data that are provided by geologists contain grids for which the material discontinuities are resolved as closely as possible by the finite volume grid.

In this example we want to compare the two quadrature approximations introduced in section 3.3. As was mentioned in Remark 5.12, although TPFA style quadrature has a worse constant in the proof, it provides qualitative advantages when the discontinuity is resolved by the grid. To compare the two approaches we introduce an illustrative example that implements the situation depicted on Figure 4. As it is shown on Figure 6, the domain is chosen to be a stripe  $1 \times 2\epsilon$  with Dirichlet boundary

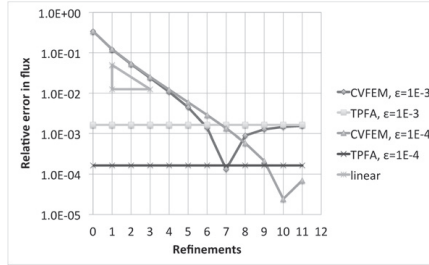


FIG. 7. Relative error in flux compared to a problem with resolved discontinuity.

conditions on left-right and periodic on top-bottom. Exactly in the middle of the domain a zigzag-shaped discontinuity is located; see Figure 6. The structure to the left of the discontinuity has a sparser pattern of the grains and hence higher permeability (around a factor of 20 contrast). Although our example is artificial, porous media with a contact zone between high- and low-permeable regions are common both in geological settings and in artificial porous media such as fuel cells and sanitation tissues.

Figure 7 presents the comparison of relative error in flux between the two strategies to choose quadrature on a relatively sparse grid compared to a solution that resolves the configuration of the quadrature. The domain initially has four degrees of freedom distributed evenly along the  $1 \times 2\epsilon$  strip that is doubled with each refinement. The figure illustrates that although CVFEM-style approximation converges to the solution with the expected rate before having stagnation near the asymptote, TPFA-type quadrature achieves that asymptotic accuracy already for the coarsest grid and maintains it. The errors for both methods will fall below the asymptotic accuracy when the structure of the discontinuity is resolved.

The reason for the poor approximation properties of CVFEM for coarse grids is that it uses a flux approximation that is close to an arithmetic mean around the discontinuity for the given setup and is not stable with respect to perturbations in general (see Figure 4(a)). This leads to overestimation of the flux for low grid resolutions, as opposed to TPFA that provides a harmonic mean, hence underestimating slightly the true behavior. The kink towards zero in the error for CVFEM-type method is due to change of sign in the approximation. Overestimation for the arithmetic means changes to underestimation because the cell problem located in the discontinuity region returns an underestimated value of permeability of about 21% emphasizing again the sensitivity to the small perturbation of the quadrature point location even for idealized cases as on Figure 6. For flows across discontinuities, the correct effective property in the limit is the harmonic mean (see, e.g., [2]) that is one of the reasons for TPFA-type methods becoming standard in reservoir simulation.

This example emphasizes that while the error of CVFEM-style method for a grid with a resolved discontinuity converges with a theoretically expected rate of  $H$ , the TPFA-style quadrature resolves the macroscopic discontinuity, and its error is proportional to “thickness” of discontinuity  $2\epsilon$ .

**7.3. Convergence of nonlinear flow to itself.** In section 6.2 the consistency between the proposed CVHMM and nonlinear homogenization was shown. In this example we provide numerical indication that verifies convergence of the method for the nonlinear case.

In absence of analytical solutions for Dupuit–Forchheimer–Ergun flows, in this example we test all solutions against a numerical solution computed on very fine grids

ANALYSIS OF CVHMM FOR FLOW IN POROUS MEDIA

359

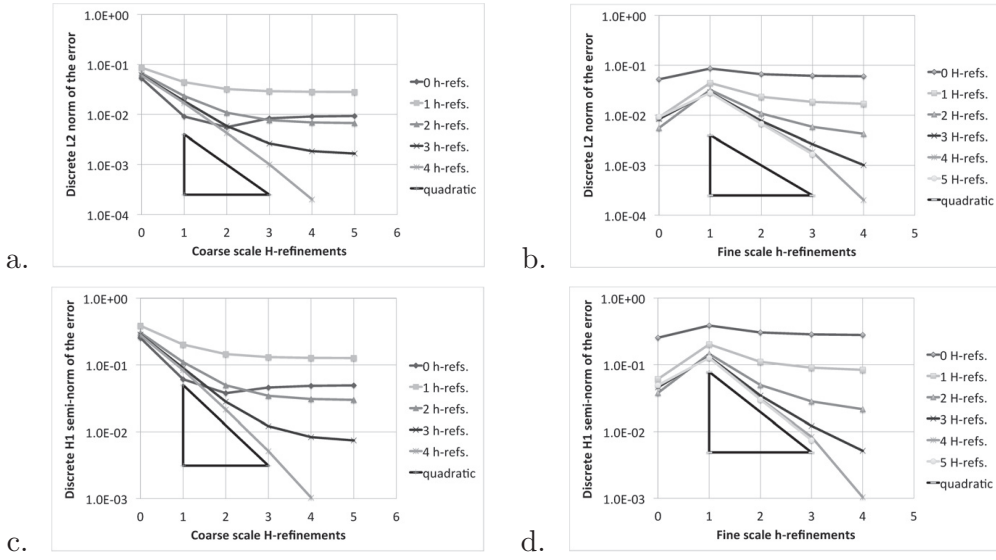


FIG. 8. Discrete error norms for nonlinear solutions with different levels of refinements plotted against coarse (a), (c) and fine (b), (d) grid sizes.

on both scales. The problem setup is analogous to section 7.1. The difference is that on the fine scale a fully nonlinear cell problem is used with  $\mu = 0.004$  (Problem 3.2) and the starting grid is one level coarser than the grid used for the linear case (see Figure 1(b)). With these parameters the discrepancy between the solution to the full nonlinearity coarse scale flux as compared to the linearized flow is up to 20%.

The discrete error norms of solutions to the nonlinear problem compared to a reference solution on detailed coarse and fine grids is presented on Figure 8. Comparing convergence plots the for nonlinear problem (Figure 8) to those verifying linear convergence (Figure 5) illustrates that the nonlinear problem converges with the same rates with respect to both fine and coarse scale refinements. As it was observed in section 7.1 for the linear case, the errors are of order  $(\frac{h}{\varepsilon})^2$  and  $H^2$ , respectively, for both norms. This gives a good indication of the robustness of the method in the nonlinear regime for which analytical results are not obtained.

**7.4. Features of nonlinear flow in heterogeneous medium.** One of the strong points of our method remains its flexibility with respect to the choice of the fine scale problem. While the focus of this paper is analysis of convergence of the CVHMM for the linear case, it is important to point out its applicability outside convergence theory.

This numerical example shows all the potential of our method and indicates problems for which nonlinearities play a crucial role. We consider a nonlinear flow problem (induced by full Problem 3.2 with  $\mu = 0.04$ ) on a heterogeneous domain composed of regions made out of cells illustrated on Figures 1(b) and 1(c) combined in an altering frame manner as shown on the bottom of Figure 9(a). The part composed of grid cells of Figure 1(b)-type gives an anisotropic region which is approximately 4 times less permeable than the isotropic region composed of the Figure 1(c)-type cells. The boundary conditions are no-flow for all outer boundaries of the domain except for one sink that is represented by the zero Dirichlet boundary condition located in the left middle on the side of the low-permeable region. The flow is driven by the load function that is nonzero in one grid point on the opposing boundary in the

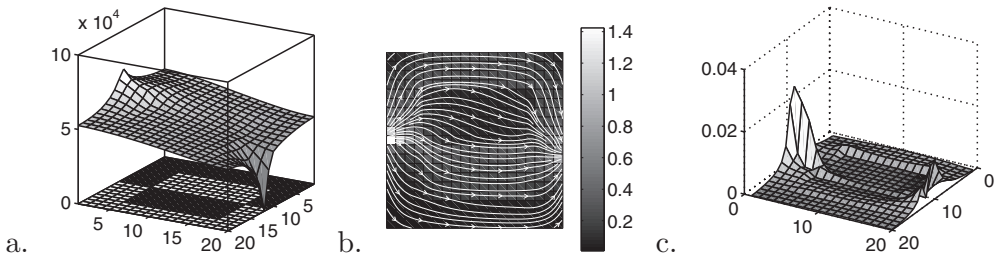


FIG. 9. Pressure solution to nonlinear problem plotted over the domain schematics (light indicate heterogeneous low-permeable areas) (a), corresponding flow solution (b), and special distribution of nonlinear effects (c).

high-permeable region, simulating a source well. To handle discontinuities correctly TPFA-type quadrature is used for sampling.

The pressure and the flow solutions to the described nonlinear problem are depicted on Figures 9(a) and 9(b), respectively. As expected most of the flow is driven along the high-permeable frame part and there are pressure buildups near the source and the sink. The latter one is larger due to lower permeability.

Another purpose of this example is to identify regions where nonlinearity is most crucial for a heterogeneous domain. Figure 9 shows the the modulus of difference between linear and nonlinear solutions in different parts of the domain. It is no surprise that the nonlinearity is biggest for parts with highest flow velocity; that is, first of all, point sources and sinks. In the rest of the domain nonlinear effects are generally larger in high-permeable areas. Moreover there is noticeable focusing effects on the outer corners of the low-permeable region in the center.

**7.5. Application to nonsymmetric porous structures.** It is well known that for general porous structures and, as a result, for general permeability fields two point methods including the methodology described in the current paper, are not consistent and therefore converge to the wrong solution (see, e.g., [3]). However, for the majority of geological applications the anisotropy is aligned with the grid to the extent that the consistency error is acceptable. Therefore TPFA remains standard in industrial reservoir simulation (such as the Eclipse software by Schlumberger). TPFA leads to linear systems that are M-matrices, which in turn guarantees monotonicity of the fluid potential and a physically reasonable solution. For the cases when the structure is not aligned with the grid there exist several methods to overcome those constraints including perturbing the grid so it is K-orthogonal and a TPVA is valid (see, e.g., [1]), modifying positions of collocation points in two-point flux scheme forming a nonlinear problem (see, e.g., [30]) or using a multipoint flux approximation (see, e.g., [2]). While the methods described above are out of the scope of this paper, here we present an example indicating that for randomly generated grain structure (as on Figure 10(a)) the errors decrease to a certain point before being limited by the consistency error of the coarse grid.

For this example we consider a coarse linear problem of the type

$$(7.3) \quad -\nabla \cdot A \nabla p = f$$

solved on the unit square, for which  $A$  is computed from solving homogenization cell problems numerically for the cell from Figure 10(a) on a refined grid. The  $f$  is than

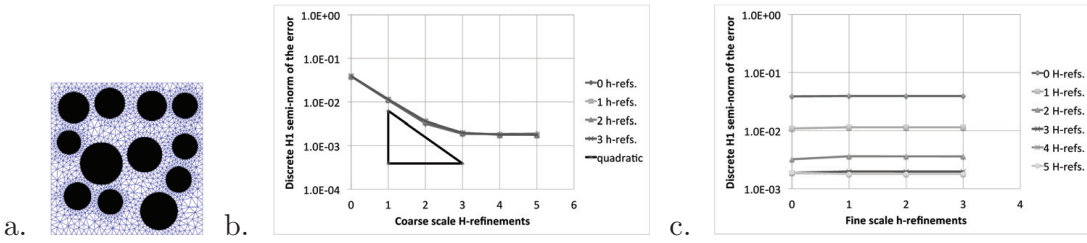


FIG. 10. An example of randomly generated anisotropic porous structure (a) and discrete error norms for solutions for domain composed of those for different levels of refinements plotted against coarse (b) and fine (c) grid sizes.

computed from (7.3) by substituting

$$(7.4) \quad p = (0.5 - |x - 0.5|)(0.5 - |y - 0.5|).$$

The comparison of the numerical results for different grid resolutions to the solution (7.4) in discrete norms is presented on Figure 10. Here, as earlier, we start out with  $H = 0.25$  on the coarse scale and grid depicted on Figure 10(a) and then perform uniform refinements.

Figure 10(b) shows expected rate of convergence for the first refinements of the coarse grid, after which the error due to lack of consistency dominates. In this example fine scale grid refinement does not provide any improvement as the error due to off-diagonal components, that is not accounted for, dominates over the propagation of fine scale error (see Figure 10(c)).

This last example provides an alternative view of our method. The TPFA discretization chosen for the coarse grid is considered sufficiently accurate for a broad range of industrial applications. We may thus choose to consider the consistency error as a sufficient tolerance for the multiscale algorithm from a practical viewpoint. This view allows us to interpret that for the current example, even the coarsest fine scale solver is sufficient to obtain the accuracy needed in practical applications.

**8. Conclusions.** In this paper we have presented a heterogeneous multiscale method for modeling flow in porous media taking explicitly into account pore scale equations. The method presumes only the continuity equation on the coarse scale and the pressure-flow relationship is numerically derived by solving problems on fine scale geometry locally. The presented implementation of the method permits both Stokes and steady state Navier–Stokes equations on the fine scale. Thus both linear and non-linear coarse scale pressure-flow relations can be modeled by this approach. Two possible choices of quadrature points for the reconstruction of the coarse scale flux were presented. Those choices result in HMMs that generalize the CVFEM and finite difference method with TPVA. HMMs with the latter choice of quadrature had not been analyzed in previous works.

The particular focus of this paper has been the convergence analysis of the presented HMM. For methods in which scales differ significantly, a reconstruction of the full fine scale solution is not important. By a comparison with the homogenization solution of the Stokes problem, we proved an a priori error estimate for the coarse scale pressure in the case of linear flow. The estimate is done in the  $\mathcal{H}^1$  norm that also implies the estimate on the coarse flux. It is shown that the error can be split into three parts: a modeling error which is zero when the flow is linear, a term proportional to the size of the coarse grid, and a term that is dependent on the fine scale geometry, grid size, and the size of the fine scale problems. We also discussed the extension of

the proof to the weakly nonlinear case, for which the modeling error is no longer zero as well as consistent with a more complicated Dupuit–Forchheimer–Ergun law for the fully nonlinear case.

Numerical results provided in the paper verify the estimate and emphasize the importance of appropriate accuracy on both the coarse and fine scales. They also indicate similar convergence behavior for nonlinear problem. We also provide an example comparing different choices of quadrature on domains with coarse discontinuity. Moreover for heterogeneous domain with discontinuity we identify some typical regions for which nonlinearities have marked influence.

**Acknowledgments.** We want to thank Jörg Willems from Johann Radon Institute for Computational and Applied Mathematics, Annette Stephansen from CMR, as well as Henrik Kalisch and Florin Radu from the University of Bergen for helpful discussions and references.

## REFERENCES

- [1] I. AAVATSMARK, *Interpretation of a two-point flux stencil for skew parallelogram grids*, Comput. Geosci., 11 (2007), pp. 199–206.
- [2] I. AAVATSMARK, *Multipoint flux approximation methods for quadrilateral grids*, in The 9th International Forum on Reservoir Simulation, Abu Dhabi, United Arab Emirates, 2007, pp. 9–13.
- [3] I. AAVATSMARK, T. BARKVE, Ø. BØE, AND T. MANNSETH, *Discretization on non-orthogonal, quadrilateral grids for inhomogeneous, anisotropic media*, J. Comput. Phys., 127 (1996), pp. 2–14.
- [4] A. ABDULLE, *On a priori error analysis of fully discrete heterogeneous multiscale FEM*, Multiscale Model. Simulation, 4 (2005), pp. 447–459.
- [5] A. ABDULLE, *The finite element heterogeneous multiscale method: A computational strategy for multiscale PDEs*, in Multiple Scales Problems in Biomathematics, Mechanics, Physics and Numerics, Math. Sci. Appl., 31 (2009), pp. 133–181.
- [6] A. ABDULLE AND W. E, *Finite difference heterogeneous multi-scale method for homogenization problems*, J. Comput. Phys., 191 (2003), pp. 18–39.
- [7] G. ALLAIRE, *One-phase Newtonian flow*, in Homogenization and Porous Media, U. Hornung, ed., Springer, New York, 1996, pp. 45–68.
- [8] S. ALYAEV, E. KEILEGAVLEN, AND J. M. NORDBOTTEN, *Multiscale simulation of non-Darcy flows*, in Computational Methods in Water Resources XIX, Urbana-Champaign, IL, 2012, pp. 1–8.
- [9] D. BRAESS, *Finite Elements: Theory, Fast Solvers, and Applications in Solid Mechanics*, Cambridge University Press, Cambridge, 2007.
- [10] A. BRANDT, *Multiscale scientific computation: Review 2001*, in Multiscale and Multiresolution Methods, Lecture Notes Comput. Sci. Eng. 20, Springer, Berlin, 2002, pp. 3–95.
- [11] H. C. BRINKMAN, *A calculation of the viscous force exerted by a flowing fluid on a dense swarm of particles*, Appl. Sci. Res. Sect. A, 1 (1947), pp. 27–34.
- [12] Z. CAI, J. MANDEL, AND S. MCCORMICK, *The finite volume element method for diffusion equations on general triangulations*, SIAM J. Numer. Anal., 28 (1991), pp. 392–402.
- [13] Z. CHEN, *On the heterogeneous multiscale method with various macroscopic solvers*, Nonlinear Anal., 71 (2009), pp. 3267–3282.
- [14] Z. CHEN, S. L. LYONS, AND G. QIN, *Derivation of the Forchheimer law via homogenization*, Transp. Porous Media, 44 (2001), pp. 325–335.
- [15] J. CHU, B. ENGQUIST, M. PRODANOVIC, AND R. TSAI, *Advances in Applied Mathematics, Modeling, and Computational Science*, Fields Institute Comm. 66, Springer, Boston, 2013.
- [16] J. CHU, B. ENGQUIST, M. PRODANOVIC, AND R. TSAI, *A multiscale method coupling network and continuum models in porous media I: Steady-state single phase flow*, Multiscale Model. Simulation, 10 (2012), pp. 515–549.
- [17] L. J. DURLOFSKY, *Numerical calculation of equivalent grid block permeability tensors for heterogeneous porous media*, Water Res. Res., 27 (1991), pp. 699–708.
- [18] W. E, *The Heterogeneous Multiscale Method and the “Equation-free” Approach to Multiscale Modeling*, Multiscale Modeling, <https://web.math.princeton.edu/~weinan/pdf%20files/HMM-eqfree.pdf> (2011).

- [19] W. E AND B. ENGQUIST, *The heterogeneous multiscale methods*, Comm. Math. Sci., 1 (2003), pp. 87–132.
- [20] W. E, B. ENGQUIST, X. LI, W. REN, AND E. VANDEN-EIJNDEN, *Heterogeneous multiscale methods: A review*, Comm. Comput. Phys., 2 (2007), pp. 367–450.
- [21] W. E, P. MING, AND P. ZHANG, *Analysis of the heterogeneous multiscale method for elliptic homogenization problems*, J. Amer. Math. Soc., 18 (2005), pp. 121–156.
- [22] Y. EFENDIEV AND T. HOU, *Multiscale finite element methods for porous media flows and their applications*, Appl. Numer. Math., 57 (2007), pp. 577–596.
- [23] G. T. EIGESTAD AND R. A. KLAUSEN, *On the convergence of the multi-point flux approximation o-method: Numerical experiments for discontinuous permeability*, Numer. Methods Partial Differential Equations, 21 (2005), pp. 1079–1098.
- [24] V. GIRAUT AND P.-A. RAVIART, *Finite Element Methods for Navier-Stokes Equations Theory and Algorithms*, Springer-Verlag, Berlin, 1986.
- [25] S. MAJID HASSANIZADEH AND W. G. GRAY, *Thermodynamic basis of capillary pressure in porous media*, Water Res. Res., 29 (1993), pp. 3389–3405.
- [26] U. HORNUNG, *Homogenization and Porous Media*, Interdiscip. Appl. Math. 6, Springer Verlag, New York, 1997.
- [27] M. K. HUBBERT, *The theory of ground-water motion*, J. Geol., (1940), pp. 785–944.
- [28] V. KIPPE, J. E. AARNES, AND K.-A. LIE, *A comparison of multiscale methods for elliptic problems in porous media flow*, Comput. Geosci., 12 (2008), pp. 377–398.
- [29] J. LI, P. G. KEVREKIDIS, C. W. GEAR, AND I. G. KEVREKIDIS, *Deciding the nature of the coarse equation through microscopic simulations: The baby-bathwater scheme*, SIAM Rev., 49 (2007), pp. 469–487.
- [30] K. LIPNIKOV, M. SHASHKOV, D. SVYATSKIY, AND Y. VASSILEVSKI, *Monotone finite volume schemes for diffusion equations on unstructured triangular and shape-regular polygonal meshes*, J. Comput. Phys., 227 (2007), pp. 492–512.
- [31] A. LOGG, K. A. MARDAL, AND G. N. WELLS, *Automated Solution of Differential Equations by the Finite Element Method*, Lecture Notes Comput. Sci. Eng. 84, Springer, Berlin, 2012.
- [32] I. LUNATI AND P. JENNY, *Multiscale finite-volume method for compressible multiphase flow in porous media*, J. Comput. Phys., 216 (2006), pp. 616–636.
- [33] A. QUARTERONI AND A. VALLI, *Numerical Approximation of Partial Differential Equations*, Springer Ser. Comput. Math. 23, Springer Verlag, Berlin, 1997.
- [34] A. TAMAYOL AND M. BAHRAMI, *Analytical determination of viscous permeability of fibrous porous media*, Internat. J. Heat Mass Transfer, 52 (2009), pp. 2407–2414.
- [35] R. VERFÜRTH, *Error estimates for a mixed finite element approximation of the Stokes equations*, RAIRO. Anal. Numér., 18 (1984), pp. 175–182.
- [36] S. WHITAKER, *Advances in theory of fluid motion in porous media*, Indust. Engrg. Chem., 61 (1969), pp. 14–28.
- [37] X. YUE AND W. E, *Numerical methods for multiscale transport equations and application to two-phase porous media flow*, J. Comput. Phys., 210 (2005), pp. 656–675.

